The structure-function relationships underlying *Drosophila* larval chemotaxis

Ibrahim Tastekin

TESI DOCTORAL UPF / 2016

Thesis Supervisor

Dr. Matthieu Louis

SENSORY SYSTEMS AND BEHAVIOUR

EMBL/CRG SYSTEMS BIOLOGY RESEARCH UNIT

CENTRE FOR GENOMIC REGULATION

upf. Universitat Pompeu Fabra Barcelona

ACKNOWLEDGEMENTS

First of all, I would like to thank Matthieu for his supervision and unconditional support and for giving me the opportunity to be a part of this project. Throughout my PhD, his constant help and motivation allowed me to see the light in the darkest hours. He has been a teacher, an understanding colleague and a sincere friend. I would like to thank Sam for helping me both inside and outside the lab. It was a really nice experience working with him. A special thanks to Avinash for being a true friend. With him, I shared both the joy and disappointment along the way. I am deeply grateful to Mariana Lopez for being so friendly and ready to help me whenever I needed. I would like to thank Moraea Phillips for being so nice to me during my first days in the lab and in Barcelona. I would like to thank Alex Gomez-Marin, who inspired me with his scientific perspective. I also want to thank Elena for the personal and professional help. I really enjoyed spending my free time and discussing science with her. I would like to thank Andi for his friendship. I will never forget the sleepless nights I spent with him in the lab. I would like to thank Daeyeon for being such a nice friend and for sharing his scientific ideas with me. I would like to thank Elie, who always cheered me up when I felt down. I am grateful to Ajinkya for the amazing time we spent together in Barcelona as well as in Janelia Research Campus. Many thanks to Aljoscha, Julia, David, Nicole, Iris, Dani and Rudra for their friendship and the scientific discussions. I am grateful to Nico for the help with the experiments. I would like to thank David and Elena for proofreading my thesis. I am grateful to Marta Zlatic for the help and the fruitful scientific discussions during our collaboration. I am thankful to all Fliact members for the wonderful moments we had during our meetings. I am grateful to the HR department of the CRG, especially Montse and

David, for the invaluable help with the paperwork. I would like to thank the members of my thesis committee, Ben Lehner, Guillaume Filion and Cedric Notredame for the inputs that helped me improve my work and my scientific skills. I am thankful to James Truman, Julie Simpson, Albert Cardona and Stefan Pulver for the help and the fruitful discussions.

I am deeply thankful to my mother, Gulser Tastekin for being the best mum in the world. Her unconditional love and support helped me achieve my goals throughout my life. I am grateful to my father, Osman Tastekin for all the things he sacrificed for my education. I would like to thank Huseyin Muratoglu for supporting me throughout my scientific career. I would like to thank Melek and Tayfun Ozmeric for always standing by me since I first met them. I would also like to thank the rest of my family (especially my dear aunt, Minenur Sunter) and friends for all the love and support. Most importantly, I would like to thank my precious wife, Gizem for her love and the support, which have been the main factors that kept me going.

ABSTRACT

Animals extract relevant information from their environment to locate favorable conditions and to avoid possible threats. Consequences of animal behavior bring about outcomes (i.e. adaptation, speciation, isolation and evolution) that are significant to the survival of the individuals as well as the species.

From the simplest jellyfish to primates, nervous systems transform patterns of sensory stimuli into behavioral actions that allow animals to increase their chances of survival. A mechanistic understanding of behavior can be achieved by studying the computations that emerge from the structural organization of the nervous systems.

The *Drosophila* larva is an excellent model organism to study the neural correlates of behavior. It possesses a tractable yet complex nervous system that is capable of integrating and transforming multimodal sensory stimuli into coherent navigational decisions. In the larva, activity of individual neurons –the building blocks of the nervous system– could be reliably monitored and manipulated thanks to the unmatched genetic tools available in *Drosophila*. Recent efforts to reconstruct the connectome of the whole larval nervous system enable circuit-level analysis of the neural mechanisms underlying the larval behavior.

The larva exhibits robust navigation in the presence of volatile chemical cues (chemotaxis). Larval chemotaxis consists in alternations between different behavioral modes: runs, pauses and turns. Here, we performed two independent forward screens to identify neurons that are involved in action selection during *Drosophila* larval chemotaxis.

In our first screen, we identified neurons that are involved in run-to-turn transitions. High-resolution behavioral analysis upon manipulation of activity in a subset of neurons in the subesophageal zone revealed that these neurons are necessary and sufficient to trigger reorientation maneuvers. Our findings suggest that the SEZ is a premotor center that mediates action selection based on integrated sensory stimuli.

In the second screen, we combined functional analysis with electron microscopy reconstruction to identify a descending neuron (PDM) that is necessary and sufficient to trigger run-to-turn transitions. EM reconstruction revealed that PDM receives olfactory inputs in the lateral horn region and connects to premotor neurons involved in peristaltic wave propagation through a set of SEZ descending neurons. By combining optogenetic activation with high-resolution analysis of behavior, we showed that PDM is responsible for terminating runs by inhibiting peristaltic wave-generating circuits in the ventral nerve cord of the larva. We believe that the elementary structural and computational principles we revealed in the larva will be generalize to more complex nervous systems in the future.

RESUMEN

Los animales extraen información relevante de su medio ambiente para encontrar condiciones favorables y evitar posibles peligros. Como consecuencia del comportamiento animal se obtienen resultados (adaptación, especiación, aislamiento y evolución) significativos para la supervivencia de los individuos así como para las especies.

Desde las simples medusas hasta los primates, el sistema nervioso transforma patrones de estimulación sensorial en acciones del comportamiento que permiten a los animales incrementar su probabilidad de supervivencia. Estudiando las computaciones que emergen de la estructura organizativa del sistema nervioso se puede llegar a entender el conocimiento mecánico del comportamiento.

La larva de *Drosophila* es un excelente organismo modelo para estudiar las correlaciones neuronales del comportamiento. Posee un dócil pero complejo sistema nervioso capaz de integrar y transformar estímulos sensoriales multimodales en decisiones de navegación complejas. En la larva, la actividad de neuronas individuales –las piezas fundamentales del sistema nervioso-puede ser controlada y manipulada de manera fiable gracias a las inigualables herramientas genéticas disponibles en *Drosophila.* Esfuerzos recientes para reconstruir el conectoma completo del sistema nervioso de la larva nos permite analizar el mecanismo neuronal a nivel de circuito subyacente al comportamiento de la larva.

La larva presenta una navegación robusta en presencia de señales químicas volátiles (quimiotaxis). La quimiotaxis de la larva alterna entre distintos modos de comportamiento: carreras, pausas y giros. Aquí, hemos llevado a cabo dos cribados independientes que nos permiten identificar

neuronas de la larva de *Drosophila* involucradas en la selección de acciones durante la quiomitaxis.

En nuestro primer cribado, hemos identificado neuronas involucradas en transiciones correr-para-girar. El análisis del comportamiento a alta resolución, habiendo manipulado la actividad de un grupo de neuronas de la zona subesofageal (SEZ), reveló que dichas neuronas son necesarias y suficientes para activar maniobras de reorientación. Nuestros descubrimientos sugieren que la SEZ es un centro premotor que media la selección de acciones basándose en estímulos sensoriales integrados.

En el segundo cribado, hemos combinado el análisis funcional con la reconstrucción mediante microscopia electrónica para identificar la neurona descendiente (PDM) que es necesaria y suficiente para activar las transiciones correr-para-girar. La reconstrucción mediante EM reveló que la PDM recibe señales olfativas en la región del asta lateral y se conecta con neuronas premotoras involucradas en la propagación de ondas peristálticas a través de un conjunto de neuronas SEZ descendientes. Combinando la activación optogenética con el análisis del comportamiento de alta resolución, hemos demostrado que la PDM es la responsable de terminar carreras inhibiendo los circuitos de generación de ondas peristálticas en el cordón nervioso ventral de la larva. Creemos que los principios básicos estructurales y computacionales que hemos descubierto en la larva se generalizarán en el futuro en los sistemas nerviosos mas complejos.

PREFACE

Santiago Ramón y Cajal – one of the most influential figures in the history of modern neuroscience – once said, "As long as our brain is a mystery, the universe, the reflection of the structure of the brain will also be a mystery." Beginning from the end of the 19th century, he combined his scientific skills with his artistic talents to create drawings of neural circuits based on the histological observations he made. His drawings – ranging from neural circuits in the mammalian retina to the hippocampal circuits of the rodents– display the daunting complexity of the nervous systems. Since then, scientists endeavor to solve the mystery of the brain by studying the structure and function of these complex neural circuits.

In his studies, Cajal observed intriguing structural parallelism between the visual circuits of the vertebrates and the flies. During the last century, his observations were corroborated by many studies showing that neural circuits share common design principles across the phylogeny. Therefore, many neuroscientists believe that basic principles of neural circuit function can be inferred by studying tractable invertebrate brains instead of dealing with the daunting complexity of the mammalian nervous system. *Drosophila Melanogaster* –which is capable of exhibiting complex behaviors– is perhaps the most popular invertebrate model organism to study neural circuits due to the presence of genetic tools to access and manipulate the neural circuits. Recently, the *Drosophila* larva –with only ~10.000 neurons– has proven itself to be a perfect model organism to study the neural basis of behavior: In addition to already existing genetic tools and high-resolution analysis of complex behaviors, larval community has made significant progress toward reconstructing the whole larval nervous system (connectome) at synaptic resolution by using electron microscopy data. Recent studies combined the functional and

behavioral analysis with the larval connectome to unravel circuit-level mechanisms underlying sensory-driven behavioral decisions. The aim of this study is to identify neural circuits involved in the sensorimotor transformation underlying chemotaxis in the tractable *Drosophila* larval nervous system. We believe that our findings will contribute to the efforts to understand the neural correlates of action selection in the Drosophila larva and eventually the basic principles we revealed would be extended to more complex nervous systems such as the human brain.

TABLE of CONTENTS

CHAPTER 1: Introductory Chapter

1.1 Introduction:

A simple definition of animal behavior would be that it is the set of actions animals undertake in response to external stimuli (e.g. food, danger, mate etc.) and their internal needs (e.g. hunger, sexual drive etc.). In this respect, a careful dissection of animal behavior is crucial to understand the mechanisms underlying the survival of individuals in short term as well as the survival of the species in long term.

Despite of its importance in understanding life, the birth of modern ethology –the study of the animal behavior– has taken place only in the 20th century. Around fifty years ago, Niko Tinbergen proposed that proper understanding of a particular behavior requires studying it at four main levels (Tinbergen 1963). In his article he states that "*... behavior is part and parcel of the adaptive equipment of animals; that, as such, its* ***short-term causation*** *can be studied in fundamentally the same way as that of other life processes; that* ***its survival value*** *can be studied just as systematically as its causation; that* ***the study of its ontogeny*** *is similar to that of the ontogeny of structure; and that* ***the study of its evolution*** *likewise follows the same lines as that of evolution of form.*" He suggested that each of these levels could be dissected with the scientific method already applied for other biological sciences. These four levels can be divided into two main groups: (1) explanation of a type of behavior by studying its underlying evolutionary processes (ultimate explanation that includes the study of its evolution and survival value) and (2) proximate explanation by studying the immediate factors giving rise to that behavior. Proximate explanation includes the short-term causation (e.g. the causation between the nervous system function and behavior) and ontogeny (the developmental changes in the behavior throughout the life

time of an organism). The framework Tinbergen postulated is still considered to be the best way to understand animal behavior (Dawkins and Hauber 2014, Taborsky and Hauber 2014).

According to Tinbergen, the ultimate explanation of 'why' a behavior exists can be understood through (1) the evolutionary processes and selective pressures that gave rise to that behavior and (2) survival value of the behavior. He stated that the evolutionary path a behavior has taken as well as its dynamics should be studied to understand why that particular behavior evolved. This could be achieved by comparing the behavior of closely related species and their recent ancestors or by investigating the behavior of different species in the same environment (Tinbergen 1963). On the other hand, the survival value of the behavior could be revealed by analyzing divergence (and convergence) of this behavior in the phylogeny. For instance, a selective pressure (e.g. environmental factors that remained constant for long time) could stabilize a particular behavior since deviations from that behavior decreases the survival success (fitness) of the species under that pressure. Therefore, the selective pressure discourages divergence from this behavior. Likewise, due to its survival value this behavior might have independently evolved by different species descended from distinct ancestors (convergent evolution).

The immediate explanation of a behavior comprises the short-term causation and the ontogeny of the behavior. The short-term causation is defined as the causal mechanisms underlying the behavior. Causal relations of the behavior can be studied at different levels e.g. molecules, cells (neurons), organs (brain), individuals or populations. Finally, the ontogeny is the explanation of the developmental changes in the behavior

throughout the lifetime of an organism. A good example of ontogeny would be the changes in the behavior machinery through learning.

All animal phyla with the exception of sponges, possess a nervous system that plays a crucial role in sensing the environment and generating coordinated behavioral responses (Budd 2015). Therefore, neuroscientists often seek the short-term causality between the sensory stimuli, the nervous system and the behavioral action. This has been one of the central goals of today's neuroscience to reach a mechanistic understanding of how nervous systems implement computations that transform the sensory information into behavioral actions (sensorimotor transformations).

Complex nervous systems (some group of insects, some molluscs and vertebrates including primates) (Roth 2015) evolved multimodal centers (e.g. mushroom bodies in insects and prefrontal cortex in primates) inside the nervous system in order to coordinate various behavioral tasks ranging from foraging and spatial orientation to social learning to instrumental learning . Multiple neuronal cell types form complex connectivity patterns within and among these multimodal centers to integrate and process the sensory information and transform them into motor outputs. The nature, number and the strength of the interactions among neurons define the characteristic computations that could be carried out by the circuit of interest (Luo, Callaway et al. 2008). Therefore, it is vital to study the organization and function of these multimodal centers to understand the mechanisms underlying sensorimotor transformations. By understanding neural mechanism of behavior and the changes in these mechanisms via learning, one can reveal the short-term causality (Tinbergen 1963) between the nervous system function and the behavior.

1.2 Dissection the neural mechanisms underlying sensorimotor transformations:

The first step to understand the causal relationships underlying the sensorimotor transformation is to monitor the neural activity while the animal is generating a behavioral action in response to sensory stimuli. Neural activity is measured by quantitative methods to reveal the dynamical properties of the activity of neurons in the sensorimotor pathway. These methods include traditional electrophysiology, functional magnetic resonance imaging and optical imaging of neural activity with dyes or genetic indicators. In simple invertebrates organisms, it is possible to correlate the activity of single neurons with the sensory stimuli and the behavioral responses (Brodfuehrer and Friesen 1986). Due to the high level of numerical and morphological complexities, in vertebrates correlations are made at the level of unique cell types that are defined based on multiple criteria such as developmental history, gene expression pattern, anatomical location and cellular morphology (Luo, Callaway et al. 2008). In this case, neurons with the same cell type identity are assumed to have the same function in the neural circuit.

Traditionally, the necessity and sufficiency of neurons in the sensorimotor processing are tested in order to further understand their roles in the sensorimotor pathway. A neuron is thought to be necessary if silencing, physically ablating or killing that neuron abolishes the generation of the behavioral response that is observed in rather intact individuals. On the other hand, if acute activation of a neuron evokes a naturally occurring behavior it is considered to be sufficient for evoking that behavior. Together, necessity and sufficiency of a neuron help unravel the relative role of the neuron in the circuit. However, one should be careful

interpreting the results of the necessity and sufficiency experiments since both sensory stimuli and function of a particular neuron are highly likely to be multidimensional (Clark, Freifeld et al. 2013). That is, multiple features of the sensory stimuli might be encoded in the nervous system (e.g. intensity and the temporal profile) and; a particular neuron might affect multiple aspects of a behavioral output. For example, the necessity experiments could be biased by the sensory stimulus defined by the experimenter and; the sufficiency experiments could be biased by the acute activation pattern.

A brain-wide map of the anatomical connectivity -the connectome- would also be instructive to dissect the neuronal computations that could possibly be implemented by the neural circuits. The first ever-reconstructed connectome of C. elegans (White et al. 1986, Varshney et al. 2011) has provided a map to study the neural correlates of behavior in this tiny nematode. Although micro (synaptic-scale connectivity) (Chklovskii, Vitaladevuni et al. 2010)) meso (long and short-range connectivity revealed by anatomical tracers) (Oh, Harris et al. 2014) and macro-scale (large-distance connectivity revealed by white matter tracts) (Van Essen, Smith et al. 2013) connectomes are available, a comprehensive whole-brain map is still absent for any vertebrate brain due to their numerical complexity and vast range of connectivity. Even if such a connectome can be achieved for a mammalian brain with billions of neurons and trillions of synapses, it might be very complicated to interpret the vast amount of data.

At this point, *Drosophila* melanogaster stands out as an excellent model organism. Both Drosophila adult and the larva display a wide range of complex behaviors (Keene and Waddell 2007, Gomez-Marin, Stephens et al. 2011, von Philipsborn, Liu et al. 2011, Zhang, Yan et al. 2013,

Asahina, Watanabe et al. 2014, Bidaye, Machacek et al. 2014, Hampel, Franconville et al. 2015) and possess complex brains with modular organization reminiscent to mammals. Unlike the mammalian brain the *Drosophila* brain is significantly smaller (100.000 neurons in the adult and 10.000 neurons in the larva), thereby making it feasible to generate brain-wide connectivity maps. In addition, individual neurons can be identified by their lineage, morphology and genetic expression patterns (Ito, Masuda et al. 2013) and neuronal identities and behavioral responses are highly stereotypic among individuals (Jefferis, Marin et al. 2001, Wong, Wang et al. 2002, Wilson, Turner et al. 2004). Finally, binary expression systems provide unprecedented genetic access to individual neurons (Pfeiffer, Jenett et al. 2008, Venken, Simpson et al. 2011, von Philipsborn, Liu et al. 2011, Li, Kroll et al. 2014). Thus, assigning functions to individual neurons and microcircuits is much easier in the *Drosophila* brain compared to complex vertebrate brains (Ohyama, Schneider-Mizell et al. 2015).

On top of the already existing genetic tools to access, manipulate and monitor the neurons (Venken, Simpson et al. 2011, Owald, Lin et al. 2015), recent efforts to reconstruct the whole-brain connectome using transmission electron microscopy data transformed the *Drosophila* larva into a model organism with which one can advance towards a brain-wide functional mapping based on the characterization of the function of individual neurons (Ohyama, Schneider-Mizell et al. 2015, Berck, Khandelwal et al. 2016, Zwart, Pulver et al. 2016). In the future, iterations through behavioral quantification, anatomical connectivity, functional analysis and mathematical modeling will contribute to our knowledge of how neural circuits perform computations underlying complex behaviors in the Drosophila larva. High level of evolutionary conservation in neural circuits (Katz and Harris-Warrick 1999) and computational principles

(Kay and Stopfer 2006) will hopefully allow generalization of these findings to higher organisms including humans.

Here, we will study the neural circuits underlying the olfactory behavior of the *Drosophila* larva for the following reasons: First, *Drosophila* larvae exhibit robust chemotaxis in odor gradients that can be quantitatively studied in laboratory conditions (Gomez-Marin, Stephens et al. 2011, Gershow, Berck et al. 2012). Second, anatomical organizations of first, second and third-order neurons are well characterized (Masuda-Nakagawa, Tanaka et al. 2005, Vosshall and Stocker 2007, Masuda-Nakagawa, Gendre et al. 2009, Masuda-Nakagawa, Awasaki et al. 2010, Das, Gupta et al. 2013, Berck, Khandelwal et al. 2016). Third, Drosophila olfactory system comprises only 21 olfactory sensory neurons (OSNs) of which response characteristics are known (Fishilevich, Domingos et al. 2005, Kreher, Kwon et al. 2005, Kreher, Mathew et al. 2008, Mathew, Martelli et al. 2013). Fourth, there exist quantitative models that can predict the transformations from olfactory stimulus to OSN activity to the probability of behavioral transitions (Gepner, Mihovilovic Skanata et al. 2015, Hernandez-Nunez, Belina et al. 2015, Schulze, Gomez-Marin et al. 2015). Although there is much more to learn about primary layers of olfactory processing, we have enough knowledge about them to guide us into the circuits that perform the sensory-motor transformations at higher levels in the larval brain.

1.3 Overview of the *Drosophila* larval nervous system:

Drosophila larval brain is composed of ganglia: While cell bodies of neurons and glial cells reside in the outer layer of the ganglia, the axonal and dendritic branches- together with the synapses among them- form the

inner layer. These axonal and dentritic branches are organized into neuropile compartments and these compartments are connected via long axonal bundles. Inside the neuropile, glial septa separate the neuropile into several anatomically distinct compartments (Younossi-Hartenstein, Salvaterra et al. 2003).

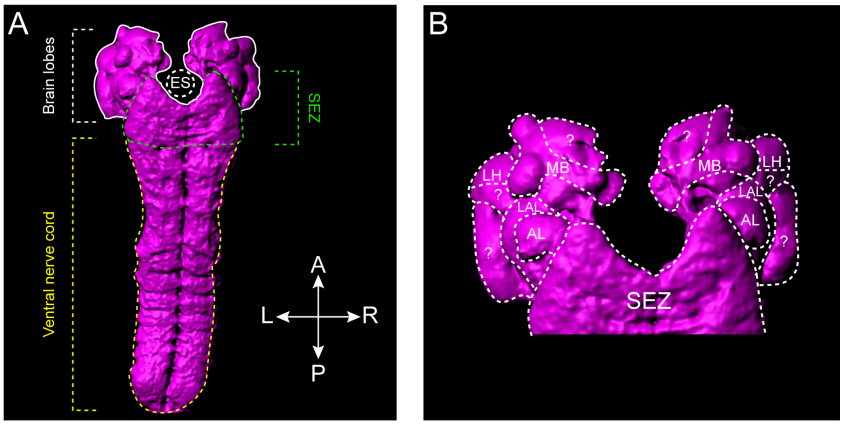

Figure 1.1: The central nervous system of the Drosophila larva A: The three main compartments of the larval CNS: the brain lobes (delineated by white dashed lines), ventral nerve cord (delineated by yellow dashed lines) and the subesophageal zone (SEZ, delineated by the green dashed lines). ES: esophagus (white dashed circle). A: anterior, P: posterior, L: left, R: right. **B:** A coarse representation of the neuropile compartments of the brain lobes. Each compartment is specialized in a particular function in sensorimotor processing. MB: mushroom body, LAL: lateral accessory lobe, LH: lateral horn, SEZ: subesophageal zone. The question marks indicate the neuropiles to which a function is not assigned yet. LAL, LH and SEZ are also not well characterized in the larva.

Like most of the Bilateria, the *Drosophila* larva has a bilateral central nervous system (CNS) that extends in the anterior-posterior axis (neuraxis). The anterior part is specialized into brain lobes (supraesophageal ganglion) and the posterior part forms a segmental

ganglia (ventral nerve cord, VNC) (Figure 1.1A). Between these two main ganglia is the subesophageal zone (SEZ), which is characterized as fused ganglia in the fly brain. The brain lobes (BLs) can be divided into three main compartments by the glial septa: Dorsal, central and basal neuropiles (Younossi-Hartenstein, Salvaterra et al. 2003). Anatomical and functional studies led to the discovery of functionally specialized neuropile compartments in both adult and larval *Drosophila* brain lobes (Figure 1.1B). The optic lobes, as the name implies, receive visual input from photoreceptor neurons in the Bolwig's organ (Sprecher, Cardona et al. 2011). It has been shown that the antennal lobe (AL), a basal neuropile, is the first layer of olfactory processing (Gerber and Stocker 2007). The mushroom body- a promiment neuropile with lobular structure- is a multi-sensory hub, which is known to be involved in multisensory integration, context-dependent decision making, learning and memory (Gerber and Stocker 2007, Hong, Bang et al. 2008, Vogt, Schnaitmann et al. 2014, Lewis, Siju et al. 2015, Rohwedder, Wenz et al. 2016). The subesophageal zone has been shown to be the primary taste center in the larval brain (Colomb, Grillenzoni et al. 2007, Kwon, Dahanukar et al. 2011) and it contains the central pattern generators (CPGs) underlying feeding behavior (Hückesfeld, Schoofs et al. 2015). Moreover, recent studies suggest that the SEZ is involved in locomotion and reorientation behavior in the larva (Lemon, Pulver et al. 2015, Pulver, Bayley et al. 2015, Tastekin, Riedl et al. 2015). The VNC is specialized in motor pattern generation. It contains central pattern generators that play role in forward and backward locomotion as well as turning behavior (Berni, Pulver et al. 2012, Berni 2015, Pulver, Bayley et al. 2015, Fushiki, Zwart et al. 2016). While the ventral side of the VNC receives sensory afferents from nociceptive and proprioceptive neurons, the dendrites of motor neurons arborize the dorsal VNC (Zlatic, Li et al. 2009, Kohsaka, Okusawa et al. 2012). Despite the substantial amount of studies on these specialized

neuropiles, there is still much to learn about the function of other neuropile compartments (Younossi-Hartenstein, Salvaterra et al. 2003) and how they are coordinated. For example, regions like the lateral horn (involved in innate olfaction, see below) and the lateral accessory lobe (involved in descending control of locomotion) (Namiki and Kanzaki 2016) are poorly characterized in the larva (Figure 1.1B).

1.4 Olfactory system of the *Drosophila* larva:

1.4.1 Peripheral organization of the larval olfactory system:

At the sensory level, the *Drosophila* larval olfactory system is a very compact system with only 21 OSNs and 25 odorant receptors (ORs). Each OSN expresses only one or two ORs together with the atypical coreceptor *Orco* (Fishilevich, Domingos et al. 2005, Kreher, Kwon et al. 2005). Dendritic arbors of OSNs innervate the 'dome' of the dorsal organ where they contact the external environment (Gerber and Stocker 2007).

By using 26 diverse odorants, Kreher et al. have shown that larval olfactory system comes with a wide range of odor response spectra (Kreher, Mathew et al. 2008): At low concentration (10^{-4} dilution) each of the ORs tested were very narrowly tuned, strongly excited by only one or two chemically related odors. At high concentration (10^{-2} dilution), however, some ORs strongly responded to a broad range of odors while at the other extreme, some ORs responded to only one odor (e.g. Or82a) or did not respond to any of the odors tested. They have observed that a single odor can be detected by several ORs (1-hexanol) or only one OR (geranyl acetate). In one particular case, they have observed that ethyl acetate can be detected by Or42a and Or42b, which respond to this odor

strongly at high and low concentrations, respectively. By constructing an odor space based on receptor activity, they suggested that odors that are closer in the odor-response space are more likely to mask each other (Boyle and Cobb 2005); therefore it is harder for the larva to discriminate between them. This might be either due to cross-adaptation or similar firing rates elicited by similar odors, which cannot be resolved by the system. However, they have neither studied the temporal profile of OSN responses nor the transformations that take place in the antennal lobe and higher brain centers. These two might potentially explain the exceptions to the relationship between the discriminative power and the distance in the odor space. Altogether, the combinatorial aspect of OSN responses (i.e. one OSN can respond to multiple odors and one odor can be detected by multiple OSNs) might help the larva broaden its dynamic range of odor sensitivity together with efficient assessment of concentration.

Interestingly, it has been shown that a few receptors, even a single functional receptor, are able to largely reproduce the behavioral phenotype exhibited with fully functional olfactory system (Fishilevich, Domingos et al. 2005, Kreher, Mathew et al. 2008, Louis, Huber et al. 2008, Asahina, Louis et al. 2009). On the other hand, Asahina et al. (2009) have shown that larvae with one or two receptors were not able to locate an attractive odor source efficiently in a wide range of concentrations while wild type larvae were invariantly attracted to the some odor across 500-fold range of concentrations. Again, this finding suggests that the combinatorial code implemented by multiple channels improve the dynamical range of sensitivity to a particular odor.

The fact that the larva can efficiently respond to an attractive odor source with only a single functional OSN suggest that the mechanisms of odor detection can be studied at single OSN level. Indeed, by using a single

functional OSN recent study in our lab has shown that OSN detects the first derivative of odor concentration together with its temporal profile (Schulze, Gomez-Marin et al. 2015). The fact that OSN is sensitive to the derivative of odor concentration enables the larva to modulate the probability of reorientation maneuvers in response to negative and positive changes in the odor concentration (see below for explanation).

1.4.2 Primary relay station of the larval olfactory system: the antennal lobe:

OSN axon terminals terminate in a specialized region called the antennal lobe (AL). In the AL OSNs mainly synapse onto two types of neurons: projection neurons (PNs) and local interneurons (LNs). PNs connect the AL to higher olfactory centers in the brain lobes, namely the mushroom body (MB) and the lateral horn (LH). The AL consists of morphological subunits called 'glomeruli'. These glomeruli are easily visualized by using neuropile markers (Python and Stocker 2002). The axon terminals of each OSN target only one glomerulus in the AL (Ramaekers, Magnenat et al. 2005, Masuda-Nakagawa, Gendre et al. 2009) creating 21-dimensions odor space. Likewise, each glomerulus is innervated by a single uniglomerular PN (uPN), which extends its dendritic branches exclusively to that particular glomerulus. Anatomical studies revealed the presence of multiglomerular PNs (mPNs) that receive input from multiple glomeruli as well as PNs that connect the AL to the subesophageal zone (Marin, Watts et al. 2005, Das, Gupta et al. 2013, Berck, Khandelwal et al. 2016). There are 14 mPNs and they mainly innervate the lateral horn and the neuropile around the MB calyx (Berck, Khandelwal et al. 2016).

In the adult *Drosophila*, PNs have been shown to encode OSN firing rate as well as acceleration of odor concentrations (Kim, Lazar et al. 2015).

However, adult and larva live in very different environments characterized by distinct statistical properties of their olfactory stimuli. For a flying *Drosophila*, turbulence is the main factor that determines the distribution of odor molecules. Under turbulent conditions, detecting acceleration as well as odor onset and offset might be the most efficient way to monitor the odor plumes for the adult fly (van Breugel and Dickinson 2014). On the other hand, diffusion is the main factor that defines the odor distribution for the crawling larva. In this case, detecting changes in odor concentration is sufficient to locate the odor source. Therefore, larval PNs might have evolved a different strategy. Early studies of PN activity in the larval olfactory system using calcium indicators are not sufficient to reveal the PN response characteristics (Asahina, Louis et al. 2009).

Lateral connections among glomeruli are mediated by the LNs in the antennal lobe. Immunostaining for neurotransmitters has shown that these local interneurons mainly express γ–aminobutyric acid (GABA), which is known to have inhibitory effects (Python and Stocker 2002). Electron microscopy reconstruction of the entire antennal lobe of the larva identified five panglomerular inhibitory LNs (Berck, Khandelwal et al. 2016). There is yet another type of LNs that receive input from only a small subset of glomeruli while inhibiting most of the glomeruli. In addition, these two LN types differ in their sites of synapses (pre-synaptic, proximal or distal post-synaptic), adding more complexity to the computations that can be performed by these inhibitory circuits. There is yet another type of LNs, which mainly target the mPNs, express glutamate instead of GABA and together tile the whole antennal lobe (Berck, Khandelwal et al. 2016). Considering the inhibitory role of glutamate in the adult *Drosophila,* these LNs are most likely to mediate inhibition in the larva as well.

What are the functional implications of panglomerular lateral inhibition in the antennal lobe? In adult flies it has been shown that lateral inhibition increases the dynamic range of PN responses through a gain-control mechanism (Wilson 2013). In addition, delayed inhibition following the activation of PNs would lead to a transient response in PNs at early OSN firing onset, potentially allowing rapid perception (Olsen and Wilson 2008, Olsen, Bhandawat et al. 2010). It has been observed that gain control is also implemented in the larval antennal lobe and it is important for obtaining a broad dynamic range (Asahina, Louis et al. 2009). Despite the thorough anatomical mapping of the larval antennal lobe, functional logic of the panglomerular lateral inhibition in the ORN-PN-LN network is still to be unraveled.

The overall AL connectivity suggests that larva might switch between panglomerular and selective glomerular inhibition. Panglomerular inhibition might be important for the system to operate in wide range of odor concentrations while the larva is approaching an attractive odor source (Asahina, Louis et al. 2009). As soon as the larva reaches the odor source (i.e. a food patch), panglomerular inhibition by strong odors might lead to undesirable inhibition of relevant but low-activity glomeruli (e.g. predator pheromones). Interestingly, selective glomerular inhibition seems to be able to suppress the panglomerular inhibition (Berck, Khandelwal et al. 2016). While the larva is feeding in the odor-rich food source, selective inhibition might render the larva sensitive to faintly active but functionally relevant glomeruli (i.e. glomeruli that receives predator pheromone cues) (Ebrahim, Dweck et al. 2015) by inhibiting panglomerular inhibition as well selective appetitive glomeruli.

1.4.3 Higher olfactory centers of the larval brain: the mushroom body and the lateral horn:

Projection neurons relay the olfactory information chiefly into two regions in the larval brain, the mushroom body (MB) and the lateral horn (LH). Developmentally, four MB neuroblasts give rise to ~300 embryonic-born Kenyon cells (KCs) that form the structures called calyx, peduncle, vertical and medial lobes (Kunz, Kraft et al. 2012). Larval PNs synapse onto the dendrites of these KCs in the calyx. Kenyon cell axons extend through the peduncle to form the vertical and medial lobes. In the MB lobes KC axon terminals synapse with other mushroom body intrinsic neurons (Rohwedder, Wenz et al. 2016) and mushroom body extrinsic neuron, the output neurons of the MB (Keene and Waddell 2007, Pauls, Selcho et al. 2010). Unlike the MB, the synaptic partners of PNs in the LH are not well characterized in the larva.

The MB has been involved in associative learning and memory formation in the larva as well as in the adult (Keene and Waddell 2007, Pauls, Selcho et al. 2010, Aso, Hattori et al. 2014). By using an intricate circuitry of neuromodulators (e.g. dopamine, octopamine, neuropeptide F etc.) (Aso, Hattori et al. 2014), the MB also regulate sleep (Sitaraman, Aso et al. 2015), thirst (Lin, Owald et al. 2014) and monitors internal states to regulate memory expression (Krashes, DasGupta et al. 2009). At the level of the calyx, Masuda-Nakagawa et al. identified 34 glomeruli (Masuda-Nakagawa, Tanaka et al. 2005). At least 23 of these glomeruli are innervated by uniglomerular PNs (Masuda-Nakagawa, Tanaka et al. 2005, Ramaekers, Magnenat et al. 2005). Each PN innervate one or two glomeruli in the MB calyx (Marin, Watts et al. 2005). In addition, an individual KC innervates ~6 glomeruli with claw like dendritic structures

(Masuda-Nakagawa, Tanaka et al. 2005). KCs that innervate the same glomerulus can have other synapses in different subsets of glomeruli. This non-stereotypic innervation pattern suggests that information from a single PN might be relayed to different KCs and KCs integrate over multiple PNs. Later, it has been shown that most AL glomeruli are stereotypically connected to MB calyx glomeruli with PN projections in one-to-one manner (Masuda-Nakagawa, Gendre et al. 2009). Physiological assessment of odor responses revealed that each AL glomerulus activate 1-3 MB calyx glomeruli (Masuda-Nakagawa, Gendre et al. 2009). The fact that KCs randomly sample from widely dispersed set of multiple MB calyx glomeruli (divergence) is considered to be the basis of memory capacity (Gerber and Stocker 2007, Keene and Waddell 2007).

A recent study argues that a subset of *odd*-expressing neurons (odd neurons) in the larval brain is involved in innate chemotaxis (Slater, Levy et al. 2015). Light microscopy suggests that these neurons have dendritic arborizations in the MB calyx and that they receive input from PNs and KCs in this region. Calcium imaging shows that odd neurons respond to odors. By performing behavioral experiments upon losses and gains of function, Slater et al. concluded that odd neurons are part of a neural circuit responsible for increasing odor sensitivity at low odor concentrations. This is an important illustration that MB can also take part in the regulation of innate chemotaxis in addition to its role in learning and memory. Indeed, there is growing evidence in the adult fly suggesting that MB is involved in context-dependent regulation of odor sensitivity (Bracker, Siju et al. 2013, Cohn, Morantte et al. 2015, Lewis, Siju et al. 2015, Owald, Felsenberg et al. 2015).

Our knowledge on the LH mainly comes from the adult *Drosophila* and other insects (Kido and Ito 2002, Jefferis, Potter et al. 2007, Gupta and

Stopfer 2012, Strutz, Soelter et al. 2014). The fact that ablation of the MB did not lead to gross defects in innate behavior led to the conclusion that the LH is involved in innate olfactory behavior (de Belle and Heisenberg 1994, Kido and Ito 2002). The topographical logic of the AL is conserved in the LH; PN axons from the same AL glomeruli converge onto stereotyped, overlapping regions in the LH (Marin, Jefferis et al. 2002, Wong, Wang et al. 2002). Jefferis et al. have shown that representation of fruity odors is restricted to dorsal and posterior LH with no considerable difference for different odors (Jefferis, Potter et al. 2007) suggesting that perception of different fruity odors is largely similar. Then, they tested pure odors and concluded that representation for pure odors can be distinguishable since they activate restricted regions in the LH.

It has also been shown that LH neurons (third order neurons downstream of PNs) arborize in distinct regions of the LH and are able to integrate across multiple PN outputs (Tanaka, Awasaki et al. 2004, Jefferis, Potter et al. 2007). This observation is further corroborated by electrophysiological studies (Fisek and Wilson 2014). Last but not the least, Strutz et al. have shown that distinct odors trigger stereotypic calcium responses in specific region of LH in a concentration dependent manner (Strutz, Soelter et al. 2014). Interestingly, they have shown that odor evoked activity in the LH for attractive odors and a repellent (benzaldehyde) are completely nonoverlapping. The stereotyped branching pattern in the LH and segregation according to odor valence is compatible with the proposed role in the innate olfactory behavior.

While it was traditionally believed that the LH is involved in innate olfaction while the MB is the center for learning and memory, this view is now changing. It is more likely that the LH and the MB form a complex network of feedback loops designed to robustly shape odor sensitivity

depending on environmental conditions and motivational states (e.g. hunger, mating etc.). Elucidating the LH-MB 'connectome' accompanied with functional characterization of this network will unravel the logic of olfactory sensory processing taking place in the *Drosophila* brain. Connecting these regions to motor pattern generators in the VNC will help us understand how sensory percepts are converted into behavioral actions. The larva – with the whole central nervous system soon to be reconstructed and its extensive genetic toolkit to manipulate neural function– will serve as an excellent model organism to study sensorimotor transformations in a complex but tractable brain.

1.5 *Drosophila* larval locomotion:

Drosophila larval locomotion mainly comprises bouts of forward movement (runs) that are separated by short periods of pauses followed by head sweeps and changing the direction of movement via turns (Figure 1.2A).

Runs are accomplished by periodically repeated strides, which could be observed in two consecutive phases (Heckscher, Lockery et al. 2012). The first phase –visceral pistoning- comprises forward movement of head, guts and the tail shifting the centroid of the larva forward. In the second phase (wave phase), the head and tail are anchored in the substrate and the abdominal segments contract in a wave like pattern from tail (posterior end) to head (anterior end). Coordinated action of these phases brings about the forward locomotion. Analysis of muscle contractions showed that dorsal and ventral muscles in a particular segment contract simultaneously with the lateral muscles in the segment posterior to it.

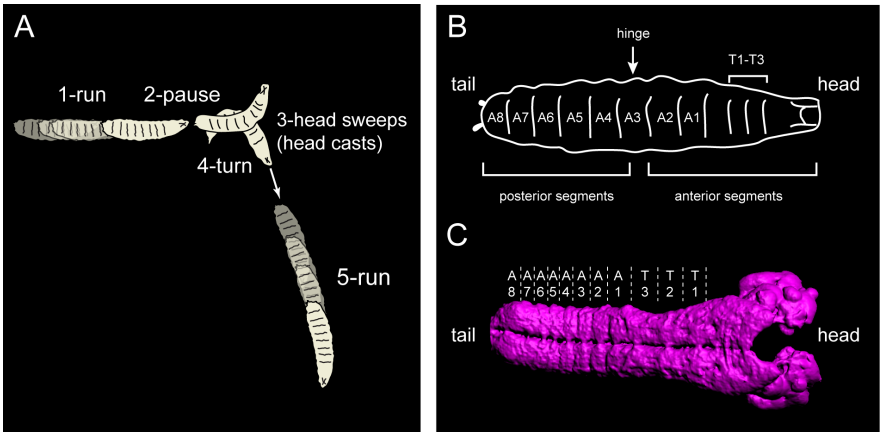

Figure 1.2: *Drosophila* larval locomotion A: The larval locomotion comprises the alternation between the runs, pauses, head casts and turns. **B:** The segmental organization of the larval body wall muscles. During the wave phase of forward locomotion, symmetrical contractions across the abdominal segments (A8 to A1) move the body forward. During head casts and turns the anterior segments (A2 to T1) contract asymmetrically. T1-3: thoracic segments. **C:** The segmental organization holds true for the central nervous system. Symmetrical motor neuron activity from A8 to A1 brings about the forward locomotion. Asymmetrical motor neuron activity from A2-T1 leads to head casts and turns.

Head sweeps (head casts) and turns are generated by breaking the symmetry of contraction in the left and the right segments in the anterior segments (Figure 1.2B). Contracting one side of the body while relaxing the other leads to asymmetric contraction. Reciprocal inhibition across the midline might mediate this asymmetry. Indeed, genetic mutants aberrant in midline crossing have revealed that asymmetry in the contraction of the left and the right segments are due to asymmetric neural activity in the thoracic segments (Berni 2015).

During forward locomotion, the motor neurons tiling the anterior-posterior axis of the larva also show wave like activity, thanks to the myotopic map between the motor neurons and the body wall muscles:

Dendritic arborizations of the motor neurons are organized into distinct domains in the VNC such that dendritic fields of the motor neurons form a myotopic map with the muscles in the body wall (Kohsaka, Okusawa et al. 2012). That is, motor neurons innervating different muscle groups have distinct dendritic arborizations in the anterior-posterior and medio-lateral axis (Landgraf, Jeffrey et al. 2003). Fictive locomotion can be observed as wave-like motor neuron activity in isolated larval central nervous system (CNS) (Berni 2015, Lemon, Pulver et al. 2015, Pulver, Bayley et al. 2015), suggesting the presence of central pattern generators (CPGs) for forward locomotion in the larval CNS (Marder and Calabrese 1996). By silencing neural activity in the brain and the subesophageal zone, Berni et al. have shown that neural substrate for generating runs and turns reside in the thoracic and abdominal ganglia of the VNC (Berni, Pulver et al. 2012). Descending inputs from the brain lobes and the SEZ are very likely to modify the temporal dynamics of motor patterns in the VNC upon sensory experience (Lemon, Pulver et al. 2015, Pulver, Bayley et al. 2015) (see Chapter 3 and 4).

Optogenetic dissection of wave propagation in the motor neurons led to several important findings (Inada, Kohsaka et al. 2011). Transient inhibition of motor neurons at the wave forefront results in relaxation of all body muscles along the anterior-posterior axis. However as soon as the inhibition is removed, the wave is re-initiated at the same segment where it was halted at the onset of the inhibition. This finding suggests that motor neurons do not only read the output of the CPGs, but that they are also involved in the pattern generation: If motor neurons were sole output neurons, inhibition of motor neurons in a particular segment would not affect the firing of the motor neurons ahead since CPG would independently generate the wave-like pattern. Moreover, these findings

imply that information about the phase of the wave propagation can be memorized in the system.

Recently, it has been proposed that a neural mechanism of alternating excitation and inhibition along the abdominal ganglia may account for the wave propagation underlying larval locomotion (Fushiki, Zwart et al. 2016). An excitatory, segmentally repeated premotor neuron (a27h) activate both motor neurons in the same segment and an inhibitory neuron in the subsequent anterior segment leading to muscle contraction in a particular segment while inducing relaxation of muscles in the next anterior segment. In this way, contraction in a particular segment induces the relaxation of the adjacent anterior segment and termination of contraction in a segment is coupled with the contraction in the next anterior segment. Anatomical reconstruction of a27h neurons revealed that they receive sensory feedback and descending input from the SEZ corroborating the observation that locomotion is modulated by the SEZ (see chapter 4).

1.6 Sensorimotor features of larval chemotaxis:

Drosophila larval chemotaxis relies on the alternation of runs, pauses and turns in a sensory experience-driven manner. Same type of organization is also observed in phototaxis and thermotaxis (Lahiri, Shen et al. 2011, Kane, Gershow et al. 2013). The probability of terminating a run is modulated by temporal changes in stimulus intensity (Gomez-Marin, Stephens et al. 2011, Gershow, Berck et al. 2012, Gepner, Mihovilovic Skanata et al. 2015, Hernandez-Nunez, Belina et al. 2015, Schulze, Gomez-Marin et al. 2015). For attractive olfactory stimuli, down-gradient runs are more likely to be ceased compared to up-gradient runs (Gomez-

Marin, Stephens et al. 2011, Gershow, Berck et al. 2012). The larva does not respond to decrease in odor concentration immediately. Instead, it seems that the larva integrates changes in stimulus intensity over time to induce transition from runs to turns (Gomez-Marin, Stephens et al. 2011). Although it has been shown that OSN is sensitive to derivative of the stimulus intensity (Schulze, Gomez-Marin et al. 2015) the site/s of integration in the larval brain remains unknown. It has been shown that the probability of terminating a run can be predicted with a generalized linear (Schulze, Gomez-Marin et al. 2015) model dependent on OSN activity or linear-nonlinear models (Gepner, Mihovilovic Skanata et al. 2015, Hernandez-Nunez, Belina et al. 2015), which are dependent on sensory experience: High OSN (increase in stimulus intensity) activity suppresses probability of interrupting runs while low OSN activity (decrease in stimulus intensity) induce termination of runs.

Runs are terminated by a short period of pause followed by lateral head sweeps (head casts). It has been suggested that head casts serve as a sampling mechanism, during which the larva monitor its environment to detect favorable direction of stimulus intensity (Gomez-Marin and Louis 2012). Indeed, the direction of the movement is often realigned by inducing turns towards favorable conditions following head casts (Gomez-Marin, Stephens et al. 2011).

Drosophila larva employs yet another strategy to improve chemotaxis. The so-called 'weathervaning' strategy relies on shallow reorientation of the direction of the runs (that is, without terminating the run) towards the favorable conditions (Gomez-Marin and Louis 2014). Gradual curling of the run direction in average depends on the strength of the local odor gradient vector perpendicular to the direction of movement. It has been argued that small amplitude head casts during runs provide a temporal

comparison mechanism that helps direct the runs towards an attractive odor source without interrupting them.

A recent computational model (Davies, Louis et al. 2015) has tested sufficiency of the qualitative model that larval chemotaxis is controlled by the sensorimotor mechanisms explained above (run-to-turn transitions, sampling via head casts, turning towards favorable conditions and weathervaning). By implementing probabilities as a function of sensory history, Davies et al. were able to reproduce behavioral statistics of real larva with an agent model. In the future, this elementary model can be improved by using OSN activity instead of sensory history (Schulze, Gomez-Marin et al. 2015). Modelling will be particularly useful to robustly test hypothesis when they are combined with experimental circuit-cracking efforts.

Temporal dynamics of sensory experience during sampling through head casts (sub second) is much faster compared to sensory dynamics in course of runs (several seconds). Perhaps that is why the phenomenon of 'active' sampling with head casts is understudied at the sensory level compared to substantial amount of knowledge about sensory determinants of run-to-turn transitions.

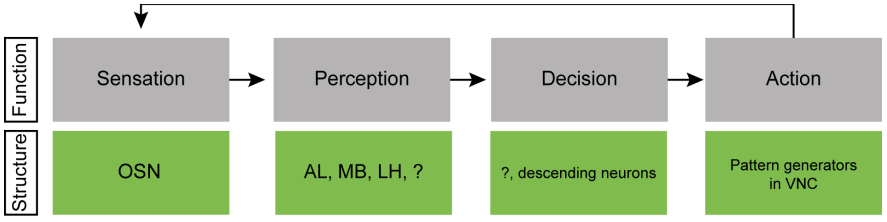

Figure 1.3: The sensorimotor loop of larval chemotaxis divided into 4 main processes The structures that are (potentially) involved in each process (function) were indicated.

Despite of the knowledge on the peripheral encoding of temporal changes in the olfactory stimuli, we still lack the identity and computations of the higher brain circuits that are involved in sensorimotor control of run-to-turn transition. In order to systematically study the sensorimotor pathway underlying larval chemotaxis we decided to divide it into four basic levels (Figure 1.3): (1) the neural circuits that sense the environment and performs the first level of sensory processing (e.g. OSNs and the antennal lobe circuitry); (2) that form a perception (e.g. going away from desired conditions) by integrating the temporal changes in olfactory stimuli together with information from other sensory modalities and internal states; (3) that implement a decision (stop running) according to the perception and convey the decision to the motor pattern generators and; (4) that execute the behavioral action (motor pattern generators). Although it might be an oversimplification of what is actually happening in the larval central nervous system, this pragmatic framework helped us dissect the functional organization of the sensorimotor transformations underlying larval chemotaxis.

1.7 Aim of this study:

The principle goal of this study is to contribute to our understanding of how a complex nervous system (Roth 2015) integrates sensory information, construct percepts and transform them into behavioral actions. It has to be stated that attempting to obtain a holistic explanation of how and why a particular behavior emerged is an ambitious endeavor (Tinbergen 1963, Taborsky and Hauber 2014), which is out of the scope of this thesis work. We rather sought causal relationships between behavioral actions (runs, pauses, head casts and turns) and neural circuit

mechanisms generating them. In other words, we aimed to understand the neural correlates of the sensorimotor transformations underlying complex behavioral decisions. In this challenge, we opted for studying the case of *Drosophila* larval chemotaxis for several reasons. First, there exist unprecedented genetic tools to manipulate neural activity in *Drosophila*. Single neurons can be morphologically characterized and rendered accessible to be silenced or activated while behavior is observed (Simpson 2009, Venken, Simpson et al. 2011, Li, Kroll et al. 2014, Nern, Pfeiffer et al. 2015, Ohyama, Schneider-Mizell et al. 2015). Second, *Drosophila* larva exhibits robust stereotypic chemotaxis behavior in simple two-dimensional laboratory assays (Gomez-Marin and Louis 2012). Third, the larva provides a very simple olfactory system with only 21 OSNs and a tractable brain with only 10,000 neurons. Fourth, peripheral olfactory and motor circuits are well characterized, making it easier to study high-order sensorimotor circuits in the brain. Finally, electron microscopy reconstruction of the whole larval nervous system makes the larva an excellent model to systematically study the neural correlates of behavior from the activity of the primary olfactory neurons to patterned activity of the motor neurons.

As a general strategy, we first assumed that the sensorimotor pathway underlying larval chemotaxis could be studied at four hierarchically organized functional levels: sensation, perception, decision and action (Figure 1.3). Then, based on our knowledge on the *Drosophila* and other insects, we tried to assign brain regions that could be involved in each of these levels. We hypothesized that multi-sensory integration and perception would take place in the mushroom body and the lateral horn since it was shown that they receive and integrate input from multiple sensory modalities (Vogt, Schnaitmann et al. 2014, Cohn, Morantte et al. 2015). Likewise, we hypothesized that neurons that receive input from the

brain lobes and output in the ventral nerve cord (descending neurons) would be the command neurons that convey the decision to the motor pattern generators in the VNC.

After the coarse matching of functions to potential brain regions we decided to identify neurons in these regions that that participate in the control of larval chemotaxis. For this purpose, we carried out two independent loss-of-function screens in which we silenced subsets of neurons and tested the chemotactic performances of the larvae. Because we wanted to bridge the gap between sensation and motor action we further biased our search toward the neurons that are potentially involved in high-level sensory integration and action selection as well as the neurons that are likely to establish the communication between the brain lobes and the ventral nerve cord.

In the **first chapter** of this thesis, we explained our motivation behind studying the neural correlates of larval chemotaxis and gave a brief overview of the literature on the anatomy and the function of the larval olfactory system. In the **second chapter**, we discussed the recent tools to manipulate neural function in the *Drosophila* larva. Then, in **the third and the fourth chapters** we presented the two independent loss-of-function (LOF) screens that we performed in order to identify neurons involved in run-to-turn transitions. In **the third chapter**, we showed the results of the first LOF screen: we argued a multi-modal region in the larval brain that is important for regulating run-to-turn transitions for chemotaxis, phototaxis and thermotaxis. **The fourth chapter** was dedicated to the results of the latest LOF screen we performed: we identified and characterized a descending neuron that is specifically involved in terminating runs. By combining our functional analysis with EM reconstruction, we were able to identify a sensorimotor pathway that

connects sensation, perception, action selection and motor pattern actuation. Altogether, we made significant progress towards our goals of finding causal relationships between neural function and behavioral control of larval chemotaxis.

CHAPTER 2: Manipulation of neural activity in the *Drosophila* larva

2.1 Introduction:

The *Drosophila* larva is premier model organism to delineate computational principles underlying how neural circuits transform sensory inputs into stereotyped behaviors (see elsewhere in this book). Traditionally, neuroscientists study circuit computation by breaking neural circuits down into their core components — individual neurons (invertebrates) or neuronal cell types (vertebrates)— and by testing the necessity and sufficiency of individual neurons to execute a behavior. The combination of community based reconstruction of the whole larval brain connectivity based on light and electron microscopy (Li, Kroll et al. 2014, Schneider-Mizell, Gerhard et al. 2016) and the presence of sophisticated genetic tools makes the larva particularly suited to progress from 'circuit mapping' to a holistic 'circuit cracking' (Olsen and Wilson 2008). The larva combines other advantages for circuit cracking: the larva has a small heat capacity facilitating thermogenetic manipulations. It is mostly transparent, which is convenient for optogenetic gain-of-function experiments and live imaging. The larva displays stereotyped behaviors on a timescale considerably slower than adult flies (Green, Burnet et al. 1983). In addition, foraging in the larva can be studied on two-dimensional substrates as basic as an agarose slab instead of complex tri-dimensional environments. As a result, tracking naturalistic behaviors is technically simpler in the larva than in the adult fly.

While the numerical complexity of the nervous system of the larva is reduced by one order of a magnitude compared to its the adult fly counterpart (10,000 versus 100,000 neurons), the *Drosophila* larva exhibits sensory-driven reorientation maneuvers in chemical, light and temperature gradients as well as robust escape behaviors in response to

threatening stimuli (Hwang, Zhong et al. 2007, Luo, Gershow et al. 2010, Kane, Gershow et al. 2013, Zhang, Yan et al. 2013, Ebrahim, Dweck et al. 2015). The larva is also capable of forming and retrieving associative memory (Gerber and Stocker 2007). The control of reorientation behavior is plastic: it can be modulated by memory traces (Schleyer, Reid et al. 2015). Genetic tools provide access to visualize and manipulate the function of small groups or even individual neurons. These tools can be efficiently combined with electron microscopy (EM) reconstruction of the entire larval brain to build circuit-level connectivity diagrams (Ohyama, Schneider-Mizell et al. 2015, Schneider-Mizell, Gerhard et al. 2016, Zwart, Pulver et al. 2016). One can perform 'circuit epistasis' by hierarchically manipulating different cell types revealed by EM connectivity diagrams (Ohyama, Schneider-Mizell et al. 2015). Altogether, recent advances in the field of larval neurobiology have created unprecedented opportunities to unravel the operation of neural circuits and to test mechanistic hypothesis with a spatio-temporal resolution that will soon match the standards in *C. elegans*.

The main objective of this book chapter is to review current genetic tools to manipulate neural functions in the *Drosophila* larva. First, we will draw the attention of the reader on the promises and the limitations of existing tools to study the function of individual neurons. Second, we will discuss on the importance of quantifying behavior to search for the neural correlates of sensorimotor functions (Egnor and Branson 2016). Third, we will discuss clonal gain-of-function strategies to dissect the contribution of distinct groups of neurons labeled by a driver line associated with a phenotype of interest. This method is intended to make the most out of driver lines with expression patterns that cover more than a couple of neurons — a problem that Drosophilists frequently face when they analyze the neural mechanisms underlying the organization of behavior.

2.2 Genetic targeting of neurons in the *Drosophila* larva:

In *Drosophila,* high stereotypy of morphology and connectivity of individual cell types allow the analysis of neural function at a population level. Transgenic expression of reporters and/or effectors in specific subsets of neurons via binary expression systems has been widely used to visualize and to functionally manipulate specific neurons (Venken, Simpson et al. 2011). Recently, two large collections of Gal4 driver lines (Pfeiffer, Jenett et al. 2008, Bidaye, Machacek et al. 2014) have been created and made accessible to the fly community to label specific subsets of neurons in *Drosophila* brain. Despite the fact that these driver lines label relatively small number of neurons compared to their predecessors (e.g., the so-called Kyoto collection), anatomical and behavioral experiments often necessitate targeting smaller subsets of neurons — ideally single neurons. Stochastic labeling methods such as flip-out, MARCM (Venken, Simpson et al. 2011) and multicolor flip-out (MCFO) (Nern, Pfeiffer et al. 2015) have been used to characterize the morphology of single neurons using Gal4 driver lines. For behavioral studies, intersectional expression combining Gal4, Gal80, LexA expression systems and Split-Gal4 technique (Luan, Peabody et al. 2006, Pfeiffer, Ngo et al. 2010) are now routinely used to restrict expression to pre-defined subsets of neurons (Aso, Hattori et al. 2014, Hampel, Franconville et al. 2015, Ohyama, Schneider-Mizell et al. 2015). However, these intersectional techniques are limited by the existence of driver lines with overlapping expression patterns. In the following sections, we will describe how driver lines with expression patterns including more than one cell can be exploited to draw hypothesis about the link between connectivity and function in specific neurons.

2.3 Inferring function by manipulating the activity of genetically labeled neurons:

Traditionally, behavioral experiments are conducted to test the necessity or sufficiency of neurons to execute a certain type of behavior in *Drosophila* (Vogelstein, Park et al. 2014, Tastekin, Riedl et al. 2015). In many cases, the necessity of a neuron to control a given function is probed by (i) hyperpolarizing the neuron upon over-expression of the inward-rectifier potassium ion channel Kir2.1 (Baines, Uhler et al. 2001) or by (ii) blocking synaptic transmission with tetanus toxin light chain (TNT) (Sweeney, Broadie et al. 1995) or the temperature-sensitive dynamin mutant *shibire* (Thum, Knapek et al. 2006). Caution must be taken while interpreting the results that follow the expression of an effector that is supposed to inhibit neural function. One should keep in mind that TNT impairs the release of neurotransmitter by cleaving neuronal synaptobrevin, a protein necessary for calcium dependent vesicle fusion (Sweeney, Broadie et al. 1995, Baines, Uhler et al. 2001). As a result, TNT does not affect synaptic transmission mediated by pathways independent of synaptobrevin (Thum, Knapek et al. 2006). In addition, it has been argued that blockage of synaptic transmission affects the electrical development of neurons (Baines, Uhler et al. 2001). Therefore, prolonged expression of TNT might lead to compensatory effects at the neuronal and/or circuit level. While UAS constructs inserted in different genomic sites can produce different expression patterns (Aso, Hattori et al. 2014), expression pattern of a given driver line can vary depending on the reporter it is coupled to (Figure 2.1). In light of this, co-expressing TNT and fluorescent indicators by using different UAS transgenes does not guarantee a perfect correlation in their respective expression patterns. One should therefore remember that the expression of a fluorescent

indicator might not faithfully reproduce that of TNT. The fact that a tagged version of TNT does not exist makes it difficult to determine whether TNT is expressed in the targeted neurons. Fortunately, a GFP-tagged version of Kir2.1 exists. Although constant hyperpolarization might lead to compensatory effects at the circuit level, it has been shown that expression of Kir2.1 does not lead to a change in the electrical properties of at least two types of motor neurons in the larva (aCC and RP2), suggesting that Kir2.1 expression does not change the electrical properties of a neuron (Baines, Uhler et al. 2001).

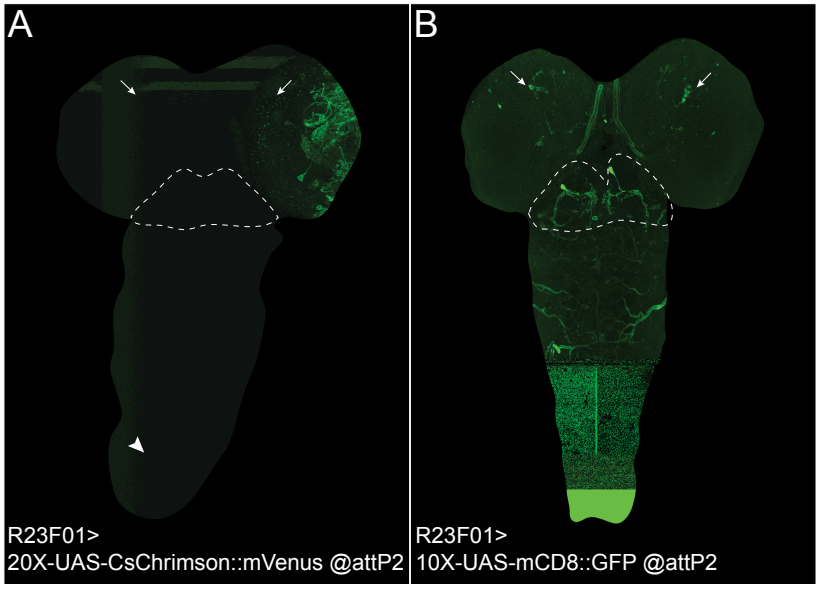

Figure 2.1: Variability in the expression pattern of the same GAL4 driver line reported by two different UAS transgenes inserted in the same landing site A: Expression pattern of R23F01>20X-UAS-IVS-CsChrimson.mVenus. Both R23F01 and 20X-UAS-IVS-CsChrimson.mVenus transgenes are at attP2 landing site on the 3rd chromosome. Dashed line encloses the subesophageal zone (SEZ). Note the high level of expression of the reporter in the SEZ. Arrows highlight expression in the brain lobes. The large arrowhead indicates the axon of a descending neuron from the SEZ. **B:** Expression pattern of R23F01>10X-UAS-IVS-mCD8:GFP (retrieved from http://flweb.janelia.org/cgi-bin/flew.cgi). Both

R23F01 and 10X-UAS-IVS-mCD8:GFP transgenes are at attP2 landing site on the 3rd chromosome. Dashed line encloses the subesophageal zone (SEZ). In contrast with panel A, only two neurons are labeled in the SEZ and very few Kenyon cells are labeled in each brain lobe. The picture shown in panel B is courtesy of the Truman lab (Li, Kroll et al. 2014). It is reproduced with the permission of the author.

In comparison with TNT and Kir2.1, the dominant-negative allele *shibire^{ts}* offers temporal control, which permits to overcome the compensatory and developmental effects of chronic inhibition. Using *shibire^{ts}*, synaptic release can be reversibly blocked under restrictive temperatures (29-34 °C). One has to remain careful while interpreting the effects of manipulations involving *shibire^{ts}* since the expression of this reagent can induce morphological changes (Gonzalez-Bellido, Wardill et al. 2009). Another caveat with the use of temperature changes is the interference with innate temperature-driven behaviors (thermotaxis). The outcome of temperature increases is therefore composite: it results from the effects of synaptic transmission block and the innate response to thermal stimulation. Moreover heat convection induced by temperature changes in the assay can perturb the geometry of the odor gradient it encloses. For this reason, it is preferable to avoid using effectors requiring temperature changes while testing the necessity of specific sets of neurons to direct orientation behaviors such as chemotaxis (Figure 2.2A). Toxins (e.g., diphtheria toxin) and proapoptotic genes (e.g., *Reaper* and *Head involution defective*) are more rarely used to block neural function by inducing cell death. Their lack of popularity is mainly due to the detrimental effects cell death might have on the development of the rest of the brain. For a more detailed discussion of the reagents commonly used to dissect neural function, we refer the reader to two thorough reviews (Simpson 2009, Venken, Simpson et al. 2011). Upon applications of

effectors inducing a loss of function, the effects of impairing the function of a given neuron or a neuronal subset should be always interpreted at the circuit level. In addition, the nonlinear dynamics generated by networks of interconnected cells imply that neural circuits must produce complex behaviors that cannot be inferred from the effect of blocking parts of the circuits.

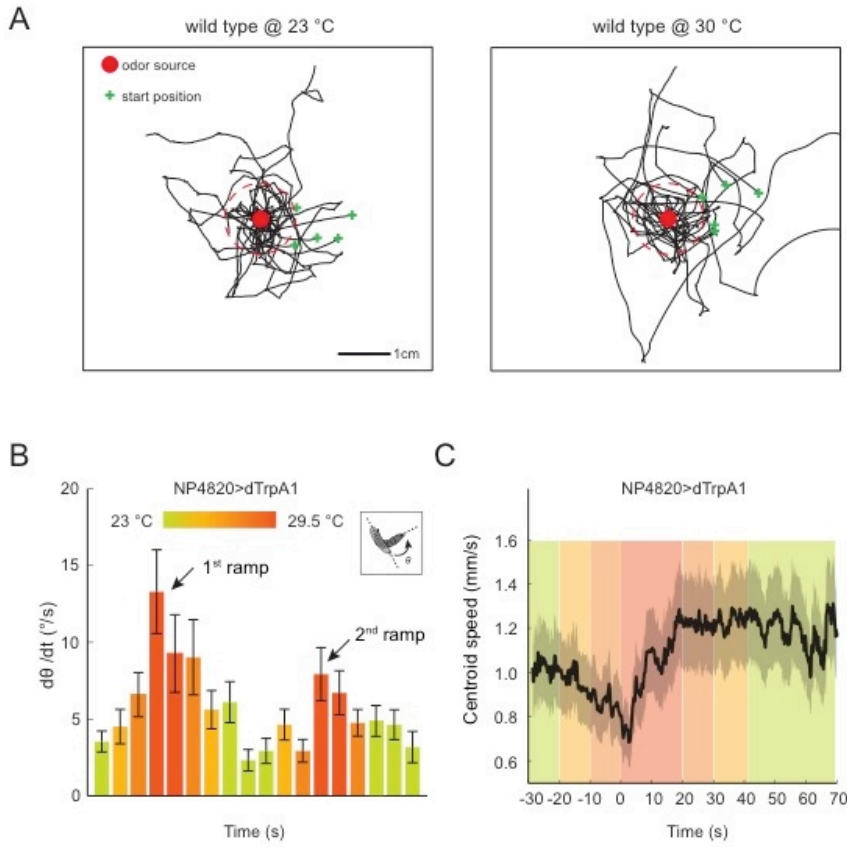

Figure 2.2: Thermogenetic gain-of-function manipulations in the *Drosophila* larva A: Effect of temperature on larval chemotaxis. An odor gradient is formed by using a point odor source (red dots, 10 μL of a 100-μM solution of ethyl butyrate). Trajectories from 5 representative larvae were plotted for 23°C (left panel) and 30°C (right panel). Note that wild type larvae tend to stay closer to the odor source when they are allowed to chemotax at 23 °C. **B:** Thermogenetic

activation of NP4820-labeled neurons by expressing dTrpA1 reagent. Temperature is raised slowly from 23°C to 29.5°C in a period of 30 seconds and decreased back to 23°C. The temperature ramp is repeated twice. Activation of NP4820-labeled neurons led to a transient increase in average head angular speed (head sweeps) during the first temperature increase phase of the temperature (arrow). However robust head sweeps cannot be elicited during the second increase in temperature (arrow labeled as 2nd ramp). Each bar indicates average head angular speed binned in 10-second windows. Error bars indicate standard error of the mean. **C:** Thermogenetic activation of NP4820-labeled neurons leads to transient increase in head sweeps followed by fast crawling. Increase in centroid speed is observed shortly after thermogenetic activation. The shaded boxes of different colors (refer to the horizontal heat map bar in (B) for corresponding temperature value) represent the windows of time during which the temperature was brought from 23°C to 29.5°C.

Sufficiency is usually defined by whether activation of a given neuron triggers a certain type of behavior or the response of a putative downstream partner. Acute activation of neurons in the larva has been successfully accomplished by using thermogenetic and optogenetic tools (Pulver, Pashkovski et al. 2009). Targeted expression of *Drosophila* TrpA1 (dTrpA1) channel (Rosenzweig, Kang et al. 2008) has been widely used to activate neurons upon temperature increases. Although this tool has proved to be useful to induce stereotypic behavioral sequences in adult flies (von Philipsborn, Liu et al. 2011, Marella, Mann et al. 2012) it lacks both temporal resolution and control over the intensity ranges of the neural activity. This is particularly important as the level and timing of a gain in neural activity might trigger distinct behavioral output due to complex circuit interactions. It has to be noticed that continuous activation of dTrpA1 might lead to depolarization block in some neuron via rapid depolarization (Inagaki, Jung et al. 2014). Furthermore, temperature manipulations necessary to activate neurons might create behavioral

interferences induced by innate responses to temperature changes, as indicated above. In recent work on the sensorimotor control of larval chemotaxis (Tastekin, Riedl et al. 2015), we were unable to trigger a reproducible gain-of-function phenotype using thermogenetics (Figure 2.2B) while optogenetic activation led to a strong and reliable phenotype in single larvae. In the next paragraphs, we will argue that the use of optogenetics has multiple advantages compared to thermogenetics.

Due to its superior temporal precision, optogenetic activation has become increasingly adopted for gain-of-function manipulations aiming to test sufficiency (Fenno, Yizhar et al. 2011). Until recently, the performances of Channelrhodopsin2 (ChR2), a blue light gated ion channel, was limited in *Drosophila* for several reasons including the low penetrance of blue light through the cuticle of adult flies and the innate responses of the adults and the larvae. In spite of this limitation, ChR2 has been successfully applied to study proboscis extension, escape responses, learning, locomotor activity (Schroll, Riemensperger et al. 2006, Gordon and Scott 2009, Zimmermann, Wang et al. 2009, Matsunaga, Fushiki et al. 2013) and orientation behaviors (Zhang, Ge et al. 2007, Gepner, Mihovilovic Skanata et al. 2015, Hernandez-Nunez, Belina et al. 2015, Schulze, Gomez-Marin et al. 2015). Since the function of ChR2 necessitates its coupling with the chromophore all-trans retina that is not endogenously produced by *Drosophila*, larvae must be grown in food complemented with all-trans retinal. Note however that a small amount of retinal is present in regular fly food (Claire McKellar, personal communication). Recent development of red-shifted optogenetic tools (ReaChr, CsChrimson and ChrimsonR) (Inagaki, Jung et al. 2014, Klapoetke, Murata et al. 2014) enabled deeper penetration of light as well as minimal innate response to visual stimulation and opened a new avenue in *Drosophila* optogenetics. It has been shown that ChrimsonR has

relatively higher off-kinetics compared to CsChrimson and it can produce sustained trains of spikes when activated at moderately high frequencies (20Hz) (Klapoetke, Murata et al. 2014).

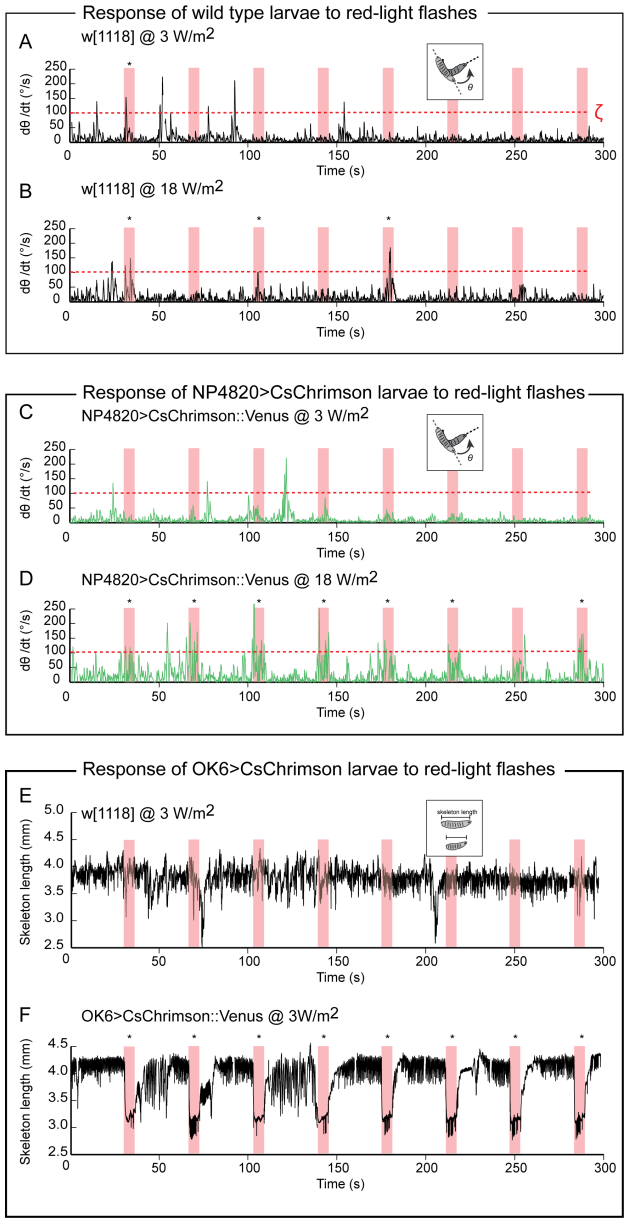

Figure 2.3: Innate sensitivity of larvae to red light and acute optogenetic activation of neural activity using CsChrimson A: We probe the response of

the control larvae subjected to 6-second flashes of red light (625 nm) at an intensity of 3 W/m^2. The behavioral response is defined by quantifying head sweeps as a function of the angular speed. A head sweep is considered to be a "cast" when the absolute value of the angular speed exceeded a threshold ζ of 100°/s. For more information about the method used to determine the value of threshold on the head angular speed, see Figure 5. The genotype used is w[1118], which corresponds to one of the most common genetic background for transgenics. At low light intensity, w[1118] only occasionally performs head sweeps that qualify as head casts (stars, 1 out of 8 flashes). **(B)** Same as panel (A) with a higher intensity (18 W/m^2) of red light. Head sweeps more frequently qualify as head casts than at a lower intensity of 3 W/m^2 (stars, 3 out of 8 flashes). **C:** Optogenetic activation of the NP4820-labeled neurons with 3 W/m^2 of red light (625 nm) upon expression of CsChrimson. Same pattern of light flashes as shown in panel (A). The larva does not respond to red light at this intensity. **D:** Same as (C) with 18W/m^2 intensity. Robust head casts are observed as a function of absolute head angular speed (stars, 6 out of 8 flashes). In panels C and D, larvae were raised on regular fly food with a concentration of 0.5 mM retinal. **E:** Response of control larvae w[1118] subjected to 6-second flashes of red light at an intensity of 3 W/m^2. Quantification of the behavioral response by the length of larva's skeleton. Red light flashes of 3 W/m^2 intensity do produce a significant decrease in body length. **F:** Optogenetic activation of OK6 neurons with 3 W/m^2 of red light (625 nm). OK6 covers most of the motor neurons in the VNC. As a result of the global activation of motor neurons, muscles across the body length contract simultaneously leading to significant decrease in the skeleton length.

Drosophila larvae are averse to blue light during most of their development (Kane et al., 2013). Abrupt changes in blue light intensity lead to increased turning. On the other hand, we observed that wild type *Drosophila* larvae show minimal to no response to changes in light intensity at 625nm when they are fed on food with all-trans retinal (Figure 2.3A and B) while 0.3-3W/m^2 is sufficient to induce paralysis when

CsChrimson is expressed in most of the motor neurons using OK6-Gal4 (Figure 2.3F). In our hands, much higher light intensities had to be applied to activate brain interneurons (10-18 W/m^2, Figure 2.3C and D). We observed that reproducible behavioral responses could be elicited over several trials using CsChrimson. However, we noted occasional time-dependent decreases in behavioral response upon the application of prolonged light stimulations (data not shown). This dampening of the gain of function is probably due to the slow off kinetics of CsChrimson and its slower recovery. It might also be related to the dynamics of the host neuron(s) independently of the effector. Therefore, the kinetics of the effector — whether it is CsChrimson, ChrimsonR or ChR2 — should be carefully considered when choosing the duration and frequency of optogenetic stimulations. In case stimulation at high frequencies is required, ChrimsonR should be favored over CsChrimson.

In the *Drosophila* larva, large-scale screens testing loss of functions (necessity) and gain of functions (sufficiency) have been performed to identify neural correlates of behavioral control (Vogelstein, Park et al. 2014, Tastekin, Riedl et al. 2015, Clark, McCumsey et al. 2016, Yoshikawa, Long et al. 2016). The number of neurons typically covered by a driver line that led to a phenotype ranged from one to a few dozens. Instead of treating each labeled neuron as a separate unit, it is convenient to group neurons by lineages. Lineages form circuit elements should be viewed as the anatomical building blocks of the brain (Hartenstein, Younossi-Hartenstein et al. 2015). For some of the hits identified in screens, an interesting behavioral phenotype could not be mapped on a single lineage due to the existence of multiple lineages covered by the driver line yielding the phenotype of interest. In these cases, alternative strategies have been deployed to restrict the phenotype to the activation/silencing of a single cell type. For example, Ohyama and

colleagues successfully utilized combination of two binary expression systems (Gal4 and LexA) together with Split Gal4 technique to narrow down the mapping of a behavioral phenotype onto one or a small set of lineages (Ohyama, Schneider-Mizell et al. 2015). This approach relies on the existence or the generation of combination of Split Gal4 lines, which is not always possible.

In recent work, we adopted a different strategy to uncover circuit elements participating in the sensory control of the timing of turning maneuvers (Tastekin, Riedl et al. 2015). In this study, we used a densely expressed Gal4 driver line (multiple cell types with more than 50 neurons in the brain lobes and the subesophageal zone). Our attempts to confine the expression of the driver line to a few neurons using traditional Gal80 and lexA intersections could only lead to the conclusion that one or more cells out of a group of ~15 located in the subesophageal zone (SEZ) are responsible for the gain of function phenotype (triggering of a turning maneuver). To enhance the precision of the circuit-function mapping, we applied an acute gain-of-function strategy combined with random labeling of neurons. We induced stochastic expression of Chrimson::mVenus in small subsets of neurons by combining the original densely expressed Gal4 driver line with a Gal80 driver whose expression is conditioned by a probabilistic flip-out recombination under the control of heat shock promoter (Figure 2.4A and B). After performing acute activation of each clone, we visualized the expression of Chrimson protein in individual clones using standard immunostaining against mVenus protein. In this way, we could directly monitor the expression of the effector (CsChrimson). This approach is more reliable than indirectly assessing the expression of an effector (e.g., TNT) through an additonal reporter (e.g., UAS-GFP). As described in the next section, we devised a statistical method to correlate the gain-of-function behavior with the expression

pattern of CsChrimson. We will detail this approach as it represents a useful alternative to infer circuit-function relationships associated with Gal4 lines expressed in multiple lineages when sparse driver lines do not exist to reduce the expression pattern of the original driver line.

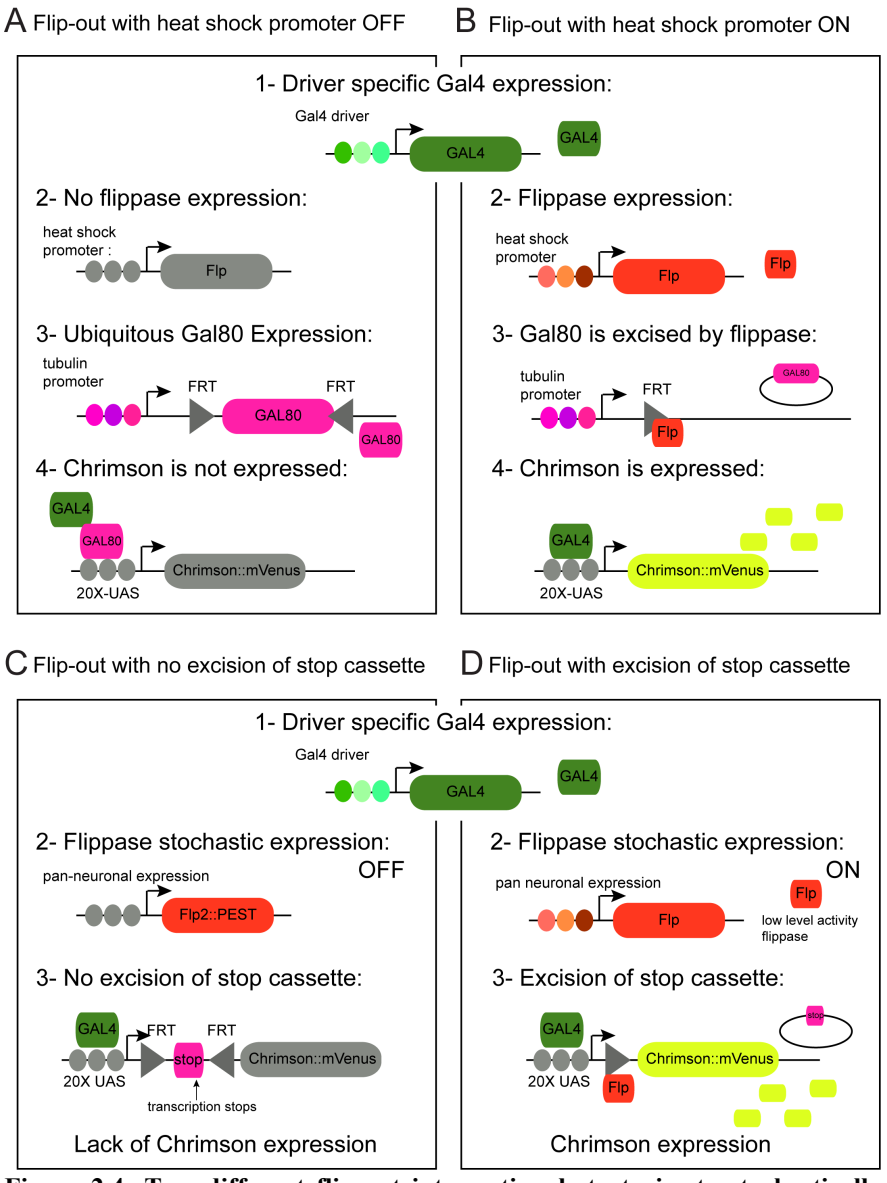

Figure 2.4: Two different flip-out intersectional strategies to stochastically express CsChrimson::mVenus in clones A-B: 'Flip-out' strategy mediated by

heat shock (hs) promoter. In panel (A), the hs promoter is OFF. As a consequence, Gal80 flanked by FRT is ubiquitously expressed under the control of tubulin promoter and inhibits Gal4-UAS dependent expression of CsChrimson::mVenus. In panel (B), the hs promoter is ON, which drives expression of the flippase protein. Flippase excises the Gal80 sequence, thereby abolishing ubiquitous Gal80 expression. Gal4 can bind to the UAS sequences and drive CsChrimson::mVenus expression in a cell-specific manner. **C-D:** 'Flip-out' strategy using pan-neuronal expression of low-level activity version of flippase (Flp2::PEST, for details see (Nern, Pfeiffer et al. 2015)). A transcriptional stop cassette flanked with FRT was placed between UAS and CsChrimson::mVenus sequences preventing Gal4-dependent expression of CsChrimson::mVenus in the absence of sufficient flippase activity (panel (C)). In panel (D), the higher level of activity of flippase in some cells is sufficient to excise the stop cassette upstream from the coding sequence of CsChrimson::mVenus. As a result, CsChrimson::mVenus is expressed in a subset of cells of the original pattern labeled by the Gal4 driver.

1.4 Stochastic labeling of neurons using Flip-out approach:

Flip-out method has been widely used to stochastically visualize subsets of neurons covered by Gal4 drivers (Venken, Simpson et al. 2011). We employed a similar strategy based on 'FLP-FRT' recombination system (Figure 2.4A and B). Following this approach, the expression of Gal80 flanked by FRT sequences is induced ubiquitously by a tubulin promoter (FLP-out Gal80) (Gordon and Scott 2009). When the flippase (FLP) recombinase is stochastically expressed under the control of heat shock promoter, it stochastically induces excision of the FRT-Gal80-FRT cassette downstream of the tubulin promoter. As a result, Gal80 is not expressed in the subset of neurons where the recombination took place,

thereby allowing full activity of Gal4 and expression of the effector (e.g., Chrimson::mVenus). This method was initially applied to stochastically silence/activate neurons involved in proboscis extension in adult flies (Gordon and Scott 2009). It enables lineage-independent expression of effectors in different combinations of neurons and it is possible to optimize the probability of flip-out events by changing the strength and duration of the heat shock. Thus, one can roughly control the number of cells in which the effector expression is allowed by the heat-shock induced loss of Gal80.

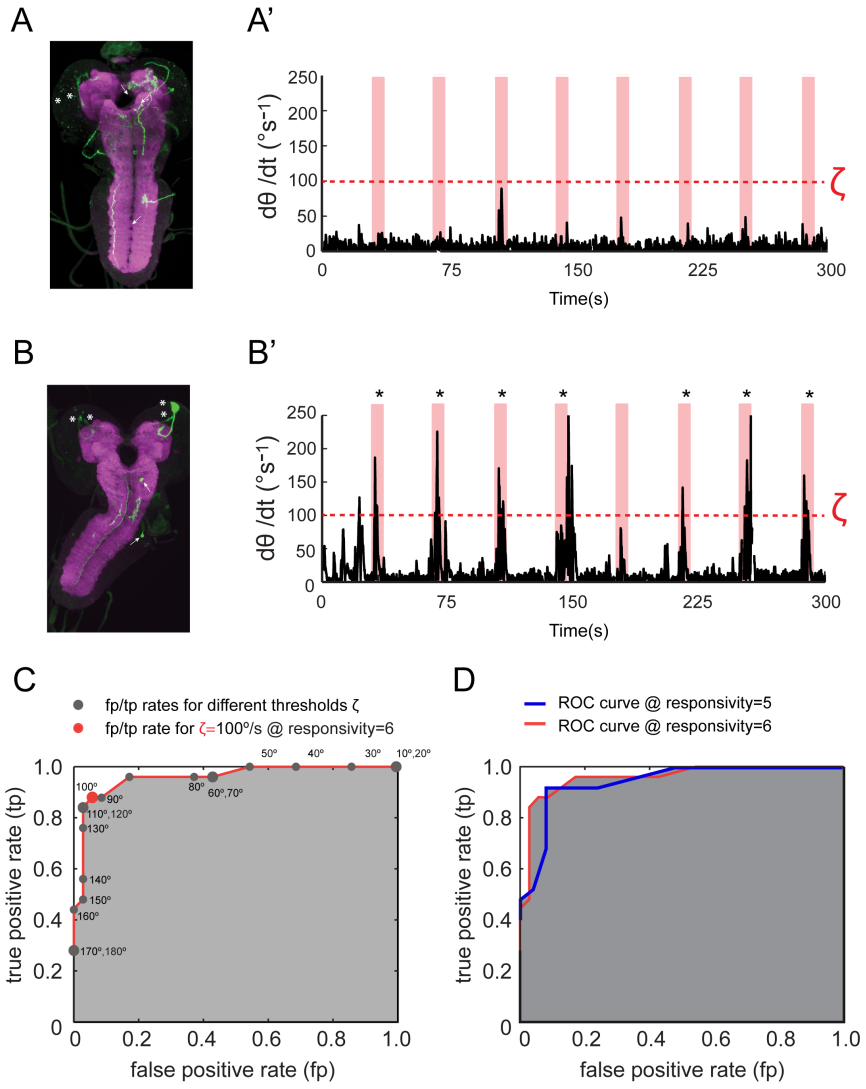

Figure 2.5: Stochastic labeling of subsets of neurons in gain-of-function clones of the NP4820-Gal4 driver line A-B: Two clones showing expression in subsets of neuron upon heat shock dependent stochastic expression (see method described in Figure 4A-B). Arrows indicate neurons that are functional in larvae at the third developmental stage. Stars indicate immature secondary lineage neurons that are unlikely to be functional at the third instar stage. Panel (A) features a clone without a behavioral phenotype while the brain displayed in panel (B) demonstrated a strong gain-of-function phenotype (see text for the explanation of positive and negative phenotypes). **A'-B':** Quantification of the

behavioral phenotype observed upon acute optogenetic gain of function of the clones shown in panels (A) and (B), respectively. The trace of panel (A') is associated with a negative phenotype since the larva does not respond to any of the light flashes. Panel (B') is associated with a positive phenotype since the larva demonstrated a strong increase in head-angular speed (|dθ/dt|) that exceeded the threshold ζ for 7 out of the 8 flashes. **C:** Receiver operating characteristic curve used to define a binary classifier for efficient detection of behaviorally positive clones. "Responsivity" is defined as the number of flashes during which head angular speed exceeds a certain threshold value (ζ). Responsivity ranges between 1 and 8. In panel (C), the ROC analysis corresponds to a responsivity of 6. The ROC is plotted for different ζ values ranging from 10 to 180 °/s (grey circles). Optimal classification (tp is as high as possible and fp is as low as possible) was obtained at responsivity=6 and for a ζ value of 100°/s (red circle). Using these criteria, the number of false positive expected for a batch of 70 tested larvae is 0.04 x 70 = 3 individuals. **D:** Comparison of the ROC corresponding to a responsivity of 5 flashes (red curve) and 6 flashes (blue curve). For both responsivity, the ROC is shown for values of ζ ranging from 10 to 180 °/s.

One disadvantage of the this flip-out approach is that hs-flp transgene and the tubulin promoter-FRT-Gal80-FRT transgene cannot be combined in the same fly stock since excision of Gal80 might occur in the germ line and lead to an irreversible loss of Gal80 in the offspring. For this reason, a new transgene must be generated for each Gal4 driver line. In order to activate and visualize the neurons that are stochastically labeled, we used red-shifted opsin CsChrimson (Klapoetke, Murata et al. 2014) fused to fluorescent protein mVenus (a collection of CsChrimson::mVenus effector inserted in different landing sites have been generated by Vivek Jayaraman; they are available from Bloomington stock center). For thermogenetic activation and simultaneous visualization of the effector, dTrpA1::myc tag fusion can be used (dTRPA1^{myc}) (von Philipsborn, Liu et al. 2011).

An alternative flip-out strategy relies on the expression of a weakened version of FLP recombinase under the control of a pan-neuronal driver (Nern, Pfeiffer et al. 2015). In this method, expression of the FLP recombinase is restricted to the differentiated neurons by driving the expression of FLP with the promoter of N-synaptobrevin gene (R57C10) (Jenett, Rubin et al. 2012). Instead of flanking ubiquitously expressed Gal80, a transcriptional stop cassette flanked by FRT (Wong, Wang et al. 2002) was introduced between UAS and CsChrimson::mVenus (dTRPA1^{myc} or dTRPA1^{mcherry} in case of thermogenetics) (von Philipsborn, Liu et al. 2011, Asahina, Watanabe et al. 2014). Low-level pan-neuronal expression of weakened FLP recombinase is expected to yield stochastic expression of CsChrimson::mVenus protein in small subset of neurons (Figure 2.4C and D). Unlike the Gal80-based method, R57C10-FLP and UAS-FRT-stop-FRT-CsChrimson::mVenus transgenes can be combined in a single fly stock since FLP expression is restricted to differentiated neurons. Thus, one can easily combine this fly stock with any Gal4 line to perform stochastic gain-of-function experiments, which makes this approach more suited for screening purposes. For both flip-out methods, we were able to reliably visualize the morphology of the labeled neurons by performing traditional immunostaning against mVenus protein with anti-GFP antibodies (Figure 2.5A and B).

1.5 Acute activation of stochastically labeled neurons: stochastic gain of function of neurons in NP4820 driver line:

Drosophila larval chemotaxis mainly involves alternation of runs (forward movements by waves of peristaltic contractions) and lateral head sweeps

(head casts) followed by directed turns (Gomez-Marin, Stephens et al. 2011). In a loss-of-function behavioral screen, we identified a Gal4 driver line (NP4820) with a reasonably sparse expression pattern. Activating these neurons by thermogenetics induced transient increase in head sweeps suggesting that NP4820-positive neurons are involved in run-to-turn transitions. Unfortunately, NP4820 labels multiple cell types in the brain lobes, the SEZ and the ventral nerve cord (VNC). Therefore, we applied a stochastic activation method to define which neurons covered by NP4820 line are responsible for triggering turning maneuvers.

We opted for optogenetic activation for several reasons. First, we observed that larvae with neural activation induced by thermogenetics (dTrpA1) failed to maintain the gain-of-function behavior — an increase in head sweeps — over several seconds. Upon thermogenetic activation of NP4820 neurons, larvae engaged in fast crawling after a short bout of increase in head angular speed (Figure 2.2C). It is possible that fast crawling results from innate avoidance triggered by high temperatures. It is equally plausible that strong activation of the neurons expressing dTrpA1 leads to a depolarization block in the neurons inducing head sweeps. Second, we were not able to reliably induce head-sweep behavior over several trials (Figure 2.2B). To limit the identification of false positives, the reproducibility of the behavioral response over several trials is crucial. A separate technical constrain came from the fact that we could not use the blue-light activated Channelrhodopsin2 as the excitation light evoked strong head sweeps in wild type larvae (Kane, Gershow et al. 2013). Therefore, we expressed CsChrimson::mVenus in NP4820 neurons. NP4820>CsChrimson::mVenus larvae robustly responded to multiple red-light light flashes (Figure 2.3D). In contrast with NP4820>CsChrimson::mVenus larvae, wild type larvae only rarely responded to a series of consecutive red-light flashes at low and

moderately high intensities (3 and 18 W/m^2, Figure 2.3A and B). We reasoned that optogenetic activation using CsChrimson would fulfill the conditions to perform stochastic gain of functions.

We took advantage of basal leakiness of heat-shock promoter at 23°C to induce low levels of flippase expression. With this reagent, we restricted CsChrimson expression to 1-5 neurons in individual larvae (clones, Figure 2.5A and B). Each clone was tested with a stimulation protocol of 8 flashes of 6 seconds at an intensity of 18 W/m^2 and a wavelength of 625 nm (Figure 2.3D). Individual flashes were separated by 30 seconds. Unlike with dTrpA1, we did not observe a decrease in the average head angular speed during consecutive gains of function (data not shown). Larval brains were dissected, fixed and immunostained for anatomical assessment with confocal imaging immediately after the behavioral experiments. To determine the behavioral phenotype of a clone, we implemented a statistical framework based on receiver operating characteristic (ROC) to optimize a binary classifier (Duda, Hart et al. 2001) that could discriminate individual larvae that showed the gain-of-function behavior (true positive, TP clones, Figure 2.5B') from the negative clones (true negative, TN, Figure 2.5A'). We combined two conditions to define TP and FP, and calculate the rate of each class of events. First, we tested different threshold values (ζ) on the head angular speed — the head angular speed reveals the increase in head activity associated with turning events — and computed the TP and FP rates for each threshold value (Figure 2.5C). Second, we evaluated how the TP and FP rates changed for different criteria on the number of flashes leading to an increase in the head angular speed that exceeded the threshold (ζ) (Figure 2.5D).

Using this approach, we were able to draw eight ROC curves each representing different criteria on the minimum number of expected responses to the 8 light flashes (two of them are shown in Figure 2.5D). The best performance was observed at a threshold ζ of 100°/s of the head angular speed and with a minimum response to 6 out of the 8 light flashes (responsivity=6, Figure 2.5C). We made use of this classifier to define the phenotype of each clone. This classifier was also used to define the expected rate of TP and TN by testing positive and negative controls (original Gal4 line driving expression of CsChrimson:: mVenus and parental control devoid of Gal4 driver, respectively). Upon behavioral tests, larvae of the positive and negative controls as well as individual clones were immunostained against the mVenus protein tagging CsChrimson using a commercial antibody against GFP (product number: A-11120, Invitrogen). We tested a total of 70 gain-of-function clones out of which we identified 10 positive hits. This ratio 10/70 was well above the expected FP rate (3-4 larvae out of 70, for calculation see Figure 2.5C). The expression pattern of a light-responsive positive clone and a light-indifferent negative clone is illustrated in Figure 2.5A and 2.5B. Finally, we determined the groups of neurons that were labeled more frequently than expected from the FP rate. Those neurons were assumed to be responsible of the gain-of-function phenotype. This stochastic gain-of-function strategy allowed us to narrow down the neurons responsible for the control of run-to-turn transitions to a three neurons in the SEZ that were not present in any of the negative clones that had been imagined.

1.6 Closing remarks:

Neural circuits form the computational units of brains. The pace at which neural circuits are identified and functionally studied has largely

accelerated in *Drosophila* after the creation of large collections of driver lines that cover sparse subset of neurons (Pfeiffer, Jenett et al. 2008, Bidaye, Machacek et al. 2014). The expression patterns of a large fraction of these two collections have been reported in the adult fly (Jenett, Rubin et al. 2012) as well as in the larva (Li, Kroll et al. 2014). Given the relatively small number of neurons that form the larval nervous system (approximately 10,000 neurons), hopes are high that a driver line labeling each neuron can be identified. With the ability to monitor genetically labeled neurons and to reproducibly interfere with their function, Drosophilists have now at their disposal an extraordinary toolkit to ask how neural circuits contribute to the organization of stereotyped behavior in the larva. However, experience has shown that this toolkit is imperfect in multiple ways: most Gal4 lines label neurons belonging to more than one lineage. Expression patterns are far from being deterministic: significant variability can be observed across individuals. While these limitations should not undermine the success of massive efforts to characterize the function of neurons of the larval brain in an unbiased way (Vogelstein, Park et al. 2014, Tastekin, Riedl et al. 2015), they call for caution in the interpretation of functional manipulations.

Variability in the expression pattern of driver lines should be viewed as the rule rather than the exception. Consequently, the action of an effector might differ substantially across individual larvae. It should be common practice to define the expression pattern of a driver with different reporters (Figure 2.1). The consistency of expression patterns should be compared across different samples as well. Inter-individual variability in the expression of an effector can produce phenotypic diversity at the level of a population of larvae undergoing the same loss-of-function or gain-of-function manipulations. In the case of thermogenetics and optogenetics, the gain-of-function manipulations might also be affected by the signal

that gates neural activity — a change in temperature or light intensity (Figures 2.2A and 2.3B). The contribution of innate responses should be accounted for and, if significant, it should be subtracted from the behavior induced by the effector. In our experience, this type of analysis necessitates to be grounded in rigorous computational analysis of behavior (Egnor and Branson 2016). In light of the variability inherent to behavioral control, searching for the neural correlate of a particular phenotype must start with the definition of metrics that robustly characterize the manifestation of a certain behavior. In the absence of such quantitative metrics, a screen or more refined manipulations are unlikely to yield conclusive results. The reader should also bear in mind that behaviors tend to form a continuum that cannot always be approximated by discrete states or actions (Szigeti, Deogade et al. 2015). In larvae, forward runs can be easily told apart from stops and backward runs. By contrast, the difference between head casts and turns is more arbitrary.

The typical absence of driver lines labeling a single neuron has also led the field to develop strategies to narrow down the expression pattern of a line with broad coverage. The most elegant approach consists in intersecting two different driver lines with Spit-Gal4 to restrict Gal4 activity to a single neuron (Aso, Hattori et al. 2014, Hampel, Franconville et al. 2015, Ohyama, Schneider-Mizell et al. 2015). This method, however, relies on the generation of complementary lines, which is often not feasible. In their absence, we argue that the expression pattern of the original driver line can still be reduced through clonal strategies. We reviewed two variants of the flip-out methods and illustrated its application to conduct clonal gain-of-function manipulations. Through this approach, we were able to nail down a phenotype — the sensorimotor control of turning maneuver — onto three neurons located in the SEZ whereas the original Gal4 lines labeled over 50 neurons in different

regions spanning the mushroom bodies and the VNC (Tastekin, Riedl et al. 2015). Interestingly the three remaining neurons included one descending neuron that projects to the VNC. Although the flip-out method did not allow us to refine the mapping beyond this resolution, nothing guarantees that the phenotype arises from a single neuron. As stated at the beginning of this section, brains are organized by network of neural circuits rather than isolated cells that carry each a different function. Extrapolating the function of a neural circuit through the manipulation of single cells might be limited since the function of individual neurons is often multiplex. The challenge that lies ahead of the reconstruction of neural circuits is to monitor the integrated function of specific circuits to explain the properties that emerge from their interactions.

CHAPTER 3: Role of the subesophageal zone in sensorimotor control of orientation in *Drosophila* larva

Tastekin I, Riedl J, Schilling-Kurz V, Gomez-Marin A, Truman JW, Louis M. Role of the subesophageal zone in sensorimotor control of orientation in Drosophila larva. Curr Biol. 2015 Jun 1;25(11):1448–60. DOI: 10.1016/ j.cub.2015.04.016

CHAPTER 4: A large-scale loss-of-function screen reveals a descending neuron involved in the sensorimotor control of *Drosophila* larval chemotaxis

4.1 Abstract:

Drosophila larval chemotaxis is organized as a set of motor actions: straight runs, short pauses and head casts followed by directed turns. The probability of transitions between these actions is modulated by the temporal changes in the intensity of olfactory stimuli. For attractive odors, run-to-turn transition is more likely to take place if the larva is engaged in a down gradient run. Upon termination of a run, active sampling through head casts enables the larva to realign its direction of motion with the local odor gradient. Although both the peripheral olfactory and motor circuits are relatively well studied in the *Drosophila* larva, little is known about the neurons that transform the activity patterns of the primary olfactory neurons into commands interpreted by the pre-motor circuits.

We performed unbiased loss-of-function screens to identify neurons that bridge the gap between the peripheral olfactory system and the motor system in the ventral nerve cord. Previously, we identified a set of interneurons in the subesophageal zone that are sufficient and necessary for to direct turning behavior. As part of a loss-of-function screen conducted within the Larval Olympiad project, here we report the identification of an olfactory descending neuron (**P**osterior-**D**orsal-**M**edial) that connects the brain lobes to the ventral nerve cord. Silencing of the PDM impairs the control of run-to-turn transitions. Acute optogenetic activation of the PDM ceases forward peristaltic waves thereby terminating runs. Using calcium imaging of motor neurons, we found that the PDM exclusively acts on the initial phase of wave propagation. Electron microscopy reconstruction of the PDM and its synaptic partners suggest that the PDM is postsynaptic to a group of neurons in the lateral horn. Here, we will discuss our progress toward

characterizing the role of the PDM in larval chemotaxis and peristaltic wave initiation by combining EM reconstruction, calcium imaging, optogenetics and high-resolution behavioral analysis.

4.2 Introduction:

Drosophila melanogaster larvae transform time-varying chemosensory inputs into stereotyped sequences of motor patterns (behavioral states) to perform robust chemotaxis. These motor patterns include runs (forward motion by means of symmetrical peristaltic contractions), stops (cessation of peristaltic waves) and head casts (lateral head sweeps) followed by directed turns (asymmetrical contractions of the body segments followed by straightening the body). It has been shown that the larva monitors the temporal profile of olfactory stimuli to modulate the transitions between these behavioral states (Gomez-Marin, Stephens et al. 2011, Schulze, Gomez-Marin et al. 2015). We refer the reader to the introductory chapter of this thesis (Chapter 1) for detailed explanation of the sensorimotor features underlying these transitions.

The peripheral organization of the olfactory system of the *Drosophila* larva is well studied. The larval olfactory system is very compact with only 21 olfactory sensory neurons (OSN), each expressing one (or in a few cases, two) odorant receptors (ORs) (Fishilevich, Domingos et al. 2005, Kreher, Kwon et al. 2005). OSN axon terminals synapse onto second-order projection neurons in a specialized brain region called the antennal lobe (AL). Here OSN axon terminals form a glomerular map with the PN dendrites such that each OSN possesses a unique glomerulus together with its uniglomerular PN (Ramaekers, Magnenat et al. 2005, Masuda-Nakagawa, Gendre et al. 2009, Berck, Khandelwal et al. 2016). The AL glomeruli are connected to each other with a sophisticated network of inhibitory interneurons (Berck, Khandelwal et al. 2016). This local network is thought to be responsible for the initial sensory

processing of the olfactory information in the larval brain (Asahina, Louis et al. 2009, Wilson 2013).

The axons of PNs project to two main neuropile centers in the larval brain lobes where further sensory processing takes place: the lateral horn (LH) and the mushroom body (MB). Early studies suggested that the MB is involved in associative learning and memory formation while the LH is responsible for innate responses. However recent findings suggest that this separation is rather ill defined (the reader is referred to the introductory chapter for detailed information). It is more likely that LH and MB are connected through feedback loops to ensure that olfactory perception is modulated by the combination of the chemical environment, past experience and the internal states.

On the other extreme of the central nervous system (CNS), motor circuits in the ventral nerve cord (VNC) are responsible for generating patterns of rhythmic motor neuron activity, which regulate the stereotyped behavioral patterns by evoking coordinated muscle contractions (Inada, Kohsaka et al. 2011, Berni, Pulver et al. 2012, Kohsaka, Okusawa et al. 2012, Berni 2015, Pulver, Bayley et al. 2015, Fushiki, Zwart et al. 2016). Across the animal phyla, it has been shown that central pattern generating (CPG) networks underlie the generation of these rhythmic activity patterns (Marder and Calabrese 1996, Katz 2016).

CPGs are defined as neural circuits that are capable of producing rhythmic neural activity in the absence of any sensory feedback or patterned inputs from other regions in the brain. The fact that the isolated larval CNS can generate segmentally coordinated motor neuron activity suggests that rhythmic patterns underlying larval locomotion are produced by CPGs

(Fox, Soll et al. 2006, Berni 2015, Lemon, Pulver et al. 2015, Pulver, Bayley et al. 2015).

The CPG network is segmentally organized in the VNC of the larva (Inada, Kohsaka et al. 2011, Berni, Pulver et al. 2012, Berni 2015). Although the it can produce coordinated motor neuron activity in the absence of sensory feedback, the CPG network has been shown that sensory input to the CPG networks modulate the duration of the runs as well as the frequency of transitions between runs and turns (Caldwell, Miller et al. 2003). It has been suggested that multi-dendritic sensory neurons serve as proprioceptive neurons that fine tune the peristaltic waves by monitoring the movement of the larva. These neurons also signal the state of the segmental contractions back to the CPGs (Hughes and Thomas 2007).

Recently, the contribution of inputs from other CNS regions — the brain lobes (BLs) and the subesophageal zone (SEZ) — to the motor pattern generation was studied in the *Drosophila* larva. By surgically removing the BLs and the SEZ, it has been shown that the abdominal and thoracic ganglia are still able to generate forward and backward waves of motor neuron activity (Pulver, Bayley et al. 2015). However the speed and the frequency of the waves are reduced, suggesting that descending input from the BL and the SEZ might modulate these features. Descending inputs are also important for producing asymmetrical motor neuron activity underlying head casts and turns (Pulver, Bayley et al. 2015). In short, the CPGs for straight runs (Berni, Pulver et al. 2012, Pulver, Bayley et al. 2015) and turns (Berni 2015) are found in the VNC. However, descending inputs from the BL and the SEZ regulate the speed and frequency of these behaviors as well as the transitions between runs and turns.

Traditionally, arthropod descending neurons are defined as neurons of which soma and dendritic arborizations reside in the brain lobes or in the SEZ while they project their axons to the ventral nerve cord. They receive integrated sensory input in the BL. Their output project onto motor circuits responsible for generating fixed action patterns. A descending neuron is often an element of a 'command' circuit whose activity is necessary and sufficient to evoke a naturally occurring behavior (Kupfermann and Weiss 1978). In light of the existence of parallel redundant pathways (Marder and Calabrese 1996), the 'necessity' condition has been relaxed to identify a descending neuron as a command neuron.

Descending neurons serve as a bottleneck in sensorimotor transformation since they mediate the communication between the sensory processing (i.e. brain lobes) and motor pattern generation (i.e. ventral nerve cord). A perfect example of descending 'command' neuron comes from the leech. A group of descending neurons with somas in the SEZ integrates mechanosensory inputs and activation of these neurons trigger segmental swim-initiating circuits in the VNC (Brodfuehrer and Friesen 1986, Brodfuehrer and Friesen 1986). Anatomical and physiological studies in other insects such as crickets (Staudacher 2001), moths (Kanzaki, Ikeda et al. 1994), locusts (Träger and Homberg 2011) and cockroaches (Burdohan and Comer 1996) have also revealed the importance of the descending control of motor output. Despite the presence of powerful genetic methods to label and manipulate neurons (that lack in other insects), DNs are relatively understudied in *Drosophila* (von Philipsborn, Liu et al. 2011, Bidaye, Machacek et al. 2014, Hsu and Bhandawat 2016).

We performed a large-scale loss-of-function screen to identify neurons in the larval brain that are necessary for larval chemotaxis. In order to silence synaptic transmission in single neurons or single cell types we induced the expression of a tetanus toxin light chain (TNT) by using Split-Gal4 (Pfeiffer, Ngo et al. 2010) driver lines generated in Janelia Research Campus. In our screen we identified a descending neuron (PDM) connecting the lateral horn to the ventral nerve cord. High-resolution behavioral analysis of the loss-of-function phenotype showed that the PDM neuron is necessary for run-to-turn transitions. Electron microscopy reconstruction of the upstream and downstream partners (performed by Avinash Khandelwal) revealed that this descending neuron receives input from Or42a and Or42b OSNs in the lateral horn region while giving output on descending neurons in the SEZ. Acute optogenetic activation of the PDM neuron led to inhibition of forward wave initiation.

Here we present our efforts to characterize the mechanisms underlying the descending control of forward peristalsis through descending inputs from the olfactory centers in the brain lobes. We suggest that the PDM neuron fulfills the necessity and sufficiency requirements of a descending 'command' neuron that terminates runs during larval chemotaxis. This descending pathway –from OSNs to motor neurons–serves as an example for an anatomical and functional basis that is capable of turning perceptions into actions. Since network motifs and computations reoccur multiple times across the phylogeny (Katz and Harris-Warrick 1999, Kay and Stopfer 2006, Katz 2016) we hope that some of the mechanisms underlying this pathway will pave the way toward a more general understanding of the anatomical and functional organization of sensorimotor transformations.

4.3 Results:

4.3.1 A loss-of-function screen to identify neurons necessary for larval chemotaxis:

In attempt to identify neurons in the larval brain involved in chemotaxis behavior we conducted a loss-of-function (LOF) screen by using Split-Gal4 driver lines generated in Janelia Research Campus. The screen took place as part of the Larval Olympiad project. Briefly, activator (AD) and DNA-binding (DBD) domains of the Gal4 sequence are separated and cloned downstream of two different enhancers as previously defined (Pfeiffer, Ngo et al. 2010). Alone, neither AD nor DBD can drive expression of UAS transgenes. However co-expression of AD and DBD in a cell leads to an active Gal4 protein, which in turn drives expression of UAS transgenes. If expression patterns of two different enhancers overlap, one can specifically access the overlapping neurons using Split-Gal4 technique. Using this technique, we were often able to restrict expression to a single neuron (or a single neuronal cell type) per hemisphere (Figure 4.1D, left panel). Thus, we could directly correlate the LOF phenotype to a single neuron (or a single neuronal cell type) without applying further intersectional techniques we had previously used (Chapter 2).

In our Split-Gal4 LOF screen, we inhibited synaptic transmission in targeted neurons by using tetanus toxin light chain as an effector. We tested chemotactic performances of larvae expressing TNT under control of 278 different Split-Gal4 driver lines. The neuron types covered by these lines include Kenyon cells (KCs), mushroom body input and output extrinsic neurons (MBIEs and MBOEs), descending neurons (DNs) that

link the BL to the VNC, neurons in the SEZ, interneurons in the BL, interneurons in the VNC and projection neurons in the BL.

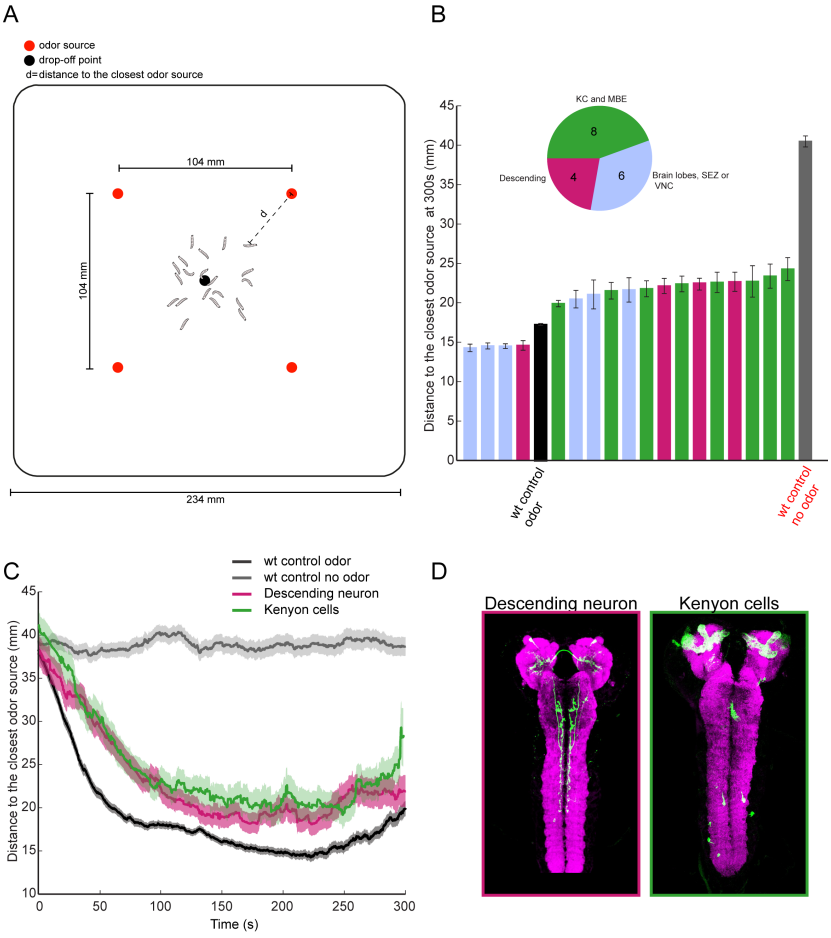

Figure 4.1: Loss-of-function chemotaxis screen using Split-Gal4 driver lines
A: Schematic of the Multi Worm Tracker used for the behavioral screen. Approximately 20 larvae were placed in the middle (black dot) of a large Petri dish covered with 4% agar. Four odor droplets of 8 µl (~15mM ETB diluted in paraffin oil) were pipetted on equidistant positions inside the lid of the Petri dish (red dots). The lid was closed and larvae were tracked for 5 min. The dimensions of the arena and the positions of the odor droplets are given in mm. **B:** Primary analysis of the chemotaxis screen. Average distance to the closest odor source was measured for each genotype (Split-Gal4>TNT). The average distances for the positive (black, wt control odor) and the negative (gray, wt control no odor)

parental controls after 300 seconds were plotted together with 18 hit lines that showed at least 2 standard deviations difference compared to the positive control. Inset: Hit driver lines color-coded according to the neuron types they label. Eight of the hit lines label MB neurons (green), four labels descending neurons (magenta) and the rest labels other interneurons in the brain, subesophageal zone and the ventral nerve cord (light blue). KC: Kenyon cells, MBE: mushroom body extrinsic neurons, SEZ: subesophageal zone, VNC: ventral nerve cord. **C:** Time course of the average distance for positive and negative controls together with two driver lines labeling KCs (green) or a descending neuron (magenta). Shaded area indicates the standard error of the mean. **D:** Maximum projections of the confocal stacks for the KCs and the descending neuron shown in panel C. Green indicates the neurons labeled by the Split-Gal4 lines driving expression of CsChrimson::mVenus. Magenta indicates the neuropile staining. Green: anti-GFP, magenta: anti-nc82 and anti-synapsin.

In order to increase the throughput in our LOF screen we made use of the multi-worm tracker (MWT) (Swierczek, Giles et al. 2011) that allowed us to track the chemotactic behavior of ~20 larvae in a single trial. In a large Petri dish (234 x 234 mm), we used four odor droplets of ~15mM ethyl butyrate (diluted in paraffin oil), with a distnance of 104 mm to each other and 130 mm to the walls of the petri dish (Figure 4.1A). We placed 20 larvae in the middle of the arena covered with a thin 4% agar slab and tracked them for 5 min.

For each driver line we performed at least 6 trials (120 larvae) together with negative and positive controls. As a negative control we used only paraffin oil instead of ETB and tracked the behavior of the parental control ($y^{-}w^{-}$; attP40; attP2 x UAS-TNT; each Split-Gal4 line is composed of two transgenes inserted into attP40 and attP2 landing sites in $y^{-}w^{-}$ background). As a positive control we assessed the chemotactic performance of the parental control larvae in a gradient identical to the

one we used for the Split-Gal4>TNT larvae. Initially, we used average distance to the closest odor source to identify larvae showing a defect in chemotaxis. Upon targeted expression of TNT, we searched for driver lines leading to at least 2 standard deviations deflection from the average distance of the parental control larvae to the closest odor source after 300 seconds.

In total, we identified 18 Split-Gal4 driver lines (Figure 4.1B): 8 driver lines labeling KCs or MB extrinsic neurons (MBEs), 4 driver lines labeling descending neurons, 2 driver lines labeling SEZ neurons, 1 driver line labeling a VNC interneuron and 3 driver lines labeling BL interneurons (Figure 4.1B). To further benchmark the chemotactic defect, we analyzed the temporal profile of the average distance to the closest odor source (2 examples are shown in Figure 4.1C). Each driver line targeted expression in only one neuron or a single neuron type (in case of KCs) per hemisphere (Figure 4.1D). Interestingly, silencing KCs and MBEs led to chemotactic defects for distinct KC and MBE driver lines suggesting that the MB is also involved in innate larval chemotaxis. However, we concentrated on DNs for further analysis, as they are the key neurons in sensorimotor transformation: they connect the sensory perception in the BLs to motor pattern generation in the VNC.

4.3.2 Identification of a descending neuron involved in larval chemotaxis:

Combining the genetic tools available for *Drosophila* with electron microscopy reconstruction, we attempted to study the chemotaxis-related descending circuits controlling motor pattern generation. In our loss-of-function screen, we have identified 4 DNs whose silencing lead to poorer

chemotaxis compared to parental control (Figure 4.1B and C).

Among these 4 DNs, one had particularly interesting morphological features (Figure 4.2F): The driver line SS01994 (each driver line is labeled as **S**table_**S**plit_XXXXX) labels a single descending neuron per hemisphere whose soma and dendrites are found in the BL and axonal projections are observed in the ventral nerve cord (Figure 4.2Fi). We named this neuron PDM (**P**osterior-**D**orsal-**M**edial) after its soma's location in the BL. By using the multi-color flip-out technique (Nern, Pfeiffer et al. 2015), we showed that PDM projects its dendrites and axons contralateral to its cell body location (Figure 4.2Fii). Closer inspection revealed that PDM has dendritic arborizations around the MB peduncle (the axonal bundle of Kenyon cells projecting form the MB lobes) and near the lateral horn (LH) region, suggesting that PDM receives olfactory input. The axon terminals of the PDM reach down to the fourth abdominal ganglion in the VNC with observably strong varicosities near the SEZ and in the thoracic ganglia (Figure 4.2Fi).

In our MWT assay, larvae with silenced PDM (SS01994>TNT) exhibited loose trajectories around the odor sources compared to the parental control (Figure 4.2A, compare left and right panel; same number of trajectories are plotted for each genotype). When we measured the distance to the closest odor source over a period of 5 min, we observed that PDM silenced larvae could not localize the odor source as efficiently as the parental control (Figure 4.2B). While the parental control larvae stay in an average distance of ~13 mm to the source between 120 and 240 s, PDM silenced larva could only get as close as ~19 mm to the source and stayed at this distance between 120 and 240 s (the minimum distance PDM silenced larvae could reach was significantly different compared to the parental control, $p<0.05$, Wilcoxon signed rank test). After 240 s, parental

controls lost interest in the odor source and; the difference between the PDM silenced and parental control larvae disappeared (Figure 4.2B). We quantified the distance to the closest odor source at the 150th second, around which the average distance reached a plateau for both parental control and PDM silenced larvae (Figure 4.2B). We showed that PDM silenced larvae reached the plateau further away from the odor sources (Figure 4.2C). In addition silencing PDM resulted in significant decrease in the average number of turns the larvae engage in in a minute, suggesting that poorer localization of the odor source might be due to delayed triggering of turns (Figure 4.2E). In order to see whether the decreases in chemotactic and turning performances are due to a defect in locomotion, we measured the average run speed for the parental control and the PDM silenced larvae. However, we did not observe any difference in the run speeds, suggesting that the chemotactic defect is not due to a direct motor defect (Figure 4.2D).

Next, we benchmarked the LOF phenotype we observed in MWT in a single larva tracking assay (SOS) that we had previously used (Gomez-Marin, Stephens et al. 2011, Tastekin, Riedl et al. 2015). Unlike the MWT assay, we previously reconstructed odor gradients for the SOS assay using FT-IR spectroscopy (Tastekin, Riedl et al. 2015). Therefore, by using the SOS we can quantify the sensory experience of the larva as a function of airborne odor concentration. To test the chemotaxis of PDM silenced larvae, we placed single PDM>TNT larva onto a 96-well plate lid covered with 3% agarose.. We used a single odor source of 100 µM ETB as previously described (Tastekin, Riedl et al. 2015). Analysis of the trajectories of PDM>TNT as well as both parental control larvae shows that PDM silenced larva could not localize the odor source efficiently, similar to what we observed in the MWT assay (Figure 4.3A). The differences between the temporal profiles of the distance to the odor

source between the single-odor assay and MWT assay (compare Figure 4.2B and 4.3B) might result from the unique shapes of the odor gradients in both assays. In the SOS assay, both parental controls and the PDM silenced larvae reached a plateau value at approximately the same distance from the odor source shortly after the beginning of the trial, although PDM>TNT larvae remained at a slightly larger distance from the odor source (Figure 4.3B). Unlike in the MWT assay, PDM>TNT seemed to lose interest in the odor source after 120 second as the average distance of the PDM silenced larva to the odor source increased while it stayed stationary for both parental controls (Figure 4.3B). Parental controls, however, lost interest only after 200 seconds similar to the MWT assay. The loss of interest in the controls might potentially occur because the steepness of the gradient cannot be preserved beyond this point due to ongoing odor diffusion (data not shown).

We compared the turn rate of PDM>TNT larvae to the parental controls in different time bins to show that the increase in the average distance to the odor source between the 120^{th} and the 180^{th} seconds is due to a decrease in the turning performance. For the parental controls, this time bin corresponds to the circling phase during which larvae have already located the odor source and keep turning under the odor droplet. As we expected, the turn rate of the PDM>TNT larva was specifically lower in this time bin while there is no difference in the turn rates for the other bins (Figure 4.3C). We have to state that one of the parental controls (SS01994 x w^-) showed significantly higher turn rates in all bins compared to the other parental control and the PDM>TNT larvae. This might be due to the significantly higher average run speed of this parental control (Figure 4.3D). Indeed, in our lab we experienced significant differences in locomotor activity for different genetic backgrounds (data not shown). To remove the effects of the speed on the turn rate, we computed the average

number of turns per unit distance rather than time during 120-180 seconds. Interestingly, there was no significant difference in the number of turns per mm for both parental controls while PDM silenced larvae had significantly lower number of turns per mm in this time bin. In this way, we uncoupled the effect of speed on the turning performance and showed that silencing the PDM neuron led to a decrease in turning performance, suggesting that PDM is involved in run-to-turn transitions.

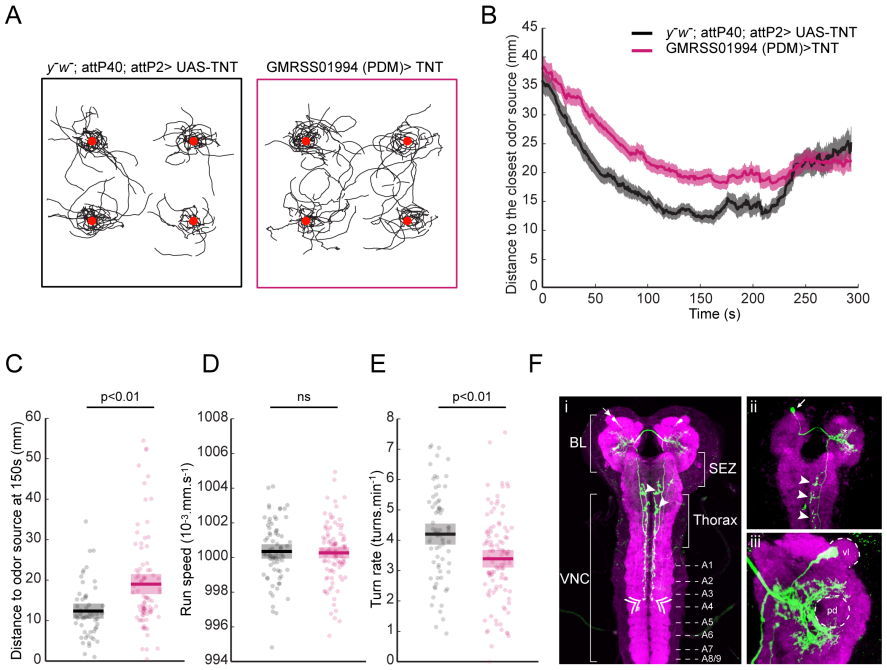

Figure 4.2: Identification of a descending neuron and analysis of its loss-of-function phenotype using Multi Worm Tracker A: Representative trajectories of the positive parental control (*y*-*w*-; attP40; attP2>UAS-TNT) and SS01994>TNT. Red dots indicate the positions of the odor droplets. **B:** Time course of the average distance to the closest odor source for SS01994>TNT (magenta line) and the positive control (black line). Shaded areas indicate the standard error of the mean. Here, positive controls that are performed during the same day with SS01994>TNT are plotted in order to avoid the effects of day-to-day variability in chemotaxis. **C:** Quantification of the average distance to the

odor source at the 150th second when a plateau was reached. SS01994>TNT (magenta) had a statistically significant difference in average distance compared to the parental control ($p<0.01$, Wilcoxon signed rank test). Boxes indicate 95% confidence interval. Dots indicate individual data points and horizontal lines indicate mean value. **D:** There is no difference between the run speeds of SS01994>TNT and $y^{-}w^{-}$; attP40; attP2>UAS-TNT (Wilcoxon signed rank test). **E:** SS01994>TNT exhibited a significantly lower turn rate compared to the parental control ($p<0.01$, Wilcoxon signed rank test). N.S.: not significant **F:** The anatomy of the descending neuron PDM labeled by SS01994>CsChrimson::mVenus immunostaining with anti-GFP antibodies that recognize mVenus protein. In panel i, the gross anatomy of the PDM neuron is shown. A1-8 indicates the approximate location of each abdominal segment. The arrow indicates the soma location. Arrowheads indicate the axon terminals in the VNC. Note the large varicosities in the initial thoracic segments and near the SEZ. Chevrons indicate the tip of the axonal projection ending around the 4th abdominal segment. In panel ii, a single PDM neuron was labeled using the MCFO method (Nern, Pfeiffer et al. 2015). Note the contralateral locations of the axon terminals (arrowhead) and the dendritic arborization (star) with respect to the soma (arrow). A detailed image of the dendritic arborizations is shown in panel iii. The dendritic tree of the PDM neuron covers a region around the mushroom body peduncle (pd) and the lateral horn. BL: brain lobes, SEZ: subesophageal zone, vl: ventral lobe of the mushroom body, VNC: ventral nerve cord.

Upon turning, the *Drosophila* larva often reorients itself toward the direction of attractive odor gradients (Gomez-Marin, Stephens et al. 2011). We tested whether silencing PDM effects the biasing of turns toward higher concentrations. We did not observe a significant decrease in the proportion of turns toward higher odor concentration when we compared PDM>TNT to $y^{-}w^{-}$; attP40; attP2 x UAS-TNT larvae. Interestingly the faster SS01994 x w^{-} larvae were poorer in terms of turning toward the local odor gradient. Perhaps, they cannot integrate

changes the sensory stimuli efficiently since they move faster and have less time to sample space around them while they are head casting. Imbalance in the speed-accuracy tradeoff while sampling the odor space might lead to poor decision-making (Chittka, Skorupski et al. 2009).

In short, the analysis of LOF data for two different assays showed that PDM is involved in run-to-turn transitions during *Drosophila* larval chemotaxis. By using two different assays with different gradient profiles we have established that silencing PDM affects the average number of turns the larva engage in to stay in close vicinity of an attractive odor source.

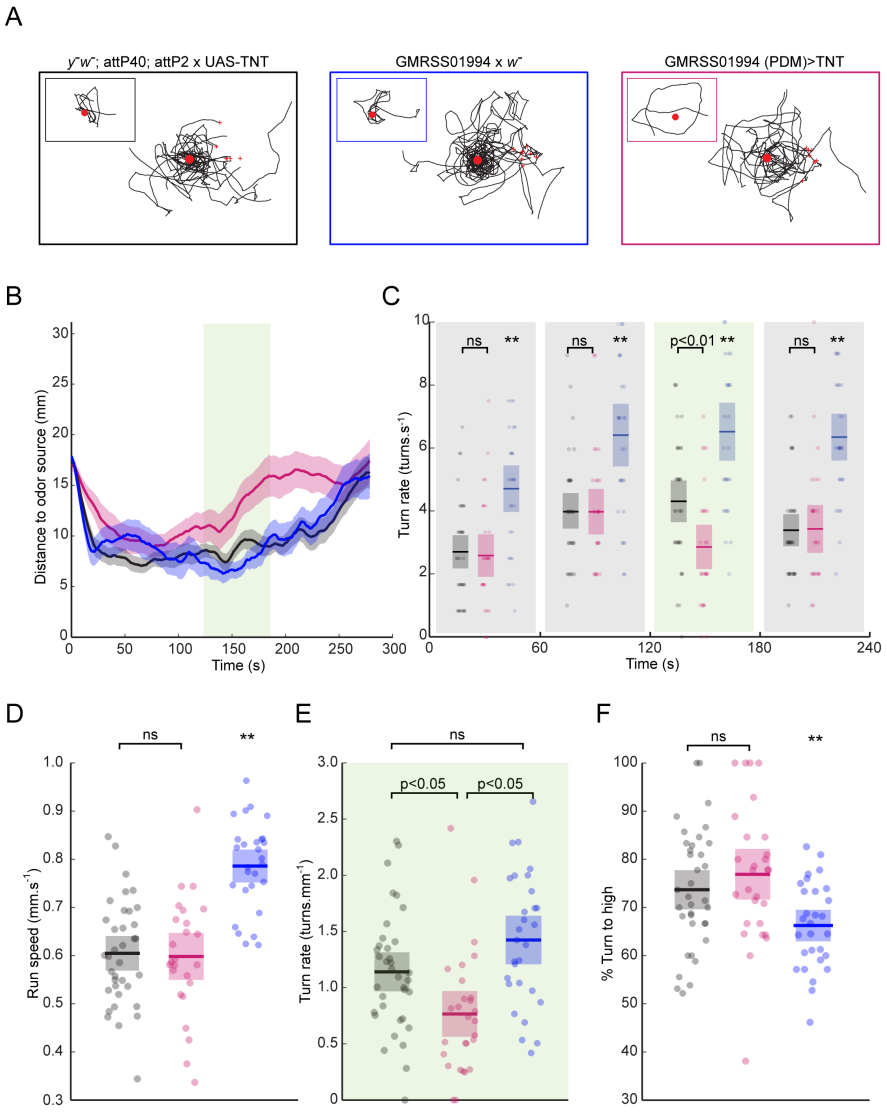

Figure 4.3: Loss-of-function behavior of the PDM>TNT larvae in single larva tracking assay A: Eight Representative trajectories of the positive parental controls (*y*-*w*-; attP40; attP2>UAS-TNT in gray box and SS01994 x *w*- in blue box) together with the PDM silenced larvae (magenta box). Insets: a single trajectory for each genotype is shown for comparison. Red squares indicate starting positions of the larvae. Red dots indicate the positions of the odor droplet. **B:** Average distance to the odor source for 300 seconds. Unlike parental controls (gray and blue), PDM silenced larvae (magenta) could not stay around the odor

source between 120-180 s (light green box). Kolmogorov-Smirnov test, $p<0.05$. Shaded areas indicate standard error of the mean. **C:** Average turns per min in four time bins: 0-60, 60-120, 120-180, 180-240 s. SS01994 x w- (blue) shows significantly higher turn rate in all bins compared to the other parental control (gray) and PDM>TNT larvae (magenta) since they are faster (see run speed in D). During 120-180 s (light green box) the turn rate of PDM silenced larvae was significantly lower compared to both controls ($p<0.05$, Wilcoxon signed rank test with Bonferroni correction). Note that this is the same time window during which the PDM silenced larvae exhibited an increase in average distance to the odor source. **D:** Average run speed. There was no difference between *y⁻w⁻*; attP40; attP2>UAS-TNT (gray) and PDM>TNT (magenta). SS01994 x *w⁻* larvae (blue) were significantly faster than both ($p<0.05$, Wilcoxon signed rank test with Bonferroni correction). **E:** In order to avoid effect of the speed on turn rate, turn rate per mm was measured in the time window in which a difference was observed for the PDM silenced larvae (light green box). The difference between parental controls did not exist for turn rate per mm while PDM>TNT larvae (magenta) had significantly lower turn rate per mm compared to both parental controls ($p<0.05$, Wilcoxon signed rank test with Bonferroni correction). **F:** Efficiency of the reorientation was measured as the percentage of the turns toward higher odor concentration. There was no difference for *y⁻w⁻*; attP40; attP2>UAS-TNT (gray) and PDM>TNT (magenta). SS01994 x *w⁻* larvae (blue) have significantly lower efficiency ($p<0.05$, Wilcoxon signed rank test with Bonferroni correction) probably due to increased speed (see a possible explanation in the text). ns: not significant.

4.3.3 Electron microscopy reconstruction of the PDM neuron and its upstream partners:

The fact that PDM>TNT larvae cannot perform chemotaxis as efficiently as their parentals control suggests that the PDM neurons is functionally connected to the olfactory system. Moreover, light microscopy shows that

dendritic arborization of PDM is found in a region around the MB peduncle and near the lateral horn (Figure 4.2Fiii). Based on these observations, we argued that PDM receives input from these two regions, which are known to be olfactory centers in the larval brain.

In order to reveal its putative anatomical connectivity in these regions, we attempted to find the PDM neuron in electron microscopy (EM) stacks of the 1st instar larval brain. Eventually, Avinash Khandelwal from our lab found and reconstructed the PDM neuron together with its upstream synaptic partners. Figure 4.4 demonstrates the strong resemblance in gross anatomy between the PDM in light microscopy images and the neuron identified in 1st instar EM stacks (Figure 4.4A left panels). We were able to find the soma of the PDM in the same approximate location (**P**osterior-**D**orsal-**M**edial) in the EM reconstruction. We also observed the same pattern of contralateral projections (Figure 4.4A right panels). In addition, the location and morphology of dendritic arborization, the axonal projection and axonal varicosities are highly correlated between the light microscopy and the EM reconstruction. This type of comparison has been successfully used in other studies to correlate between EM and light microscopy (Ohyama, Schneider-Mizell et al. 2015). Altogether, we are confident that the neuron we found in the EM dataset is the PDM neuron we identified in our screen.

In our LOF experiments we used ETB as an attractive odor which strongly activates only two receptor neurons: Or42a and Or42b (Kreher, Mathew et al. 2008). We hypothesized that PDM should be connected to Or42a and/or Or42b OSNs, because silencing PDM led to defects in chemotaxis in ETB gradients (Figure 4.2 and 4.3). Preliminary analysis of the EM connectivity revealed that PDM indeed receives input from the Or42a and Or42b channels in the lateral horn region (Figure 4.4B). Although the EM

reconstruction is yet to be finalized and reviewed (Figure 4.4B, gray arrows indicate connections that so far have only been identified on one side of the brain but for which symmetrical connectivity is expected) we observed that there is a feed-forward connectivity from the Or42a and Or42b PNs to the PDM neuron: Or42a and Or42b PNs directly output to LHB3 (**L**ateral-**H**orn-**B**ilateral axon-**3**) in the lateral horn region. This neuron receives ipsilateral input in the lateral horn and sends axonal projections bilaterally synapsing onto another bilateral axon neuron in the LH, LHM2 (**L**ateral-**H**orn-**M**ediator-2) as well as the PDM neuron (Figure 4.4C, right). In turn, LHM2 also outputs to the PDM neuron bilaterally (Figure 4.4C, left), forming a feed-forward motif from the PNs to the PDM neuron (Figure 4.4B-D and Figure 4.12A-B).

We observed two interesting features in the upstream connectivity of the PDM neuron. First, preliminary reconstruction revealed that LHM2 is one of the most strongly connected pre-synaptic partners of the PDM neuron (data not shown). Moreover, PDM is the strongest downstream partner of LHM2 receiving ~5% of the total output of the LHM2 neuron (weakest partner receives 0.46% of the total output). Although ongoing EM reconstruction might change the total number of synapses these neurons form with other neurons as well as with each other, the strong partnership between PDM and LHM2 suggests that this pathway is functionally important for the larva. Second, the PDM neurons on each side of the brain receive bilateral input from LHM2 and LHB3 neurons from both sides of the brain while PNs synapse onto LHB3 only ipsilaterally. It seems that the PN inputs from each side are equally distributed onto the PDM neurons on both sides, thereby abolishing bilateralism. Previously, it has been shown that larvae with one OSN active only on one side of the brain can perform sufficient chemotaxis (Louis, Huber et al. 2008). We argue that bilaterally distributing the olfactory signals at the level of

lateral horn might account for the sufficiency of one OSN on either side of the body to drive chemotaxis. Finally, LHB3 and LHM2 form feedback loops with their contralateral partners (LHB3 to LHB3 and LHM2 to LHM2).

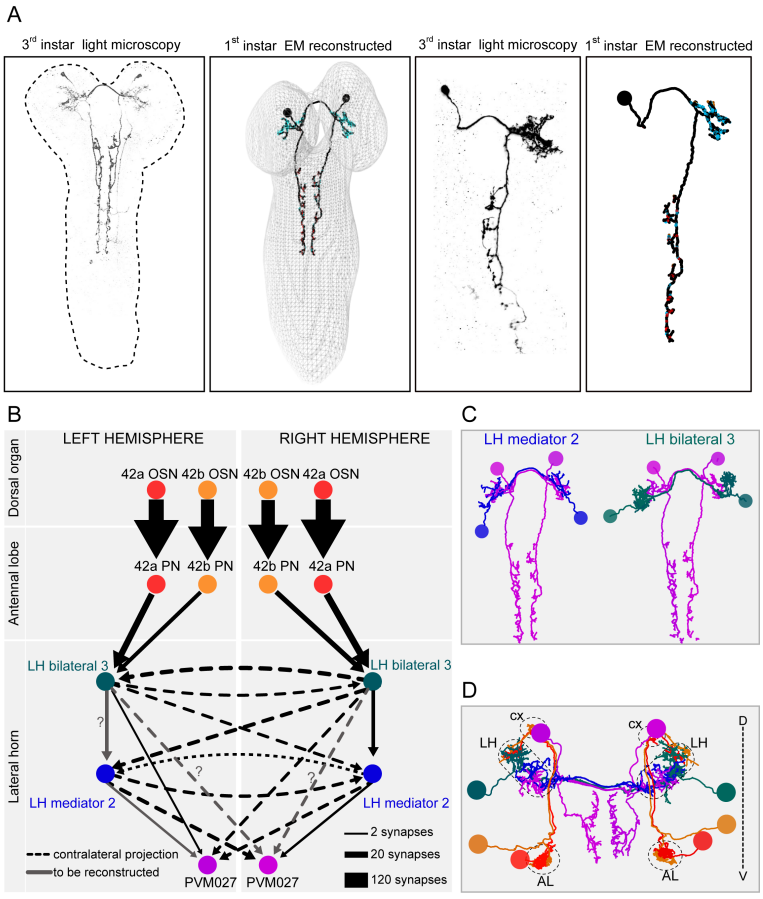

Figure 4.4: Upstream connectivity of the PDM in the EM reconstruction of the 1st instar larva A: Comparison of the 3rd instar light microscopy (LM) morphology of the PDM neuron to the PDM reconstructed in the EM volume of a 1st instar larva. On the left, gross morphology of the PDM neuron in the LM and the EM is very similar. On the right a single cell clone of the PDM neuron was compared to the EM reconstruction. Dendritic arborizations and axonal projection patterns exhibit high level of similarity. In the EM images red dots indicate post-

synaptic sites and cyan dots indicate pre-synaptic sites. **B:** Upstream connectivity diagram of the PDM neuron. PDM receives input in the lateral horn (LH) region from two LH neurons: LH bilateral 3 and LH mediator 2. LH bilateral 3 (LHB3) receives input from Or42a and Or42b PNs and outputs onto LH mediator 2 (LHM2) as well as PDM forming a feed forward motif. Dashed arrows indicate contralateral projections. LHMB3 forms a feedback loop with its contralateral partner. The same observation is true for LHM2. Gray arrows indicate connections missing on one side of the brain and to be reconstructed. PDM receives bilateral input from both LHB3 and LHM2. The thickness of the arrows was scaled according to the number of the synapses the arrow is connecting. **C:** Dorsal view of LHB3 (right, green) and LHM2 (left, blue) are shown together with the PDM neuron (magenta). **D:** Anterior view of the PDM neuron was shown together with the Or42 and Or42b PNs, LHM2 and LHB3. Antennal lobe (AL), lateral horn (LH) and the calyx of the mushroom body (cx) were delineated by dashed circles. Same color codes were used in B, C and D. V: ventral, D: dorsal.

In the future, identifying driver lines for the LHB3 and LHM2 neurons will help us characterize the functional relevance of the feed-forward connectivity and bilateral distribution of PN outputs in the lateral horn region. Identification of the neurotransmitters of these neurons (excitatory or inhibitory) will shed light on the nature of the feed-forward motif (coherent or incoherent types) (Shoval and Alon 2010). The characteristics of the feed-forward motif will eventually define the sensory processing taking place upstream of the PDM neuron. Therefore, we are currently in the process of identifying driver lines for the LHB3 and LHM2 neurons.

4.3.4 Sufficiency of the PDM neuron to trigger pauses during larval locomotion:

LOF experiments suggest that PDM is involved in run-to-turn transitions. In order to test the sufficiency of the PDM neuron to trigger transitions from runs to turns, we acutely activated the PDM neuron by using optogenetics. Upon expression of CsChrimson in the PDM neuron, we applied 6 s of red light flashes to induce an acute activation of the PDM neuron. Intriguingly, we found that PDM activation reliably evoked pauses for 8 consecutive flashes that were interspersed by 30 seconds. We quantified this behavior by measuring the tail speed of the larva (Figure 4.5A and B). In order to test whether PDM activation also triggers turning behavior, we quantified the average head angular speed as well as the absolute head angle upon PDM activation. The parental control showed a characteristic startle response upon red light flashes, readily quantifiable by a decrease in the tail speed (Figure 4.5A and B) concurrent with an increase in the head angular speed at the onset of the red light (Figure 4.5C and D, black lines). Unlike the parental controls, PDM activation led to a strong decrease in the average tail speed followed by an increase in the average head angular speed 3 seconds only into the light activation (Figure 4.5C and D, magenta lines).

Then we tested whether different levels of PDM activation can reliably induce run-to-turn transitions (Figure 4.5E-G). We observed that activating PDM with a range of different light intensities could reliably trigger pausing behavior although the minimum average tail speed was higher for lower light intensities (Figure 4.5E). However, the effect of evoking head sweeps was more ambiguous for lower light intensities, resembling the startling response of the parental control (Figure 4.5F and

G). In short, activation of the PDM neuron is sufficient to trigger pausing behavior while it can (but does not necessarily need to) evoke turning behavior following the pause (for a possible explanation see Figure 4.6E and below).

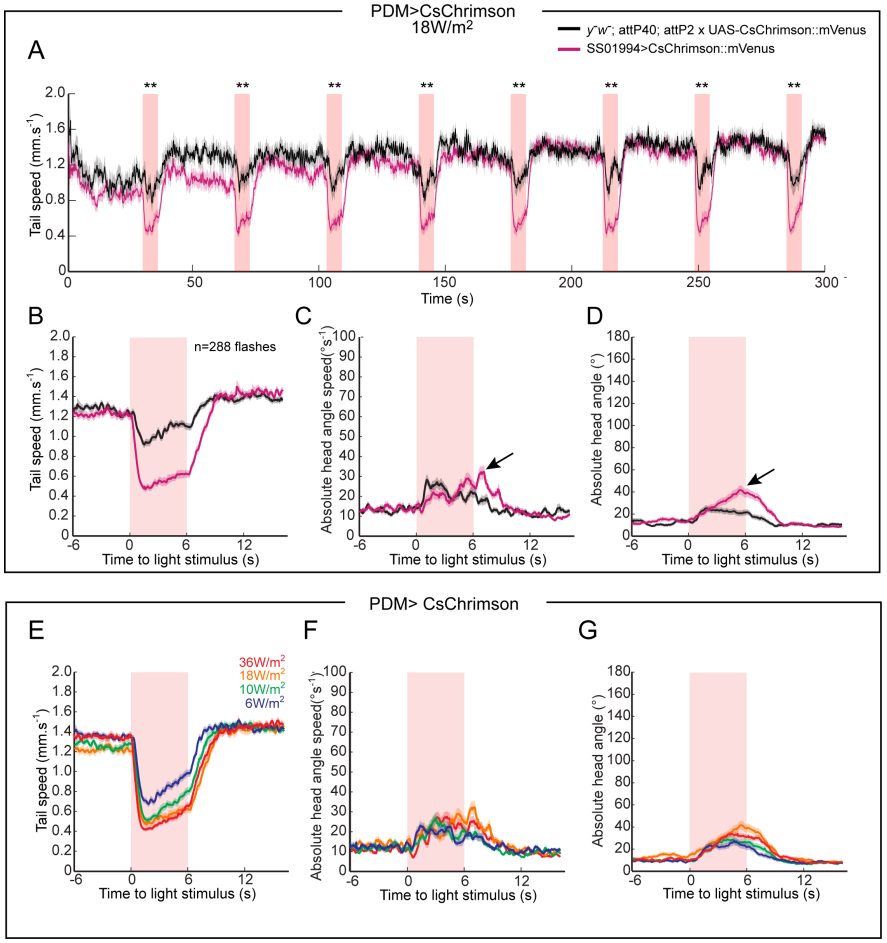

Figure 4.5: Sufficiency of the PDM neuron to evoke pauses A: Pausing behavior was quantified as a function of tail speed. Average tail speed of the SS01994>CsChrimson (magenta) and the parental control (black) larvae were quantified for a duration of 5 min during which 8 consecutive light flashes interspersed by 30 seconds were applied (light red boxes). For each light flash, the average tail speed was significantly lower for SS01994>CsChrimson compared to the parental control ($p<0.05$, Kolmogorov-Smirnov test). Parental

control larvae exhibited a slight decrease in the tail speed due to the startle response. Shaded area indicates standard error of the mean. **B:** The average tail speed for all the flashes (n=288 flashes). The difference between the PDM>CsChrimson (magenta) and parental control (black) is clearly visible. **C**: In order to quantify the reorientation maneuvers (head casts and turns), average head angular speed was measured upon PDM activation. Parental control exhibited an increase in the head angle speed at the onset of the light stimulus as a part of the startle response. Conversely, PDM>CsChrimson larvae showed a delayed increase in the head angular speed (arrow) following the pausing behavior. **D:** Absolute head angle upon activation of the PDM neuron. The delayed response of the PDM activated larvae was shown (arrow). **E-G:** The PDM activation phenotype was quantified for different strengths of activation. Four red light intensities were tested (6, 10, 18 and 36 W/m^2). **E:** Robust pausing behavior was observed except for 6 W/m^2 (blue). **F and G:** The delayed increase in the head angular speed is observable only at high intensities (18 and 36 W/m^2, orange and red). For 6 and 10 W/m^2 (blue and green) the response resemble the startle response of the parental control.

We asked whether unilateral activation of the PDM neuron would still induce pausing behavior. To answer this question, we stochastically expressed Chrimson in the PDM neuron only on one side of the brain Figure 4.6A, left panel) using the previously mentioned 'Flip-out' technique (for Flip-out technique see Figure 2.4). We showed that unilateral activation of the PDM neuron was sufficient to trigger pausing behavior (Figure 4.6A, right panel), suggesting that PDM activity is bilaterally distributed in its downstream circuitry to affect both sides of the brain (see below and Figure 4.10 for the EM connectivity)

We tested whether the pausing behavior could be sustained with prolonged PDM activity. To this end, we applied 12 s red light flashes to PDM>CsChrimson larvae. We observed an initial pausing behavior,

which lasted 3 seconds (similar to what we observed in 6 second activation paradigm). Then, larvae continued forward locomotion albeit with a decreased tail speed that plateaued around 7 s after the onset of the light flash and returned to normal after the light offset (Figure 4.6B). That is, although prolonged activation of PDM cannot keep the larva in the pausing state for more than 3 s, it is able to slow down the locomotion for longer time. This observation suggests that the neural circuitry underlying the PDM-induced pausing behavior must have evolved to ensure that the larva does not stay in pausing state for more than a couple of seconds.

Does the pausing behavior triggered by activation of the PDM neuron depend on the behavioral state? To answer this question, we activated the PDM neuron exclusively when the larva engaged in turning behavior (Figure 4.6C). By quantifying the tail speed, we showed that PDM is able to evoke pausing behavior during turns as well; suggesting that PDM-triggered pausing behavior independent of the behavioral state the larva at the moment of PDM activation.

Activation of the PDM neuron in the absence of olfactory sensory information suggests that PDM is involved in pausing behavior (Figure 4.5 and 4.6). Moreover, PDM activation can also induce delayed head sweeps and turning behavior depending on the activity level of the PDM neuron (Figure 4.5C and D). We then decided to study the effects of PDM activation during chemotaxis in odor gradients. We placed the larva in 12x12 cm Petri dish covered with 2% agarose. We used a single droplet of 10mM ETB in the middle of the square petri dish and randomly activated the PDM neuron during chemotaxis. We performed a post-hoc analysis of PDM activation for up-gradient and down-gradient runs defined by the absolute value of the bearing angle θ. We defined 4 bins of absolute bearing angle (Figure 4.6D): $0° < |\theta| < 45°$ and $45° < |\theta| < 90°$ for up-gradient

runs and 90°<Iθ I<135° and 135°<Iθ I<180° for down-gradient runs. We observed that PDM activation robustly evoked pausing behavior for all bearing angles tested (Figure 4.6E). An intriguing observation was the differential modulation of the head sweeps by the bearing (Figure 4.6F). When the larva was approaching the odor source in a relatively straight path (0°<Iθ I<45°) the head angular speed did not increase upon PDM activation (Figure 4.6F, red line). During suboptimal up-gradient runs (45°<Iθ I<90°), the average head angular speed increased only slightly but it was below the threshold for a head cast (Figure 4.6F, orange line). That is, during up-gradient runs PDM activation does not seem sufficient to evoke head casting and turning behavior. Conversely, activating PDM during down-gradient runs (90°<Iθ I<135° and 135°<Iθ I<180°) triggered a strong increase in the average head angular speed, suggesting that PDM-induced pauses are followed by reorientation during down-gradient runs (Figure 4.6E, green and blue lines).

Altogether, we concluded that the PDM neuron robustly evokes pauses, irrespective of the behavioral state. Moreover, unilateral activation of the PDM neuron is sufficient to trigger pauses. However, the reorientation behavior triggered by strong activation of PDM depends on the sensory experience: reorientation is observed only if PDM is activated following a negative sensory experience. In short, we suggest that PDM activation is involved in the pausing phase of the run-to-turn transitions. However, it does not necessarily lead to changes in direction although it is permissive to reorientation: if PDM activity is preceded by a negative sensory experience, PDM-evoked pauses are often followed by reorientation maneuvers. Otherwise, larvae continue forward runs following the pauses.

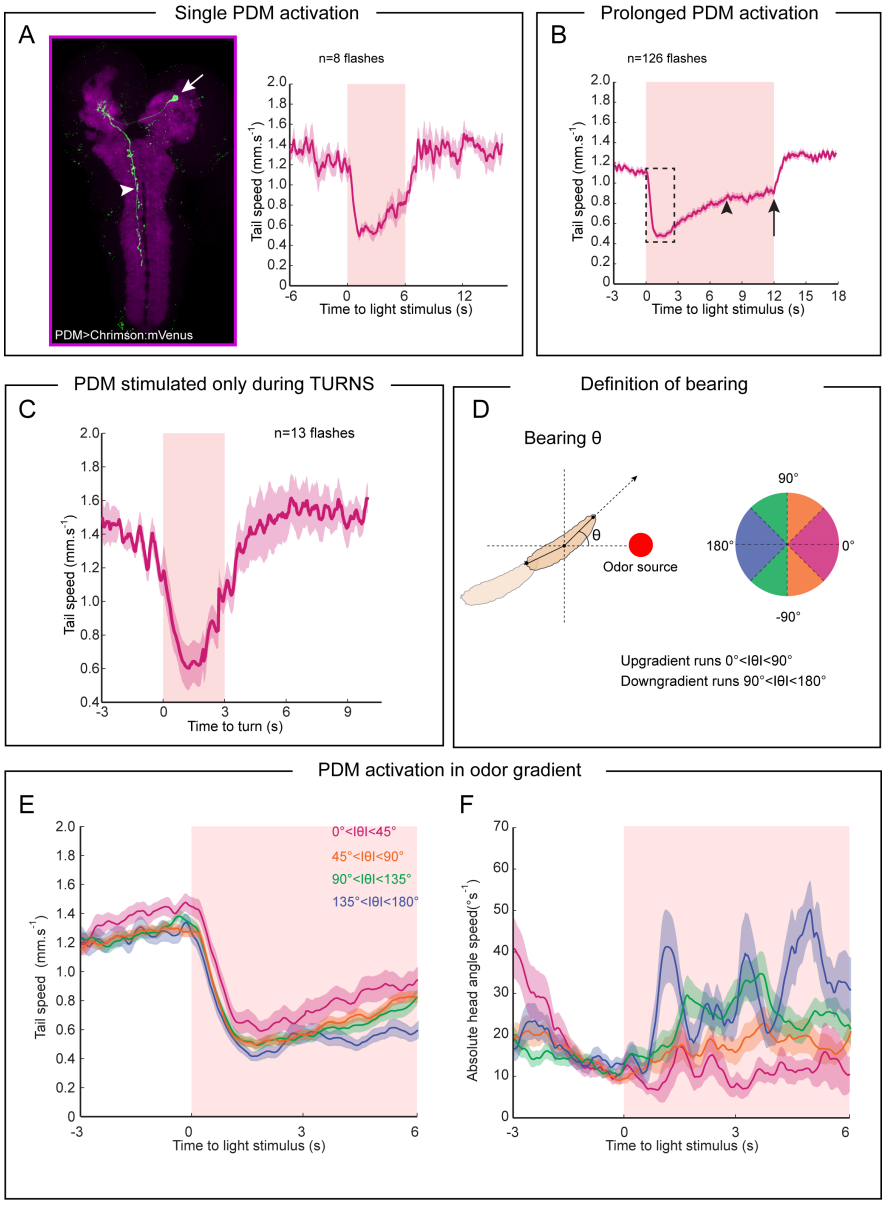

Figure 4.6: High-resolution analysis of PDM>CsChrimson larvae upon acute optogenetic activation A: Unilateral activation of PDM by stochastically expressing CsChrimson::mVenus in a single PDM neuron using the 'Flip-out' technique explained in Chapter 2 (Figure 2.4 C and D). Immunostaining against mVenus protein confirmed that CsChrimson::mVenus was expressed unilaterally (left panel). Acute optogenetic activation of a single PDM neuron was sufficient

to evoke pauses quantified as average tail speed (right panel). Shaded area indicates SEM. **B:** Prolonged activation of the PDM neuron led to a transient pause (dashed box) followed by slower locomotion that plateaus around the 7th second of optogenetic activation (arrow head). Upon light offset, larvae immediately switched back to normal crawling speed (arrow). **C:** The pausing triggered by PDM activation was indifferent to the behavioral state. The PDM neuron was activated only when the larva engaged in a turn. Strong drop in the tail speed suggests that PDM activation during turns could trigger pausing. **D** Definition of bearing (θ) in odor gradients. Absolute bearing values between 0° and 90° correspond to up-gradient runs. Absolute bearing values between 90° and 180° correspond to down-gradient runs. We defined four bins for our analysis: Straight up-gradient: 0°<Iθ I<45°, sub-optimal up-gradient: 45°<Iθ I<90° and two down-gradient bins: 90°<Iθ I<135° and 135°<Iθ I<180°. **E-F:** The effect of PDM activation in odor gradients. **E:** PDM-induced pauses were indifferent to bearing. Upon PDM activation, strong drop in tail speed was observed for all four bins. **F:** For up-gradient runs (magenta and orange) PDM did not evoke strong head casts measured as the head angle speed. On the other hand, PDM activation during down-gradient runs led to strong increase in head angular speed (blue and magenta), especially when the odor source was at the back of the larva (135°<Iθ I<180°, blue). Shaded areas indicate standard error of the mean.

4.3.5 Neurotransmitter profiling of the PDM neuron:

In order to find out whether the PDM neuron is excitatory or inhibitory, we made use of immunostainings for three main neurotransmitters of the larval brain: Gamma-aminobutyric acid (GABA), glutamate and acetylcholine (Figure 4.7A). GABA is an inhibitory neurotransmitter in the larva while acetylcholine was shown to be excitatory. Glutamate might be either excitatory or inhibitory depending on the glutamate receptors expressed in the downstream neurons. Immunostaining for GABA and glutamate together with PDM labeling

(SS01994>CsChrimson::mVenus) showed that PDM did not express either of them (Figure 4.7A, left and middle column). Choline acetyltransferase (ChaT) enzyme is necessary for the synthesis of acetylcholine. Therefore, we used antibodies against ChaT to see whether PDM is cholinergic. Indeed, PDM labeling showed colocalization with ChAT staining (Figure 4.7A, right column), suggesting that PDM is cholinergic. We further showed that PDM is cholinergic by using RNAi against ChaT while activating the PDM neuron using optogenetics. RNAi knock down of ChaT abolished the PDM activation phenotype (we compared minimum average tail speed for both genotypes, $p<0.05$ Wilcoxon signed rank test), suggesting that acetylcholine release is necessary for PDM-evoked pauses (Figure 4.7B). Therefore, we concluded that PDM is likely to be a cholinergic excitatory neuron.

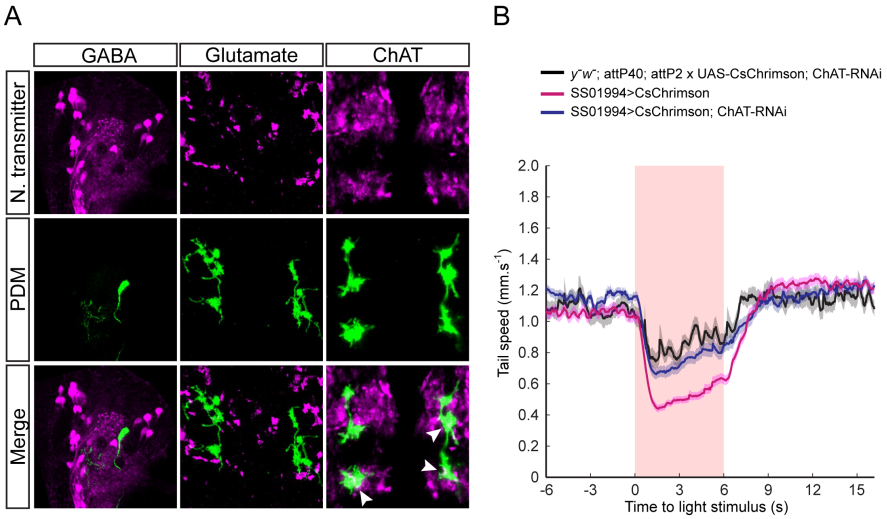

Figure 4.7: Neurotransmitter profiling of the PDM neuron A: SS01994>CsChrimson::mVenus larvae were immunostained against the mVenus protein (green) together with immunostaining against each of the three main neurotransmitters of the larval nervous system (magenta): Acetylcholine, gamma-aminobutyric acid (GABA) and glutamate. GABA was clearly visible in neuronal cell bodies in the larval nervous system. However, there was no colocalization of

GABA signals in the soma of the PDM neuron (left column, MERGE). Glutamate was not colocalized in the PDM axon terminals (middle column, MERGE) while it was clearly visible as magenta puncta for other neurons (upper row). PDM labeling colocalized with choline-acetyltranferase immunostaining shown as white puncta (bottom row, MERGE), suggesting that the is cholinergic. B: RNAi knockdown of acetylcholine (ChaT) alleviated the pausing behavior triggered by optogenetic activation of the PDM neuron. CsChrimson::mVenus was co-expressed with choline-acetyltranferase RNAi (SS01994>CsChrimson, ChAT-RNAi, blue line). Responses induced by red light flashes were analyzed as a function of tail speed. Shaded areas indicate standard error of the mean.

4.3.6 Effect of PDM activation on the peristaltic waves:

After showing that PDM is sufficient to evoke pauses during larval chemotaxis, we decided to study the effect of the PDM activity at the level of muscle contractions. Larval forward locomotion comprises repetitive cycles of wave-like peristaltic contractions starting from the most posterior segments and ending at the anterior segments (Heckscher, Lockery et al. 2012). Each of the eight abdominal segments sequentially relaxes and contracts beginning from the most posterior abdominal segment, leading to peristaltic waves traveling from tail to head. At the beginning of the peristaltic wave, tail speed is maximized due to a mechanism called visceral piston phase (see section 1.5 for the explanation of visceral piston phase) (Heckscher, Lockery et al. 2012). This feature could readily be seen as wave-like pattern of the tail speed (Figure 4.8A, bottom trace). Then each abdominal segment contracts sequentially, advancing the body forward. At the end of the wave the skeleton length is maximal since all body segments finished their forward movements (Figure 4.8A, top trace). Therefore, we can define the wave cycle as the period between the maxima of the local tail speed and the

skeleton length (Figure 4.8A) since they mark the beginning and the end of a wave cycle, respectively.

Next, we decided to find whether PDM activation could cease the peristaltic wave propagation immediately at the initial phase of the wave cycle. We coarsely divided the peristaltic wave into six equal phase bins from 0° to 360° (Figure 4.8B). We run a post-hoc analysis of the tail speed upon PDM activation at different phases of peristaltic contraction. In the phase plot in Figure 4.8B, each point represents an independent PDM activation event together with its corresponding segment, color-coded according to the defined phase bins (Figure 4.8B, top panel). Thus, we could study the effect of PDM activation during the initial phase of the peristaltic wave after the wave was initiated.

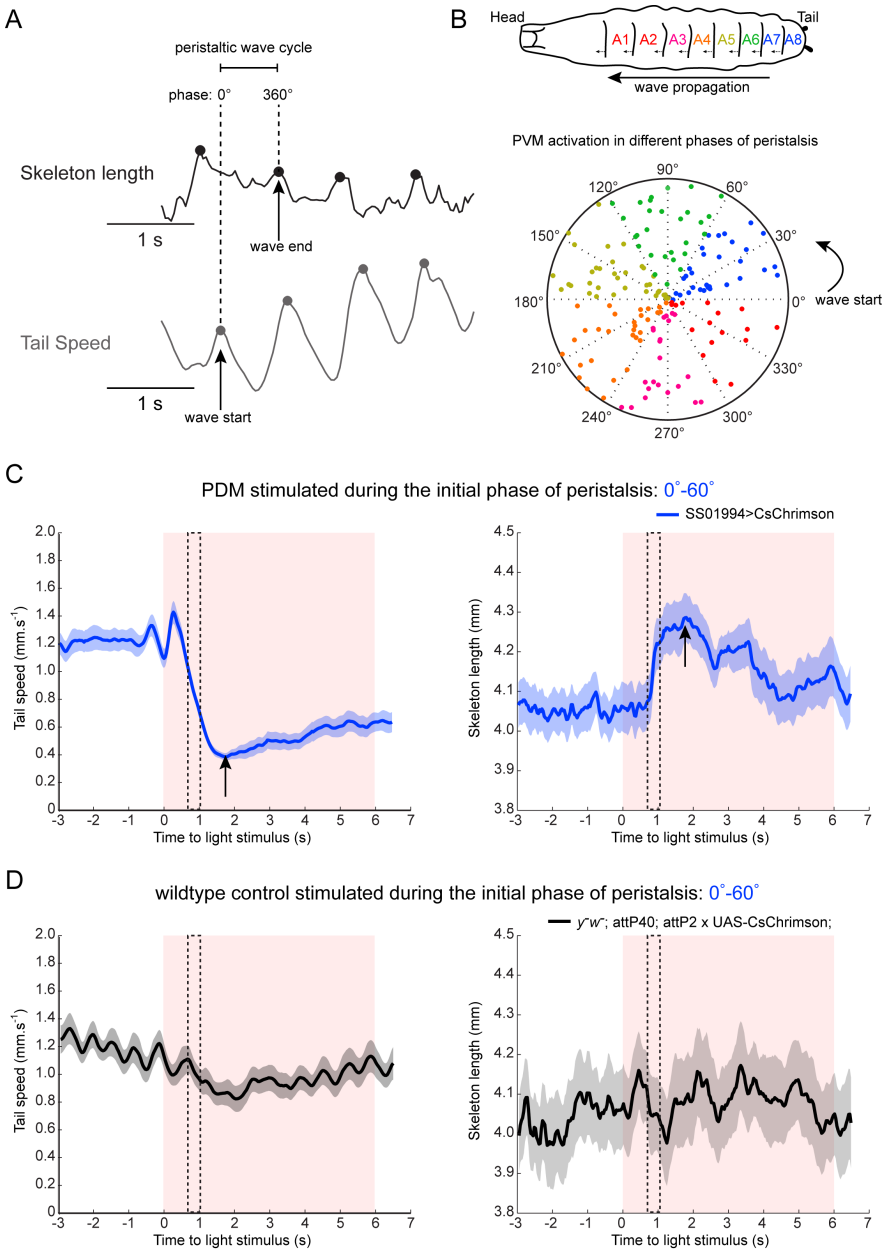

Figure 4.8: Effect of on the peristaltic waves A: Skeleton length (upper trace) and tail speed (bottom trace) exhibit wave-like pattern during forward locomotion. At the beginning of a peristaltic wave tail speed (gray dots) is maximized followed by the extension of the larval body to its maximum length at the end of the wave (black dots). The peristaltic wave cycle was defined as the

period between consecutive tail speed and skeleton length maxima. **B:** The wave cycle was divided into six equal phase bins. Upper panel indicates the abdominal segments color-coded according to phase bin during which they contract (blue: 0°- 60°, green: 60°- 120°, yellow: 120°- 180°, orange: 180°- 240°, magenta: 240°- 300° and red 300°- 360°). A1-A8 indicates the abdominal segments. Upon post-hoc analysis of PDM activation, the corresponding phases of the onsets of PDM activation were shown on a phase plot (bottom panel). Identical color-codes are used for both panels. **C:** Tail speed (left panel and skeleton length (right panel) was quantified for the PDM activation during the initial phase of the peristaltic wave (0 °- 60°, blue). In the left panel, larvae experienced a sharp decrease in the tail speed shortly after the onset of the light flashes (left panel, dashed rectangular box) and the tail speed quickly reached its minimum value (left panel, arrow). During the same period the skeleton length increased steeply (right panel, dashed rectangular box) reaching a maximum around the same time the tail speed was minimized (right panel, arrow). **D:** Same as C for the parental control. The skeleton length was not maximized (right panel) upon light stimulation although there was a slight decrease in the tail speed (left panel). For comparison, the dashed rectangular boxes are placed at the same time point they were placed in C.

When PDM activation coincided with the initial phase of the peristaltic wave (phase: 0° to 60° corresponding to A7-A6 segment color-coded in blue), we observed a sharp decrease in tail speed shortly after the onset of the activation (Figure 4.8C, left panel dashed box). In the same time window, the skeleton length exhibited a steep increase (Figure 4.8C, right panel dashed box), reaching its maximum value concurrent with the dip in the tail speed (Figure 4.8C arrows). We had previously discussed that PDM activation could keep the larva in pausing state for maximum ~3 seconds (Figure 4.6B). Consistently, we observed that the skeleton length was significantly higher than the baseline only during the initial 3 seconds of PDM activation, suggesting that the larva stayed in a fully stretched

(relaxed) pausing state in this period. Although the parental control showed a shallow decrease in tail speed we did not observe any increase in the skeleton length upon the same pattern of light stimulus utilized to activate the PDM neuron (Figure 4.8D). This observation implies that the larva does not stop the wave immediately upon PDM activation. The wave is rather completed and the larva reaches its maximal length at the end of the wave. However, a new peristaltic wave could not be initiated, keeping the larva in the fully stretched pausing state.

4.3.7 Segmental analysis of the PDM activation phenotype:

We wanted to corroborate our finding that the PDM neuron cannot cease an already initiated wave, but it prevents the initiation of a new cycle. In order to achieve this, we decided to study the segmental contractions upon PDM activation. We made use of the fact that each abdominal segment can be distinguished by visualizing the pigmented denticle bands (hairy structures that help each abdominal segment attach and pull themselves on the substrate during locomotion) on the ventral cuticle of the larva (Berni 2015, Pulver, Bayley et al. 2015). We pinned the larva on a polydimethylsiloxane (PDMS) slab and visualized the movements of the denticle bands upon optogenetically activating the PDM neuron (Figure 4.9A). We collected a dataset in which PDM activation coincided with the contraction of each segment at least once. Consistent with our previous observation, PDM activation could not cease peristaltic wave immediately but it prevented the larva from initiating a new wave (Figure 4.9B-H).

We quantified peristaltic waves as sequential displacement of the abdominal segments from A7 to A1 (Figure 4.9B-H, vertical dashed lines

indicate each wave cycle). When PDM was activated between the end of a wave and the start of the next cycle, we observed that a new cycle could not be initiated (Figure 4.9B). For other segments we observed that the wave was finalized upon PDM activation but the next wave could not be initiated (Figure 4.9C-H), corroborating the results of our previous analysis with the tail speed and the skeleton length (Figure 4.8).

In our segmental analysis, we observed an interesting phenotype when PDM activation coincided with the contraction of A7. Upon activating PDM, the wave continued but was immaturely ceased in the middle segments (Figure 4.9I). This suggests that the PDM neuron is capable of ceasing peristaltic wave immaturely only if its activation precisely coincides with the wave initiation. However the effect was still slightly delayed since the wave was often terminated in A4 or A5 (~70% of all observations). As discussed later in this chapter, the circuit motif downstream the PDM neuron might help us explain this phenotype (see Figure 4.11). Our findings suggest that the PDM neuron is more likely to act on the motor pattern generators in the VNC that are responsible for the initiation of the peristaltic waves. Once the wave initiation is completed, PDM is no longer capable of ceasing the cycle until the initiation of the next wave.

4.3.8 Analysis of fictive locomotion in motor neurons upon PDM activation:

High-resolution behavioral analysis (Figure 4.8) and the dissection of the effect of PDM activation at the level of segmental contractions (Figure 4.9) suggest that the PDM neuron influences the initiation of the

peristaltic wave in the most posterior abdominal segments. Next we asked how PDM activation is implemented in the motor neuron activity.

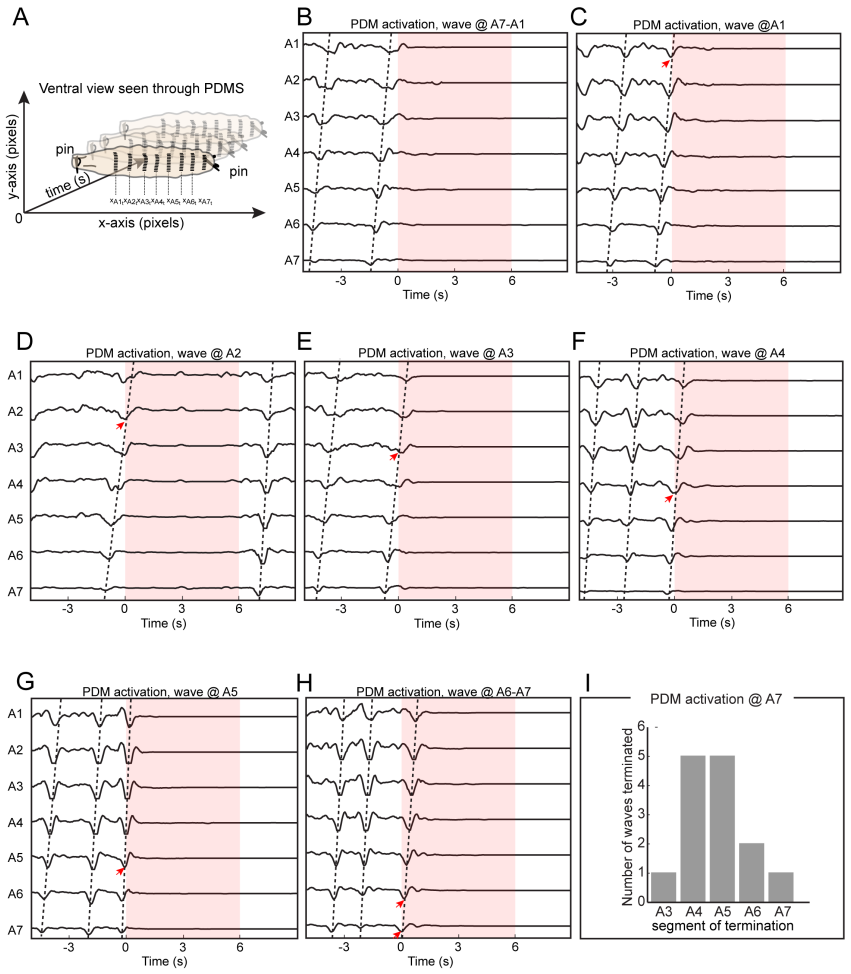

Figure 4.9: Characterization of the PDM activation phenotype at the level of segmental contractions A: Schematic for the experimental setup. 3rd instar larvae were pinned down on a PDMS slab ventral side touching the PDMS surface. The contractions of the abdominal segments could be quantified by visualizing the denticle bands on the ventral side of the body (each abdominal segment has a denticle band). **B-H**: The contractions of the abdominal segments upon PDM activation were quantified as a function of denticle band displacement for A1-A7. Each horizontal dashed line indicates a complete peristaltic wave such

that wave starts with the contraction of A7 and ends with A1. **B:** Onset of PDM activation was between the end of a wave and start of a new wave (A7-A1). **C:** Onset of PDM activation was between the contractions of A1 and A2 and so on for **D-H**. For all cases, a wave that had already started could not be ceased immediately by the PDM activation but a new wave could not be initiated at least until the offset of the PDM activation. **I:** When the onset of PDM activation coincided with the beginning of A7 contraction, the wave was immaturely ceased at different segments ranging from A3 to A7. The wave was immaturely terminated often at the 4^{th} and the 5^{th} segments (10/14 or ~70% of all cases).

Motor neurons and abdominal muscles form a myotopic map: motor neuron dendrites are organized into distinct domains in the VNC that represent the segmental organization of their target muscles at the periphery (Landgraf, Jeffrey et al. 2003). It is also very likely that motor pattern generators (CPG) are organized in a similar topographical way (Kohsaka, Okusawa et al. 2012, Fushiki, Zwart et al. 2016) to ensure that oscillations in these networks are coordinated with the sequential contractions of the segmental muscles. Therefore, we decided to study the effects of PDM activation on the motor neuron activity as a first step to understand the mechanisms of the PDM-induced pausing behavior at the neuronal level.

It has been shown that isolated larval CNS devoid of any sensory input can still produce rhythmic patterns of motor neuron activity (fictive locomotion) coordinated in a similar way with the segmental muscle contractions (Lemon, Pulver et al. 2015, Pulver, Bayley et al. 2015). We expressed a calcium indicator in motor neurons (VGLUT-lexA>GCamP6f) to monitor the effect of optogenetic PDM activation (SS01994>CsChrimson::mVenus) on fictive locomotion (Figure 4.10A). In an isolated CNS preparation (Pulver, Bayley et al. 2015), we observed rhythmic patterns of motor neuron activity generating fictive forward

locomotion (Figure 4.10B). Like muscle contractions, motor neuron activity started in the most posterior segments (A8/9) and sequentially progressed to the most anterior segment A1 (Figure 4.10C, black dashed lines labeled as F). However, the frequency of wave generation was ~5-10 times lower compared to the intact larval locomotion as reported previously (Berni 2015, Pulver, Bayley et al. 2015).

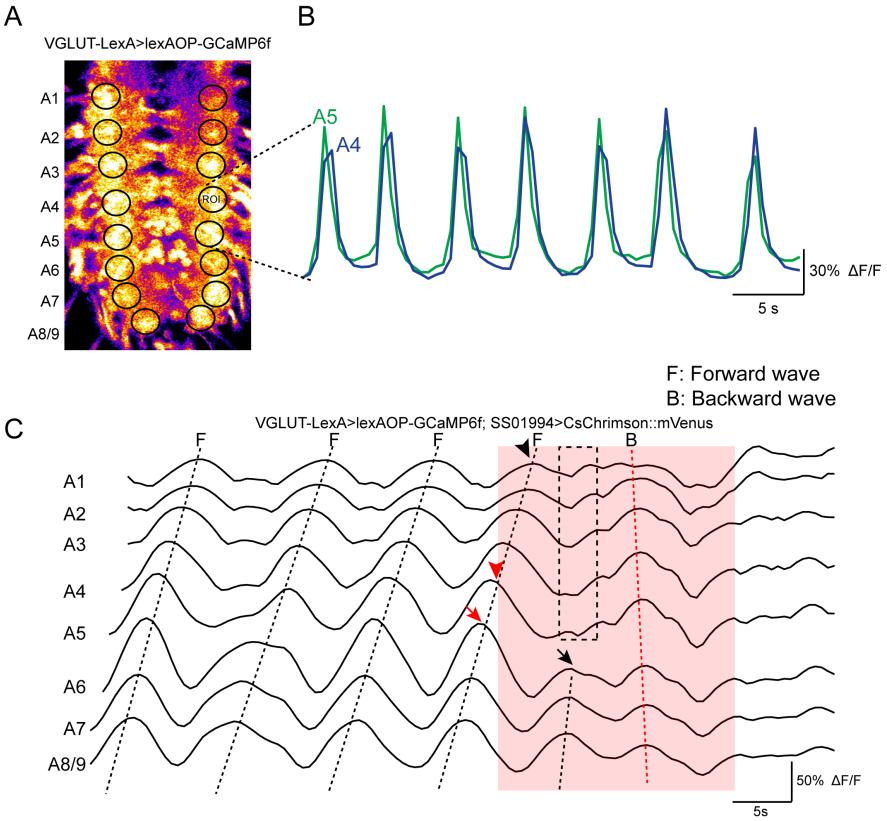

Figure 4.10: The effect of PDM activation at the level of motor neurons A: In order to measure neural activity, motor neurons were labeled by expressing GCamP6f under the control of VGLUT-LexA driver line. For each abdominal segment, isometric regions of interest (ROIs) were drawn where motor neuron axons from the same segment bundle together (circles). A1-A8/9 indicate the segment locations. **B:** Motor neuron activity in an isolated CNS was quantified from ROIs as a function of normalized change in fluorescence intensity (ΔF/F). In

an isolated CNS covered with saline, motor neurons formed wave-like activity pattern from posterior to anterior resembling the peristaltic waves of muscle contractions (fictive locomotion). **C:** Fictive locomotion shown as waves of motor neuron activity. Each horizontal dashed line indicates a single fictive peristaltic wave beginning at A8/9 and ending at A1. After a sequence of forward waves (F), The PDM neuron was optogenetically activated (SS01994>CsChrimson::mVenus) with stimulus onset coinciding with the increase in the motor neuron activity at A4 (red arrowhead). The wave was successfully finalized at A1 (black arrowhead). Then, although a weak wave was reinitiated at A8/9 it was immaturely terminated at A6 (arrow) without observable waves of motor neuron activity from A5 to A1 (dashed box). Eventually a backward wave (B) was generated. Red box indicates the red light flash to activate the PDM neuron.

After successfully monitoring the rhythmic motor neuron activity, we activated the PDM neuron (a representative case was illustrated in Figure 4.10C, note the forward waves as horizontal dashed lines before the PDM activation). When the onset of PDM activation coincided with the peak of the motor neuron activity in A4 (Figure 4.10C, red arrowhead), the wave was completed (black arrowhead) consistent with what we observed in the segmental analysis (compare to Figure 4.9F). As for the next wave, the motor neuron activity sequentially increased from A8 to A6 although the peak level of activity for these segments were much lower compared to the previous cycles (compare the corresponding intensity changes for the red and black arrows). Expectedly, the wave was terminated at A6 with absence of increase in the motor neuron activity from A5 to A1 (dashed box). Unlike what we observed in the segmental analysis, a backward wave was initiated after the inhibition of the forward wave. We did not observe this reversal in our segmental analysis. Since the relative frequency of backward waves are significantly increased in isolated CNS preparations (Lemon, Pulver et al. 2015, Pulver, Bayley et al. 2015), we

speculate that the reversal might be due to the change in the dynamics of forward and backward wave generating networks.

In short, by showing the effect of PDM activation on segmental contractions and motor neuron activity we conclude that PDM evokes pausing behavior by inhibiting forward wave initiation in the posterior segments. However, the mechanisms underlying this inhibition are yet to be explained at the level of the motor pattern generating circuits downstream of the PDM neuron.

4.3.9 EM reconstruction of the downstream partners of the PDM neuron:

Identification of the downstream partners of the PDM neuron is a crucial step toward studying the mechanisms of the forward wave inhibition mediated by the PDM neuron. Therefore we decided to find the downstream partners of the PDM neuron in the EM dataset (section 4.3.3) generated in Janelia Research Campus.

Avinash Khandelwal identified several downstream partners of the PDM neuron, by connecting the PDM neuron to the neurons that were already reconstructed by the other members of the collaborative EM reconstruction project led by Albert Cardona. EM reconstruction of the circuits downstream of the PDM neuron is still in progress. Nevertheless, we here present an interesting motif that we observed while analyzing the EM connectivity data.

Recently, Fushiki et al. reported a circuit mechanism for forward wave locomotion (Fushiki, Zwart et al. 2016). They characterized an excitatory

premotor neuron, A27h together with an inhibitory interneuron called GDL. GDL and A27h form segmentally repeated alternating excitatory and inhibitory connections throughout the abdominal and the late thoracic segments. They showed that A27h excites motor neurons in the same segment that connect to the longitudinal muscles involved in forward locomotion (Kohsaka, Okusawa et al. 2012). Moreover, A27h neuron excites the inhibitory GDL neuron in the adjacent anterior segment. GDL neuron in turn suppresses the activity of the A27h neuron in the same segment. Therefore, A27h activity in a particular segment leads to contraction of the muscles in that segment while relaxing the muscles in the adjacent anterior segment by activating inhibitory GDL neuron. The connectivity pattern of the A27h neurons suggests that the alternating excitation-inhibition mechanism might underlie the forward wave propagation.

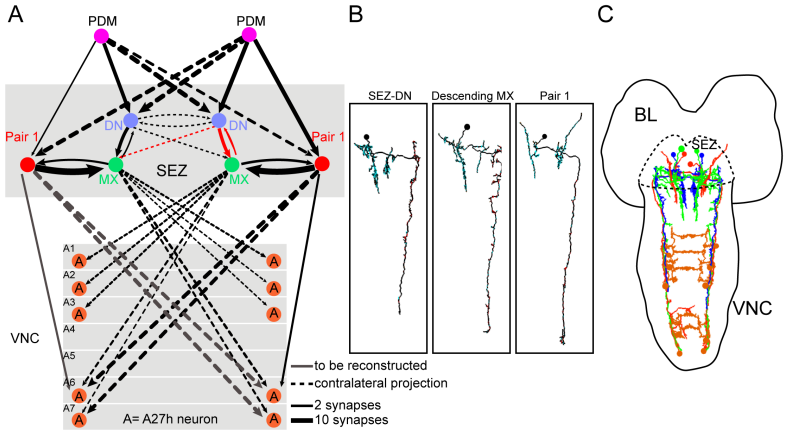

Figure 4.11: Downstream partners of the PDM neuron revealed by EM reconstruction A: Downstream connectivity diagram of the PDM neuron in the EM volume. PDM gives bilateral outputs on the Pair 1 neuron as well as the Descending SEZ (DN) neuron. Pair 1 and SEZ-DN ipsilaterally synapse on the Descending MX (mx) neuron. Pair 1 neuron is bilaterally connected to the A27h neurons in the posterior segments A7 and A6. Descending MX neuron is contralaterally connected to the A27h neurons in all segments except A4 and A5.

Note that descending inputs from the SEZ skip the 4th and the 5th segments. **B:** Morphology of the descending SEZ neurons downstream of the PDM neuron. Cyan dots indicate post-synaptic sites. Red dots indicate pre-synaptic sites. **C:** Overall connectivity of the descending SEZ neurons. Pair 1 (red), Descending MX (green) and Descending SEZ (blue). A27h neurons are shown in orange.

Interestingly, preliminary analysis of the EM connectivity data showed that the PDM neuron is connected to the A27h neuron through a set of descending neurons in the SEZ region (Figure 4.11A). Since PDM is responsible for ceasing forward locomotion presumably by inhibiting the A27h neuron we decided to analyze this pathway in detail.

We observed that the PDM neuron is differentially connected to the A27h neuron in the anterior and the posterior segments. In segments A6 and A7, the A27h neurons receive bilateral input from the Pair 1 descending neuron (Figure 4.11A and Figure 4.11B right panel), which itself receives direct bilateral input from the PDM neuron. In addition, they also receive contralateral input from another SEZ descending neuron called MX neuron (Figure 4.11A and Figure 4.11B middle panel). MX neuron receives direct ipsilateral input from the Pair 1 neuron together with indirect input from the PDM neuron via yet another SEZ descending neuron called DN (Figure 4.11A and 4.11B left panel). Unlike the posterior segments, A27h neurons in A1-A3 receive contralateral input only from the MX neuron. Altogether, these SEZ descending neurons form an intricate network of connectivity with the A27h neuron that spans across the entire abdominal ganglia (Figure 4.11C and 4.12A and C).

In short, the PDM neuron excites a network of SEZ descending neurons (SEZ-DNs, Figure 4.12A and C) that connects to the circuit involved in the actuation of forward wave propagation. The SEZ-DNs form a feed

forward motif that presumably inhibits the contraction of the anterior and the posterior segments (Figure 4.12C). Differential connection of the SEZ-DNs to the posterior and the anterior segments might provide dynamical features underlying the fact that PDM cannot cease the wave during the later phases of wave propagation. In the future, identification of the SEZ-DNs will help us unravel the neural mechanisms of the PDM-evoked pauses.

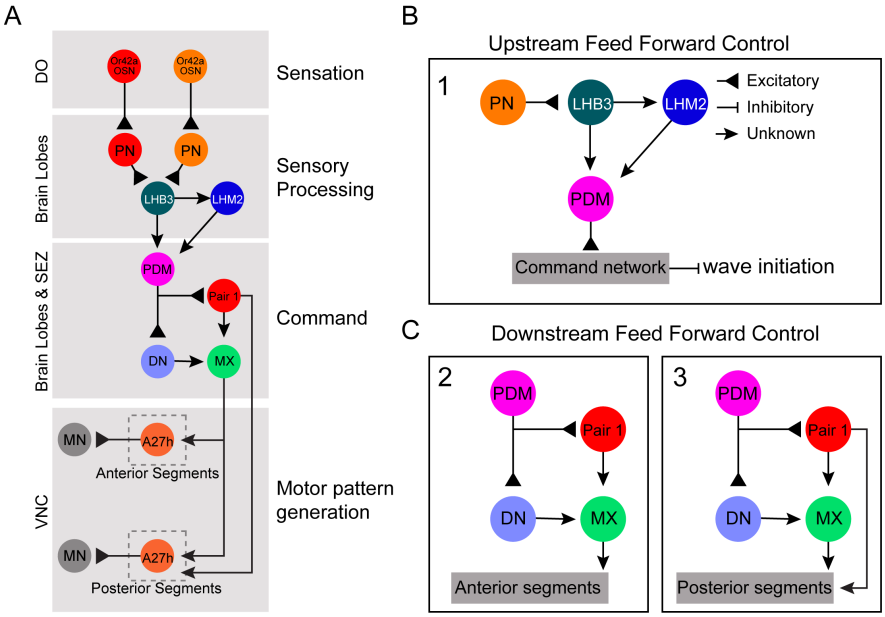

Figure 4.12: Summary of the PDM connectivity A: Connectivity diagram of the PDM pathway from OSNs to motor neurons. For simplicity only unilateral connections are shown. Odorant molecules are sensed in the dorsal organ by OSNs. Sensory processing takes place in the brain lobes starting with the antennal lobe and continuing with the lateral horn. Upstream of the PDM neuron, LHB3 and LHM2 form a feed-forward motif. We propose that PDM is part of a descending command circuit that also includes the downstream neurons of the PDM in the SEZ: Pair 1, DN (SEZ-DN) and MX (Descending MX). This descending command circuit receives integrated sensory input from the LH and sends the 'pause' signal to the motor pattern generators in the VNC. Downstream

neurons of PDM also form feed-forward control on the pattern generating circuits. The command circuit is differentially connected to the anterior and the posterior segments in the VNC. The functional implications of this connectivity pattern are yet to be unraveled. **B:** The feed-forward motif upstream of the PDM neuron (1). To determine the type of the feed-forward motif (coherent types or incoherent types) PDM participate in, one will have to study the neurotransmitters released by the LHB3 and LHM2 neurons. We propose a possible network motif in Figure 4.13. **C:** Downstream feed-forward control. PDM sends excitatory inputs to SEX-DN and MX neurons. Since the descending circuit is supposed to inhibit the excitatory pre-motor neuron A27h, we speculate that Pair 1 neuron is excitatory and MX neuron is inhibitory. This type of network motif together with differential connections in the anterior (2) and the posterior (3) segments might explain the delayed pausing in A4 and A5 when PDM activation coincides with A7 contraction.

4.4 Discussion:

4.4.1 Sensorimotor processing in the larval brain:

Despite the considerable amount of knowledge about the peripheral olfactory coding (Wilson 2013, Kim, Lazar et al. 2015, Schulze, Gomez-Marin et al. 2015) and the motor control (Kohsaka, Okusawa et al. 2012, Berni 2015, Pulver, Bayley et al. 2015, Fushiki, Zwart et al. 2016), we still lack the anatomical and functional information on how olfactory sensory information is transformed into coordinated actions in the *Drosophila*. Recent advances in genetic tools and EM reconstruction of the whole larval brain transformed the larva into an excellent model organism to map and crack the circuits governing chemotaxis.

Sensorimotor processing in the larval brain is likely to comprise at least four main steps (Figure 4.12A). First, sensory neurons at the periphery receive the sensory signals and carry them to specialized neuropiles in the brain lobes such as the antennal lobe (Gerber and Stocker 2007) and the optic neuropile (Sprecher, Cardona et al. 2011). Early sensory processing already takes place in these regions (sensory coding) (Wilson 2013). Second, information from multiple sensory modalities converges on higher brain centers (i.e. the lateral horn and the mushroom body) (Vogt, Schnaitmann et al. 2014) and; they are integrated here (sensory integration) together with the internal states (hunger, circadian clock etc.) (Wang, Pu et al. 2013). Third, after forming a sensory perception and decision upon multi-sensory integration, commands are sent down to the motor pattern generators in the VNC via descending fibers to trigger a certain type of behavior (action selection). Finally, pattern-generating networks in the VNC produce rhythmic activity in motor neurons to

trigger coordinated muscle contractions (actuation). In turn, movement of the larva leads to a change in the local sensory environment, reinitiating the sensorimotor loop. In reality, the borders among these abstract hierarchical levels are very likely to be more indistinct. Sensory processing can be distributed all over these levels and sensory integration can take place at multiple levels (Ohyama, Schneider-Mizell et al. 2015).

4.4.2 Loss-of-function screen and identification of a descending neuron that is necessary for run-to-turn transitions in larval chemotaxis:

We performed a loss-of-function screen in order to identify neurons involved in the sensorimotor control of the larval chemotaxis. We biased our screen toward driver lines labeling the neurons potentially involved in the sensory-processing and the descending networks. The motivation behind this bias was to bridge the gap between the first layers of the olfactory processing (e.g. OSNs, PNs) and the motor circuits in the VNC. We assumed that the amount of the information about the early sensory processing (Kim, Lazar et al. 2015, Schulze, Gomez-Marin et al. 2015) and the motor pattern generation (Berni, Pulver et al. 2012, Kohsaka, Okusawa et al. 2012, Berni 2015, Pulver, Bayley et al. 2015, Fushiki, Zwart et al. 2016) would allow us to study the information processing in the neurons between them.

In our screen, we obtained 18 driver lines that label neurons involved in innate larval chemotaxis (Figure 4.1B). Interestingly, eight of these driver lines targeted the mushroom body (MB) region, which is known to be involved in learning, memory, multi-sensory integration and context-

dependent innate decision making (Gerber and Stocker 2007, Vogt, Schnaitmann et al. 2014, Lewis, Siju et al. 2015). In the future, it will be indispensible to study the role of the MB (together with the lateral horn) in innate chemotaxis to understand the sensory processing taking place in the brain lobes.

However, we initially decided to focus on the neurons that are responsible for mediating communication between the brain lobes (sensory processing and decision making) and the motor networks in the VNC (action). Through a purely anatomical assessment, we identified 4 neurons that received input from the brain lobes and projected axons down to the VNC. This type of neurons are called descending neurons due to their morphology. Descending neurons are likely to be the bottlenecks in sensorimotor transformation since they convey decisions (or action selection) made in the brain lobes to the motor pattern generating networks. In invertebrates, it has been shown that some descending neurons are capable of turning a particular motor pattern on or off (Brodfuehrer and Friesen 1986, Brodfuehrer and Friesen 1986, Kanzaki, Ikeda et al. 1994, Burdohan and Comer 1996, Staudacher 2001, Träger and Homberg 2011, Bidaye, Machacek et al. 2014, Hampel, Franconville et al. 2015). First defined in crayfish (Wiersma and Ikeda 1964), these descending neurons are traditionally called 'command' neurons (Kupfermann and Weiss 1978). By definition, command neurons receive integrated sensory input and trigger a motor pattern-generating network that is responsible for generating a fixed action pattern.

The morphology and loss-of-function phenotype of one of the descending neurons we identified (PDM) made us hypothesize that it could be a command neuron (Figure 4.2): Its dendritic arborization was around the MB and LH region and silencing this neuron led to a defect in chemotaxis.

We argued that PDM receives olfactory inputs in the LH-MB regions and; it is necessary for triggering a behavior routine important for larval chemotaxis. By using two different assays, we showed that PDM silenced larvae exhibited a decrease in turn rates in odor gradients (Figure 4.2 and 4.3). However, once the run was terminated they successfully reoriented themselves toward the odor source (Figure 4.3). These findings suggest that the PDM neuron is specifically necessary for triggering run-to-turn transitions.

4.4.3 The PDM neuron receives olfactory inputs in the lateral horn region:

We reconstructed the upstream synaptic partners of the PDM neuron to prove its connection to the olfactory centers in the larval brain. Indeed, we could show that PDM receives input from the Or42a and the Or42b channels (Figure 4.4) together with Or74a and Or82a (data not shown). Interestingly, Or42a and Or42b are the main ORs that mediate chemotaxis toward the odor we used in our screen (ethyl butyrate) (Kreher, Mathew et al. 2008, Asahina, Louis et al. 2009). Thus, EM reconstruction corroborates our findings that the PDM neuron is involved in *Drosophila* larval chemotaxis.

4.4.4 The PDM neuron is sufficient to evoke pauses during larval locomotion:

During run-to-turn transitions in chemotaxis, the larva pauses for a short period and then turns toward the gradient upon sampling its local environment via head casts (Gomez-Marin, Stephens et al. 2011). After

showing that PDM is necessary for run-to-turn transitions, we asked whether the PDM neuron is sufficient to trigger any of the behavioral subroutines (pausing, head casting and turning) taking place during these transitions. We showed that acute optogenetic activation of the PDM neuron triggered robust pausing behavior (Figure 4.5 and 4.6).

The posterior part of the larval body should be kept in pausing mode to avoid forward locomotion during the sampling period via head casts. This period is usually only a few seconds long as the larva tends to trigger a turn upon one or two head casts (Gomez-Marin, Stephens et al. 2011). The larva often triggers a turn upon a single head cast probably since in most of the cases the first head cast is already toward the direction of the gradient. In cases where the first head cast leads to a decrease in odor concentration, the larva often triggers a second head cast toward the gradient and turns in that direction. The larva rarely engages in more than 2 head casts prior to turns (less than 10% in our data set, data not shown). Since the temporal dynamics of head casts are quite fast, the larva needs only a few seconds to make sure that it reorients itself toward the odor source.

Interestingly, we showed that the PDM neuron could keep the larva in the pausing state for maximum ~3 seconds (Figure 4.6B). In order to see whether this is due to the dynamics of CsChrimson (CsChrimson has been reported to produce unreliable pattern of spike trains upon high frequency light stimulus, see section 2.3 for explanation), we used different frequencies of light flashes instead of constant activation. By using relatively low frequencies (10Hz) at which CsChrimson can produce spike trains for longer durations (Klapoetke, Murata et al. 2014), we reproduced the pausing behavior (data not shown). However, we were not able to prolong the effect. This finding suggests that the 3-second time window of

pausing is not due to the CsChrimson dynamics and it is rather implemented in the neural circuitry underlying the pausing behavior.

Although mechanisms underlying the head cast dynamics are yet to be studied it is possible that the larval nervous system restricts the sampling window to only a few seconds. In most cases, this would be sufficient to realign the direction of movement toward the gradient since the gradient direction could be detected in maximum 2 head casts (Gomez-Marin, Stephens et al. 2011). In extreme conditions where the odor information is too noisy or the gradient is too shallow, the larva might need more time to make a decision. In this case, it might be more efficient to engage in a run rather than continuing sampling via head casts. Therefore, the system might have evolved in a way that PDM activation cannot evoke pauses longer than a certain period of sampling. It is important to study the head cast dynamics and the decision rules underlying the sampling period to make a solid connection between the pausing dynamics and the PDM-evoked pauses.

How can the PDM pathway produce pauses that are no longer than ~3 seconds? It might be possible that the PDM neuron enters a depolarization block and stops firing upon sustained input from the upstream neurons. Alternatively, PDM might trigger a negative feedback mechanism such that it activates a neuron (neuron X in Figure 4.13) that in turn inhibits the PDM neuron. Thus, the temporal dynamics of the delayed inhibition might define the time window that activation of the PDM neuron can sustain the pausing behavior (Figure 4.13A and B).

4.4.5 The PDM activation phenotype in odor gradients:

When we used high intensity light to activate the PDM neuron we observed that pauses were followed by an increase in head angular speed, suggesting that larvae engaged in head casts and turn. We decided to see whether PDM activation in odor gradients is sufficient to reorient the larva toward the odor source.

Activation of the PDM neuron evoked robust pausing behavior independent of whether the larva had engaged in an up-gradient or a down-gradient run (Figure 4.6C). Notably, PDM activation evoked strong head casting only during down-gradient runs. On the other hand, the larva tended to engage in a straight run following pauses if the PDM neuron was activated during an up-gradient run. Based on this observation, we argue that pausing and sampling via head casts can be uncoupled depending on the sensory experience of the larva. That is, PDM-evoked pauses do not necessarily lead to sequential recruitment of the head casts unless the larva is experiencing negative changes in olfactory stimuli. Although pausing during an up-gradient run is likely to be rare in naturalistic conditions, the larva further ensures that turning behavior is induced upon negative sensory experience by uncoupling the pausing and the sampling behaviors.

4.4.6 The PDM neuron acts on the peristaltic wave mainly at the posterior segments:

By restricting our analysis of PDM activation to the initial phases of the peristaltic wave propagation we showed that PDM activation was not sufficient to trigger immediate pauses once the wave was already initiated. However, it did not allow the initiation of the next wave (Figure 4.8). We further corroborated this observation by analyzing the segmental contractions in intact larva (Figure 4.9) and fictive locomotion in isolated CNS preparations (Figure 4.10) upon PDM activation.

We made an intriguing observation during our analysis of the segmental contractions upon PDM activation. When the onset of PDM activation coincided with the beginning of the contraction in segment A7, the wave was immaturely terminated mostly in the middle segments A4 and A5 (Figure 4.9I). Therefore it might also be possible that PDM activation leads to a delayed inhibition at the posterior segments. Despite the delay, PDM input was sufficient to terminate the wave before it propagates to the anterior segments. However once the wave passed the segment A7, PDM was no longer able to cease the wave but it prevents initiation of a new wave cycle (Figure 4.8C, and 4.9B-H). Therefore we argue that PDM activation has stronger effect at the posterior segments.

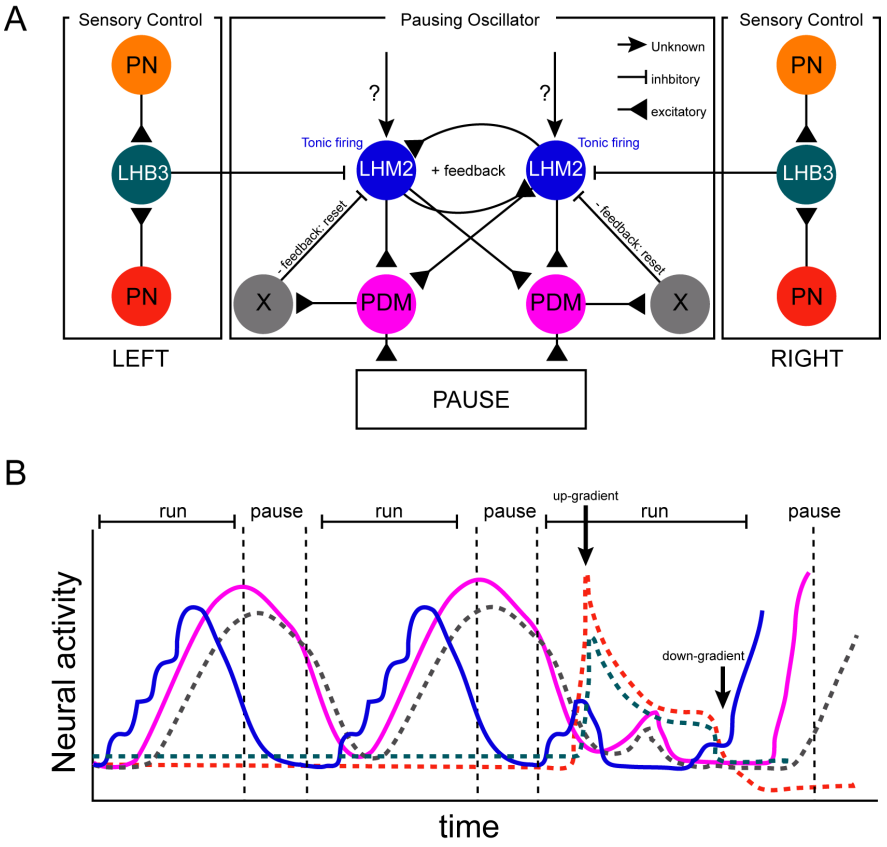

Figure 4.13: A qualitative model of the PDM pathway A: Schematic of the model (see the text for explanation). Question mark indicates a putative excitatory pathway upstream of LHM2. For example, olfactory information might converge on LHM2 from multiple pathways. It is also possible that other sensory modalities input on LHM2. X indicates a neuron that is responsible for giving negative feedback to LHM2. **B:** A qualitative graph for the proposed regulatory dynamics. Blue curve; LHM2 activity, magenta curve: PDM activity, gray curve: activity of the negative feedback neuron X, red curve: activity of the PNs and green curve: activity of LHB3. See the main text for detailed explanation.

It was shown that head casts are mediated by asymmetrical contraction in the segments anterior to segment A4 (Berni 2015, Pulver, Bayley et al. 2015). It might be possible that PDM inhibits segments posterior to A4 to

inhibit forward locomotion while allowing the generation of head casts through asymmetrical contractions in the anterior segments. Indeed, we observed an increase in head angular speed shortly after the onset of PDM activation during down-gradient runs (Figure 4.6F). On the other hand, the anterior segments remained largely inactive together with the posterior segments in our segmental analysis of PDM activation with occasional asymmetrical contractions in the anterior segments. We speculate that this might be due to the absence of olfactory input in this assay.

We also imaged fictive locomotion in isolated CNS preparations (Pulver, Bayley et al. 2015) by expressing the calcium indicator GCamP6f in the motor neurons while optogenetically activating the PDM neuron (Figure 4.10). This method allowed us to study the effects of PDM activation at the neuronal level. When we activated the PDM neuron while the motor neuron activity peaked at A4, we observed that the wave successfully propagated and terminated at A1. Then, despite an attempt to initiate at the posterior end (A8/9), the wave gradually faded away and was completely terminated before it reached A5. Conversely, a new wave cycle never started in our segmental analysis. It might be possible that low level of motor neuron activity from A8/9 to A6 is not sufficient to trigger muscle contractions that are strong enough to move the segments forward. Alternatively, isolated CNS preparation might have different dynamics due to the absence of sensory feedback (Berni 2015, Pulver, Bayley et al. 2015).

4.4.7 The PDM neuron connects to the circuits involved in forward wave propagation through a network of SEZ descending neurons:

Preliminary EM reconstruction of the downstream partners of the PDM neuron revealed that it is connected to the forward wave propagation circuitry (Fushiki, Zwart et al. 2016) through a network of descending neurons in the SEZ (Figure 4.11). We showed that PDM gives excitatory input (Figure 4.7) to this network of descending neurons. In the EM reconstruction, we observed that two of these descending neurons (MX and Pair 1) give input to the excitatory pre-motor neuron A27h that is involved in forward wave propagation (Fushiki, Zwart et al. 2016).

A27h is a segmentally repeated pre-motor neuron tiling the abdominal segment. During peristaltic wave, A27h activity is in phase with the motor neuron activity (aCC motor neuron) in the same segment. It has also been shown that A27h is capable of activating aCC motor neurons. Inhibition of A27h in the same segment by the GABAergic GDL neuron leads to relaxation of that segment (Fushiki, Zwart et al. 2016). Therefore, we suggest that the descending network downstream of PDM should inhibit the A27h neuron. Consequently, we predicted that at least one of these descending neurons should be inhibitory.

We observed that the SEZ descending neurons output differently on the posterior and the anterior segments (Figure 4.12A and C). In the posterior segments A7, both Pair 1 and MX neurons output contralaterally to the A27h neuron in a feed forward manner such that Pair 1 also outputs to the MX neuron ipsilaterally (Figure 4.12A and C). Interestingly, A27h neuron does not receive any input from this descending network in A4 and A5

(Figure 4.11A). This type of connectivity might be important for uncoupling the effect of PDM in anterior and posterior segments. At the anterior end, A27h receives contralateral input only from the MX neuron. We speculate that this differential connection pattern might underlie the stronger effect of PDM activation at the posterior segments. In the future, we aim to monitor the activity of the A27h neuron while activating the PDM neuron to test this hypothesis. However, it will be crucial to identify at least the neurotransmitters expressed by each member of the SEZ descending network to be able to understand the functional relevance of this connectivity pattern.

4.4.8 A model for olfactory control of pausing behavior with a command neuron:

In the light of the functional analysis and EM connectivity of the PDM neuron, we proposed a series of hypotheses that we hope to experimentally test in the future, as described below.

Kupfermann and Weiss proposed 3 conditions that are necessary to define a neuron as a 'command' neuron (Kupfermann and Weiss 1978). (1) The response pattern of the putative command neuron to a particular sensory stimulus should be revealed and correlated with a fixed action pattern (behavior); (2) the putative command neuron should be necessary to elicit that behavioral response and; (3) normal firing pattern of the putative command neuron should be sufficient to evoke the action pattern.

First of all, our functional analysis suggests that the PDM neuron is necessary for run-to-turn transitions and it is sufficient to trigger a behavioral subroutine of run-to-turn transitions satisfying the 2nd and 3rd

criteria. Although we showed the anatomical connectivity of the PDM neuron to the olfactory input with EM reconstruction, we still lack the necessary information to fulfill the first criterion: the response of the PDM neuron to olfactory stimuli. Nevertheless, we propose that PDM is a member of a 'command' circuit whose function is to trigger pauses during larval locomotion (Figure 4.12A). We argue that sensory processing in the upstream LH network (Figure 4.12B) modulates the activity of this command circuit. In turn, the command circuit outputs onto pre-motor circuits that generate fixed patterns of motor neuron activity underlying pauses (Figure 4.12C).

Second, since run-to-turn transitions are triggered with OSN inhibition, we hypothesize that OSN inhibition due to a decrease in odor concentration should trigger PDM activity. Likewise, high level of OSN activity should suppress the activity of the PDM neuron. Therefore we aim to study the response profile of the PDM neuron to olfactory stimuli by using functional imaging. By controlling the OSN activity with either controlled odor delivery or optogenetics (Schulze, Gomez-Marin et al. 2015) we will aim to establish the response profile of the PDM neuron to olfactory stimuli. This will also allow us to unravel the transformations that take place in the LH network (Figure 4.12B) upstream of the PDM neuron.

Third, we propose a qualitative model that might explain our observations (Figure 4.13). If we assume that LHM2 is a tonically firing excitatory neuron, contralateral connections between LHM2 neurons can form a positive feedback loop that enhances the LHM2 activity. As the activity of the LHM2 neuron increases, it activates the PDM neuron, which in turn evokes pausing behavior (Figure 4.13B). Then, PDM activates a negative feedback (X in Figure 4.13A) that inhibits the LHM2 neuron resetting it to

the baseline activity. This network might form a pausing oscillator that switches between two steady states: runs and pauses. Interestingly, we found a multi-synaptic feedback connection from the PDM to the LHM2 neuron (data not shown). We are currently trying to find out whether this could be the negative feedback we propose in the model.

This pausing oscillator is amenable to sensory modulation via the LHB3 neuron. Since high level of OSN activity during up-gradient runs suppresses run-to-turn transitions (Schulze, Gomez-Marin et al. 2015) and LHB3 receives excitatory input from the PNs, we assume that LHB3 neuron suppresses the LHM2 activity to prevent it from activating the PDM neuron. Therefore, we propose that LHB3 inhibits the LHM2 activity during up-gradient runs. As the larva experiences a decrease in sensory experience OSN activity is inhibited (Schulze, Gomez-Marin et al. 2015). In turn, LHB3 activity goes down, releasing the inhibition on the LHM2 neuron. In turn, rapid increase in LHM2 activity would trigger PDM-mediated pausing behavior. In case of rapid drops in odor concentration, strong OSN inhibition might trigger a parallel excitatory pathway to quickly activate the LHM2 neuron (question mark in Figure 4.13A). This excitatory pathway might also be utilized by other sensory modalities (e.g. a rapid increase in visual stimuli might trigger this pathway to immediately terminate runs by quickly activating LHM2). We identified candidate pathways that might allow this excitatory input upon OSN inhibition (data not shown). In order to verify this qualitative model, we have to characterize LHM2 and LHB3. Therefore, it is necessary to identify driver lines labeling these neurons. Upon identification of the driver lines, we will be in a position to proceed with functional analysis and quantitative modeling to challenge our current hypothesis.

4.4.9 Conclusion:

In summary, we identified a descending command neuron that elicits pauses during larval locomotion. This command neuron is part of a sensorimotor pathway that is controlled by temporal changes in the olfactory stimuli. By combining functional analysis with EM reconstruction we were able to map a sensorimotor pathway from the sensory neurons to the motor neurons. In the future, characterization of the downstream and upstream partners of this descending neuron will contribute to our understanding of the computational principles underlying the *Drosophila* larval chemotaxis.

4.5 Author Contributions:

The loss-of-function screen was performed by Samuel Francis Reid and me and the behavioral analysis script was written by Vani G. Rajendran. All functional experiments were conducted and analyzed by me. Nico Fessner helped me with the generation of the data in Figure 4.3 and Figure 4.9. Elena Knoche helped me with the experimental set ups explained in Figure 4.9 and 4.10. EM reconstruction data was generated by Avinash Khandelwal and the members of a collaborative project led by Albert Cardona. Avinash Khandelwal and I analyzed the EM data. All figures were prepared by me.

4.5 Materials and methods:

Fly stocks: The following fly stocks were used: *w*$^{-}$; UAS-TNTE, *w*$^{+}$; UAS-TNTE, *y*$^{-}$*w*$^{-}$; *w*[1118]; P{y[+t7.7]*w*[+mC]=20XUAS-IVS-CsChrimson::mVenus}attP2 (stock#: 55136, Bloomington), *w*[1118]; P{y[+t7.7]*w*[+mC]=20XUAS-IVS-CsChrimson::mVenus}attP18 (stock#: 55134, Bloomington), CG9887(VGlut)-LexA in su(Hw)attP8 (a kind gift from Julie Simpson), w[1118]; P{y[+t7.7] w[+mC]=13XLexAop2-IVS-GCaMP6f-p10}su(Hw)attP5 (stock#: 44277, Bloomington), *w*[1118];P{y[+t7.7]*w*[+mC]=20XUAS-IVSCsChrimson::mVenus}attP18; CG9887(VGlut)-LexA in su(Hw)attP8; w[1118]; P{y[+t7.7] w[+mC]=13XLexAop2-IVS-GCaMP6f-p10}su(Hw)attP5 (a kind gift from Stefan Pulver). Split-Gal4 Driver line SS01994: *y*$^{-}$*w*$^{-}$; AD_R23E07; DBD_R124H03 (Larval Olympiad, Janelia Research Campus. Vesicular acetylcholine transporter RNAi (stock#: 40918, VDRC). R57C10-Flp2 in su(Hw)attP8; ; HA_V5_FLAG (a kind gift from Aljoscha Nern) (Nern, Pfeiffer et al. 2015).

Multi worm tracker experiments: 20 larvae were kept in 15% sucrose solution for 20 min. Then, they were placed on 4% agar in a 245mm x 245mm square dish (07-200-600, Corning). As odor sources we used ~15mM ethyl butyrate (CAS: 105-54-4, Sigma-Aldrich) diluted in paraffin oil (Sigma-Aldrich). Four odor droplets of 8 microliters were pipetted in equidistant positions on the lid of the plate and the lid was closed. The larvae were tracked for 5 min using the previously defined Multi Worm tracker software (http://sourceforge.net/projects/mwt). Behavioral data was analyzed by custom written Matlab scripts (Matlab, MathWorks).

Single larva tracking experiments: Single larvae tracking experiment were performed as stated in Chapter 3 and (Gomez-Marin, Stephens et al. 2011). The behavioral data was analyzed by using custom script in Matlab (Matlab, MathWorks).

Histology: Histology was performed as stated in Chapter 3. For Multi-Color Flip Out (MCFO) experiments we used 1:500 anti-HA tag antibody (C29F4. Cell Signaling Technology). Monoclonal N-terminal rabbit anti-glutamate was used at 1:1000 dilution for glutamate immunostaining (a kind gift from Hermann Aberle). For GABA staining, we used 1:2000 anti-GABA produced in rabbit (A2052, Sigma-Aldrich).

Image analysis: Confocal stacks were analyzed by using Fiji software (http://fiji.sc).

Optogenetic activation experiments: As it was described in Chapter 3, SS01994-GAL4 driver was crossed to UAS-CsChrimson::mVenus. As a negative control we used $w^{-/-}$ x UAS-CsChrimson::mVenus. Flies were kept in complete darkness on food supplemented with 0.5mM all trans-retinal (Sigma, R2500). For optogenetic stimulation we used a red LED with peak emission at 625 nm (PLS 0625-030-S, Mightex Systems, Toronto, Canada). Single larvae were placed on a 2.5% agarose slab (Seakem-LE, Lonza) and tracked for 5 min using the Close-Loop Tracker (Schulze, Gomez-Marin et al. 2015). We applied total 8 light flashes that are 6 seconds long and separated by 30 seconds.

Analysis of the segmental contractions: 3rd instar larvae were pinned down on a PDMS slab (Sylgard 184 Silicone Elastomer Kit, Dow Corning) using stainless steel pins (26002-10, Fine Science tools). The pins were placed at the anterior part between the mouth hooks and at the

posterior part between the tail spiracles. The segmental contractions were tracked by visualizing the denticle bands on the ventral side of the larva. 1280 x720 pixels resolution videos were recorded at 20Hz by using a USB3.0 CMOS camera (Grasshopper 3-41C6M-C, Point Grey). The movements of the denticle bands were analyzed by using Fiji (http://fiji.sc) and custom-written scripts in Matlab (Matlab, MathWorks). For optogenetic stimulation we used a red LED with peak emission at 625 nm (PLS 0625-030-S, Mightex Systems, Toronto, Canada). We applied 6-second long flashes that are separated by 20 seconds. The camera and the LED were controlled with a NI-DAQ (NI USB-6525, National Instruments) and a custom written LabVIEW software (LabVIEW, National Instruments).

Analysis of motor neuron activity: Central nervous system of VGlut-lexA>LexAOp-GCamP6f; SS01994>UAS-Chrimson::mVenus larva was dissected using thin forceps (11252-20, Fine Science Tools) in a saline described in Pulver et al. 2015 (Pulver, Bayley et al. 2015). The isolated CNS was placed on a poly-L-lysine-covered coverslip (CAS: 25988-63-0, Sigma-Aldrich) and covered with saline. Changes in fluorescence intensity in motor neurons were recorded with a Leica SP5 Upright confocal microscope using a 20X multi-immersion objective (15506343, Leica). For optogenetic stimulation we used a red LED with peak emission at 625 nm (PLS 0625-030-S, Mightex Systems, Toronto, Canada). We applied 20-second long flashes. The microscope acquisition (LAS-AF software, Leica) and the optogenetic stimulation were controlled with a NI-DAQ (NI USB-6525, National Instruments) and a custom written Matlab script.

CHAPTER 5: General discussion and future directions

5.1 General discussion and future directions:

From the simplest nervous system to the most complex human brain, nervous systems evolved complex neural computations to coordinate their behavioral actions in response to their environments and internal needs. The main goal of today's neuroscience is unequivocally to understand how nervous systems implement these computations that create behavior by transforming sensory information into motor actions.

Complex brains possess multimodal units (micro circuits) to perform computations that could satisfy their intricate behavioral needs (Budd 2015, Roth 2015). A complete understanding of how these multimodal units function would only be possible by studying them as a part of the whole system (Koch and Laurent 1999). In this respect, the daunting complexity of the mammalian brain (Van Essen, Smith et al. 2013) hinders the efforts toward understanding the coordinated action of these multimodal neural circuits giving rise to behavior. Luckily, the evolutionary conservation of basic computational principles and their underlying neural network motifs (Marder and Calabrese 1996, Katz and Harris-Warrick 1999, Katz 2016) makes it possible to study them in invertebrate models (e.g. *C. elegans*, *Drosophila*, cockroach etc.) that are able to perform complex computations with a reduced number of neurons in their nervous system.

Drosophila melanogaster brain provides an excellent tradeoff between the numerical complexity and experimental tractability. As of complexity, unlike *C. elegans* its central nervous system is organized in structures reminiscent to that of mammalians (e.g. brain lobes-cerebrum, ventral nerve cord-spinal cord). They possess multimodal units such as mushroom

bodies and central complex that are involved in the generation of complex behaviors such as sensory-driven navigation, memory formation and learning. As far as experimental tractability is concerned, the genetic toolkit available in *Drosophila* to monitor and manipulate neural function is unrivalled by any other insect model (e.g. locusts, cockroaches).

The *Drosophila* larva shares all the merits of its adult counterpart while decreasing the numerical complexity by one order of magnitude (~10.000 neurons vs. ~100.000 neurons). In addition, the EM reconstruction of the whole larval nervous system will allow us to study the neural circuits underlying particular behaviors as a part of the overall connectivity of the brain (Ohyama, Schneider-Mizell et al. 2015). Therefore, we chose to study the sensorimotor processes in the *Drosophila* larval brain. Combining the experimental tractability with the EM reconstruction of the larval connectome, we aimed to unravel basic principles of sensorimotor transformations, hoping to uncover computational principles generalizable to the more complex brains of mammals.

As a model system, we decided to investigate the sensorimotor transformations underlying the olfactory behavior of the *Drosophila* larva for the following reasons: The kinematic features of larval chemotaxis are well characterized (Gomez-Marin, Stephens et al. 2011, Gershow, Berck et al. 2012, Gomez-Marin and Louis 2012, Gomez-Marin and Louis 2014, Davies, Louis et al. 2015). Moreover, the molecular and anatomical organizations of the peripheral olfactory layers are well defined (Fishilevich, Domingos et al. 2005, Kreher, Kwon et al. 2005, Kreher, Mathew et al. 2008, Berck, Khandelwal et al. 2016). Finally, the anatomical organization of the motor circuits is relatively well understood (Inada, Kohsaka et al. 2011, Berni, Pulver et al. 2012, Kohsaka, Okusawa et al. 2012, Berni 2015, Pulver, Bayley et al. 2015, Fushiki, Zwart et al.

2016, Zwart, Pulver et al. 2016). Thus, by using the larval chemotaxis as a model system we intended to focus our efforts on bridging the gap between the peripheral sensory system and the motor circuits.

In order to identify neurons involved in larval chemotaxis, we carried out two forward screens. We silenced synaptic transmission in subsets of neurons with targeted expression of tetanus toxin light chain (TNT) using the Gal4-UAS technique and tested the effects of this manipulation on the chemotactic performance of the larva. Since we were specifically interested in higher brain regions that could connect the sensory system to the motor circuits, we focused on the Gal4 driver lines that label brain interneurons, SEZ neurons and the interneurons in the VNC and tried to avoid targeting sensory neurons and the motor neurons. We further ignored the driver lines labeling neurons that led to a pure motor defect to make sure that the changes in the chemotaxis were due to a defect in the sensorimotor processing. Since TNT might not silence some neuronal cell types (Thum, Knapek et al. 2006), our screen was somewhat biased toward the neurons that can be silenced by TNT expression. For example, we might have not been able to silence neurons that secrete neuromodulators although they were targeted by the driver lines we used.

Due to the absence of Gal4 driver lines at the time of the first loss-of-function (LOF) screen, we had to use driver lines that labeled multiple neuronal cell types. In order to narrow down the LOF phenotype to individual cell types, we attempted to perform multiple genetic intersectional manipulations using traditional reagents (Venken, Simpson et al. 2011). Eventually, we had to develop a stochastic gain-of function strategy to restrict the acute optogenetic activation to individual neurons. We believe that the stochastic activation method we developed will be useful whenever sparsely labeling driver lines do not exist.

In the second LOF screen, we utilized Split-Gal4 driver lines that often labeled a single neuron. Thus, we were able to correlate the chemotactic defect to individual neurons without carrying out further intersections. However, this techniques is restricted by the existence of driver lines with overlapping expressions for single neurons. For example, in our Split-Gal4 screen neurons in the mushroom body region were overrepresented, as many overlapping driver lines have already been identified for these neurons (Aso, Hattori et al. 2014). Fortunately, we had a number of driver lines labeling single neuron in other regions of the larval brain. The coverage being incomplete, we could nonetheless not test the function of all the neurons identified in the screens.

Presumably, the sensorimotor pathway underlying larval chemotaxis comprises neural circuits (1) encoding relevant features of the sensory input; (2) creating perceptions by integrating olfactory signals with other sensory modalities and internal states; (3) transforming the perception into a decision to switch between runs and turns; and (4) executing the motor actions based on the decision. These circuits should be connected via short-range and long-range interneurons to allow communication among them. In our screens, we aimed to identify neurons that are involved in the selection of proper actions based on the perceived value of the olfactory signals as well as neurons that convey this decision to the motor pattern generating circuits.

In our first screen (Chapter 3) we identified a group of neurons in the subesophageal zone (SEZ). Silencing these neurons impaired the timing of run-to-turn transitions in odor gradients while activating them was sufficient to trigger head casting and turning maneuvers. Interestingly, the loss-of-function phenotype was also present for phototaxis and

thermotaxis, suggesting that these neurons receive integrated input from these regions.

To which step of the sensorimotor pathway are these neurons functionally contribute? Recent studies suggest that asymmetrical motor neuron activity underlying the turning behavior is generated in the thoracic ganglia (Berni, Pulver et al. 2012, Berni 2015). However, surgical removal of the SEZ severely impairs the generation of asymmetrical motor neuron activity in the VNC (Pulver, Bayley et al. 2015), suggesting that descending inputs from the SEZ regulate the turning behavior. We also observed that silencing the neurons in the posterior part of the SEZ (Becker et al. 2016) by using Scr-Gal4 severely reduced the turning frequency (data not shown). In locusts, SEZ has also been shown to be involved in sensory-driven control of locomotion via descending inputs from the brain (Kien and Altman 1992). In the light of these observations, we argue that SEZ neurons we identified in the first screen are involved in conveying the decisions made in the brain to the motor pattern generators in the VNC. Moreover we found the same SEZ neurons are involved in chemotaxis, phototaxis and thermotaxis, suggesting that they might be a part of a descending command circuit that receives integrated input from multiple sensory modalities. Reinforcing our argument, in our second screen we discovered SEZ descending neurons that are part of a command circuit involved in triggering pauses (see Chapter 4 and below). In the future, EM reconstruction and functional analysis of the SEZ circuits will help us reveal the exact role of the SEZ networks in sensorimotor processing.

In our second screen, we identified a descending neuron (PDM) of which silencing also leads to a defect in run-to-turn transitions (Chapter 4). Acute optogenetic activation of this descending neuron evokes pauses that

are occasionally followed by head casting and turning. Activation of PDM in odor gradients revealed that large-amplitude head casts and turns follow pauses only if the larva is engaged in a down-gradient run at the onset of the activation. We showed that while this neuron cannot cease an already initiated wave at the anterior segments it does not allow the initiation of the next wave from the very posterior segments. By studying the activation of this neuron at segmental contraction and motor neuron activity levels, we concluded that this neuron acts strongly at the posterior segments.

We then questioned the role of the PDM-induced pausing behavior in run-to-turn transitions. After the *Drosophila* larva terminates a run, it samples its immediate environment via head casts. During the head cast, the posterior segments stop contracting, while the anterior segments contract asymmetrically to generate head casts. We argue that PDM inhibits the contraction of the posterior segments while allowing the asymmetrical contraction of the anterior segments. Thus, PDM evoked pauses ensure that the larva samples its environment sufficiently before it reinitiates a forward wave. Interestingly, Berni suggested that unlike the symmetrical waves, the asymmetrical waves start at the anterior thoracic segments and propagate posteriorly and the origin of the symmetrical and asymmetrical waves can be anatomically uncoupled in the VNC (Berni 2015). It is conceivable that the premotor circuits that generate the forward waves and asymmetries are different and PDM acts specifically on the forward wave generation while being permissive to the asymmetrical activity in the anterior VNC.

If PDM is responsible for ensuring that the larva can sample its environment before reinitiating a forward wave, silencing the PDM neuron might affect the decision of where the larva turns to. However,

when we quantified the proportion of the turns toward the higher concentration we did not see any defect in PDM-silenced larvae. Since nervous systems tend to be redundant and circuit-level compensation is possible (Venken, Simpson et al. 2011), we speculate that the 'where to turn to' decision is not severely affected due to either the presence of redundant neurons for the same function or the circuit level compensation.

As opposed to the first screen, we were able to identify the PDM neuron in the EM volume. Reconstruction of the upstream partners of the PDM neuron showed that it receives olfactory input in the lateral horn region. At the other extreme, PDM outputs onto a set of SEZ descending neurons that synapses onto the excitatory premotor neuron A27h (Fushiki, Zwart et al. 2016) in the abdominal segments. The fact that the SEZ descending neurons directly acts on the premotor circuits while receiving integrated sensory input from the lateral horn region via the PDM neuron corroborates our previous arguments that SEZ is involved in communicating the selected action to the motor pattern generators. It is probable that the SEZ descending networks further integrate and transform the signal rather than passively conveying it. For example, they might integrate the proprioceptive inputs to fine-tune the behavioral output (Kien and Altman 1992).

In the light of the upstream EM connectivity of the PDM neuron, we proposed a hypothetical model in which PDM and its upstream neuron LHM2 forms a pausing integrator that is modulated by the olfactory inputs via LHB3 neuron (Figure 4.13). LHM2 neurons on both side of the brain connected to each other, forming a positive feedback loop. Tonic activity of the putative excitatory LHM2 neuron would be enhanced by this feedback loop and the system would drift toward a threshold at which the PDM neuron is activated. In turn, PDM would activate the

downstream SEZ descending network that specifically inhibits the forward waves by silencing the A27h neuron. In order to ensure that the system can go back to the forward locomotion state, we proposed that PDM in parallel activates a negative feedback pathway to silence the LHM2 neuron. Thus, activation and delayed inhibition of LHM2 neuron can generate a 'pausing oscillator' by drifting between LHM2 ON and OFF states. Interestingly, in EM reconstruction we found a feedback pathway from the PDM neuron to the LHM2 neuron. We are now searching for driver lines to label these neurons and to characterize their functions.

We proposed that the pausing oscillator could be modulated by olfactory inputs. The putative inhibitory LHB3 neuron receives excitatory inputs from the uniglomerular PNs of Or42a and Or42b. During an up-gradient run, high level of PN activity would activate the LHB3 neuron to suppress the pausing oscillator by inhibiting the LHM2 neuron. As soon as the larva experiences a down-gradient run, the inhibition would be released and eventually the pausing oscillator would kick in to terminate the run. Then, the larva samples its environment via head casts. An increase in OSN activity due to a head cast toward higher odor concentration would trigger the PN activity. In turn, LHB3 would get activated and LHM2 neuron would be inhibited to turn off the pausing state. If the larva cannot locate an increase in odor concentration via head casts until the PDM-evoked negative feedback kicks in, the pausing state would anyway be terminated by the negative feedback. Thus, the larva engages in a new run unless it experiences further decrease in odor concentration. The decrease in odor concentration might also activate the LHM2 neuron via an LHB3 independent pathway in order to stop the larva immediately in response to sudden decreases in odor concentration. We are currently analyzing the EM data for this possibility.

In order to challenge our current hypothetical model, we are trying to identify driver lines specifically labeling the LHM2 and LHB3 neurons. In short term, we aim to characterize the odor response profile of the PDM neuron to see whether it responds to the changes in odor concentration as the model proposes. In the long term, identification of driver lines sparsely labeling the LHM2 and LHB3 neurons will allow us perform functional studies similar to the ones we performed for the PDM neuron. Furthermore, identification of the downstream SEZ descending neurons will help us unravel the mechanisms of how the pauses are implemented on the premotor circuits underlying the forward wave initiation and propagation.

In short, by performing forward screens we were able to identify neurons that are involved in sensory-driven selection of different subroutines in run-to-turn transitions. EM reconstruction helped us map a sensorimotor pathway at each level from the sensory neurons to the motor neurons. Functional analysis allowed us to characterize a descending neuron in this pathway that is necessary and sufficient to trigger a fixed motor pattern (a function comparable with the definition of command neurons). Finally, we proposed a qualitative model that can explain the role of this sensorimotor pathway in larval chemotaxis. In the near future, we will take advantage of the amazing genetic toolkit available for functional analysis in *Drosophila* to study the computational logic of this sensorimotor pathway. Altogether, we believe that our work contributes to understanding the sensorimotor transformations underlying animal behavior. We hope that the structural and functional mechanisms we unravel will be generalized to more complex brains in the future.

6. Bibliography:

Asahina, K., M. Louis, S. Piccinotti and L. B. Vosshall (2009). "A circuit supporting concentration-invariant odor perception in Drosophila." J Biol **8**(1): 9.

Asahina, K., K. Watanabe, B. J. Duistermars, E. Hoopfer, C. R. Gonzalez, E. A. Eyjolfsdottir, P. Perona and D. J. Anderson (2014). "Tachykinin-expressing neurons control male-specific aggressive arousal in Drosophila." Cell **156**(1-2): 221-235.

Aso, Y., D. Hattori, Y. Yu, R. M. Johnston, N. A. Iyer, T. T. Ngo, H. Dionne, L. F. Abbott, R. Axel, H. Tanimoto and G. M. Rubin (2014). "The neuronal architecture of the mushroom body provides a logic for associative learning." Elife **3**: e04577.

Baines, R. A., J. P. Uhler, A. Thompson, S. T. Sweeney and M. Bate (2001). "Altered electrical properties in Drosophila neurons developing without synaptic transmission." J Neurosci **21**(5): 1523-1531.

Becker, H., Renner, S., Technau, G. M., & Berger, C. (2016). "Cell-Autonomous and Non-cell-autonomous Function of Hox Genes Specify Segmental Neuroblast Identity in the Gnathal Region of the Embryonic CNS in Drosophila." PLOS Genet, **12**(3), e1005961.

Bednar, J., P. Furrer, V. Katritch, A. Z. Stasiak, J. Dubochet and A. Stasiak (1995). "Determination of DNA persistence length by cryo-electron microscopy. Separation of the static and dynamic contributions to the apparent persistence length of DNA." J Mol Biol **254**(4): 579-594.

Berck, M. E., A. Khandelwal, L. Claus, L. Hernandez-Nunez, G. Si, C. J. Tabone, F. Li, J. W. Truman, R. D. Fetter, M. Louis, A. D. Samuel and A. Cardona (2016). "The wiring diagram of a glomerular olfactory system." Elife **5**.

Berni, J. (2015). "Genetic dissection of a regionally differentiated network for exploratory behavior in Drosophila larvae." Curr Biol **25**(10): 1319-1326.

Berni, J., S. R. Pulver, L. C. Griffith and M. Bate (2012). "Autonomous circuitry for substrate exploration in freely moving Drosophila larvae." Curr Biol **22**(20): 1861-1870.

Bidaye, S. S., C. Machacek, Y. Wu and B. J. Dickson (2014). "Neuronal control of Drosophila walking direction." Science **344**(6179): 97-101.

Boyle, J., & Cobb, M. (2005). "Olfactory coding in Drosophila larvae investigated by cross-adaptation." Journal of Experimental Biology, **208**(18), 3483-3491.

Bracker, L. B., K. P. Siju, N. Varela, Y. Aso, M. Zhang, I. Hein, M. L. Vasconcelos and I. C. Grunwald Kadow (2013). "Essential role of the mushroom body in context-dependent CO(2) avoidance in Drosophila." Curr Biol **23**(13): 1228-1234.

Brittain, E. H. (1987). "P-values for the multi-sample kolmogorov-smirnov test using the expanded bonferroni appoximation." Communications in Statistics-Theory and Methods **16**(3): 821-835.

Brodfuehrer, P. D. and W. O. Friesen (1986). "Initiation of swimming activity by trigger neurons in the leech subesophageal ganglion." Journal of Comparative Physiology A **159**(4): 489-502.

Brodfuehrer, P. D. and W. O. Friesen (1986). "Initiation of swimming activity by trigger neurons in the leech subesophageal ganglion." Journal of Comparative Physiology A **159**(4): 511-519.

Budd, G. E. (2015). "Early animal evolution and the origins of nervous systems." Philosophical Transactions of the Royal Society B: Biological Sciences **370**(1684): 20150037-20150037.

Burdohan, J. A. and C. M. Comer (1996). "Cellular Organization of an Antennal Mechanosensory Pathway in the Cockroach, Periplaneta americana." The Journal of Neuroscience **16**(18): 5830-5843.

Caldwell, J. C., M. M. Miller, S. Wing, D. R. Soll and D. F. Eberl (2003). "Dynamic analysis of larval locomotion in Drosophila chordotonal organ mutants." Proc Natl Acad Sci U S A **100**(26): 16053-16058.

Cardona, A., S. Saalfeld, S. Preibisch, B. Schmid, A. Cheng, J. Pulokas, P. Tomancak and V. Hartenstein (2010). "An integrated micro- and macroarchitectural analysis of the Drosophila brain by computer-assisted serial section electron microscopy." PLoS Biol **8**(10).

Chittka, L., P. Skorupski and N. E. Raine (2009). "Speed-accuracy tradeoffs in animal decision making." Trends Ecol Evol **24**(7): 400-407.

Chklovskii, D. B., S. Vitaladevuni and L. K. Scheffer (2010). "Semi-automated reconstruction of neural circuits using electron microscopy." Current Opinion in Neurobiology **20**(5): 667-675.

Clark, D. A., L. Freifeld and T. R. Clandinin (2013). "Mapping and cracking sensorimotor circuits in genetic model organisms." Neuron **78**(4): 583-595.

Clark, M. Q., S. J. McCumsey, S. Lopez-Darwin, E. S. Heckscher and C. Q. Doe (2016). "Functional Genetic Screen to Identify Interneurons Governing Behaviorally Distinct Aspects of Drosophila Larval Motor Programs." G3 (Bethesda) **6**(7): 2023-2031.

Clyne, J. D. and G. Miesenbock (2008). "Sex-specific control and tuning of the pattern generator for courtship song in Drosophila." Cell **133**(2): 354-363.

Cohn, R., I. Morantte and V. Ruta (2015). "Coordinated and Compartmentalized Neuromodulation Shapes Sensory Processing in Drosophila." Cell **163**(7): 1742-1755.

Colomb, J., N. Grillenzoni, A. Ramaekers and R. F. Stocker (2007). "Architecture of the primary taste center of Drosophila melanogaster larvae." J Comp Neurol **502**(5): 834-847.

Das, A., T. Gupta, S. Davla, L. L. Prieto-Godino, S. Diegelmann, O. V. Reddy, K. V. Raghavan, H. Reichert, J. Lovick and V. Hartenstein (2013). "Neuroblast lineage-specific origin of the neurons of the Drosophila larval olfactory system." Developmental Biology **373**(2): 322-337.

Das, A., T. Gupta, S. Davla, L. L. Prieto-Godino, S. Diegelmann, O. V. Reddy, K. V. Raghavan, H. Reichert, J. Lovick and V. Hartenstein (2013).

"Neuroblast lineage-specific origin of the neurons of the Drosophila larval olfactory system." Dev Biol **373**(2): 322-337.

Davies, A., M. Louis and B. Webb (2015). "A Model of Drosophila Larva Chemotaxis." PLoS Comput Biol **11**(11): e1004606.

Dawkins, M. S. and M. Hauber (2014). "Tribute to Tinbergen: Questions and How to Answer Them." Ethology **120**(2): 120-122.

de Belle, J. S. and M. Heisenberg (1994). "Associative odor learning in Drosophila abolished by chemical ablation of mushroom bodies." Science **263**(5147): 692-695.

Duda, R. O., P. E. Hart and D. G. Stork (2001). Pattern classification. New York, Wiley.

Ebrahim, S. A., H. K. Dweck, J. Stokl, J. E. Hofferberth, F. Trona, K. Weniger, J. Rybak, Y. Seki, M. C. Stensmyr, S. Sachse, B. S. Hansson and M. Knaden (2015). "Drosophila Avoids Parasitoids by Sensing Their Semiochemicals via a Dedicated Olfactory Circuit." PLoS Biol **13**(12): e1002318.

Egnor, S. E. and K. Branson (2016). "Computational Analysis of Behavior." Annu Rev Neurosci **39**: 217-236.

Fawcett, T. (2006). "An introduction to ROC analysis." Pattern recognition letters **27**(8): 861-874.

Fenno, L., O. Yizhar and K. Deisseroth (2011). "The development and application of optogenetics." Annu Rev Neurosci **34**: 389-412.

Fisek, M. and R. I. Wilson (2014). "Stereotyped connectivity and computations in higher-order olfactory neurons." Nat Neurosci **17**(2): 280-288.

Fishilevich, E., A. I. Domingos, K. Asahina, F. Naef, L. B. Vosshall and M. Louis (2005). "Chemotaxis Behavior Mediated by Single Larval Olfactory Neurons in Drosophila." Current Biology **15**(23): 2086-2096.

Fishilevich, E., A. I. Domingos, K. Asahina, F. Naef, L. B. Vosshall and M. Louis (2005). "Chemotaxis behavior mediated by single larval olfactory neurons in Drosophila." Curr Biol **15**(23): 2086-2096.

Fox, L. E., D. R. Soll and C.-F. Wu (2006). "Coordination and Modulation of Locomotion Pattern Generators in Drosophila Larvae: Effects of Altered Biogenic Amine Levels by the Tyramine β Hydroxlyase Mutation." The Journal of neuroscience : the official journal of the Society for Neuroscience **26**(5): 1486-1498.

Friesen, W. O. and W. B. Kristan (2007). "Leech locomotion: swimming, crawling, and decisions." Curr Opin Neurobiol **17**(6): 704-711.

Fushiki, A., M. F. Zwart, H. Kohsaka, R. D. Fetter, A. Cardona and A. Nose (2016). "A circuit mechanism for the propagation of waves of muscle contraction in Drosophila." Elife **5**.

Gepner, R., M. Mihovilovic Skanata, N. M. Bernat, M. Kaplow and M. Gershow (2015). "Computations underlyingDrosophilaphoto-taxis, odor-taxis, and multi-sensory integration." eLife **4**.

Gerber, B. and R. F. Stocker (2007). "The Drosophila larva as a model for studying chemosensation and chemosensory learning: a review." Chem Senses **32**(1): 65-89.

Gershow, M., M. Berck, D. Mathew, L. Luo, E. A. Kane, J. R. Carlson and A. D. T. Samuel (2012). "Controlling airborne cues to study small animal navigation." Nature Methods **9**(3): 290-296.

Gjorgjieva, J., J. Berni, J. F. Evers and S. J. Eglen (2013). "Neural circuits for peristaltic wave propagation in crawling Drosophila larvae: analysis and modeling." Front Comput Neurosci **7**: 24.

Gomez-Marin, A. and M. Louis (2012). "Active sensation during orientation behavior in the Drosophila larva: more sense than luck." Curr Opin Neurobiol **22**(2): 208-215.

Gomez-Marin, A. and M. Louis (2014). "Multilevel control of run orientation in Drosophila larval chemotaxis." Front Behav Neurosci **8**: 38.

Gomez-Marin, A., N. Partoune, G. J. Stephens and M. Louis (2012). "Automated Tracking of Animal Posture and Movement during Exploration and Sensory Orientation Behaviors." PLoS One **7**(8): e41642.

Gomez-Marin, A., G. J. Stephens and M. Louis (2011). "Active sampling and decision making in Drosophila chemotaxis." Nat Commun **2**: 441.

Gonzalez-Bellido, P. T., T. J. Wardill, R. Kostyleva, I. A. Meinertzhagen and M. Juusola (2009). "Overexpressing temperature-sensitive dynamin decelerates phototransduction and bundles microtubules in Drosophila photoreceptors." J Neurosci **29**(45): 14199-14210.

Gordon, M. D. and K. Scott (2009). "Motor control in a Drosophila taste circuit." Neuron **61**(3): 373-384.

Green, C. H., B. Burnet and K. J. Connolly (1983). "Organization and patterns of inter- and intraspecific variation in the behaviour of Drosophila larvae." Animal Behaviour **31**(1): 282-291.

Grueber, W. B., L. Y. Jan and Y. N. Jan (2002). "Tiling of the Drosophila epidermis by multidendritic sensory neurons." Development **129**(12): 2867-2878.

Gupta, N. and M. Stopfer (2012). "Functional analysis of a higher olfactory center, the lateral horn." J Neurosci **32**(24): 8138-8148.

Hampel, S., R. Franconville, J. H. Simpson and A. M. Seeds (2015). "A neural command circuit for grooming movement control." Elife **4**: e08758.

Hartenstein, V., A. Younossi-Hartenstein, J. K. Lovick, A. Kong, J. J. Omoto, K. T. Ngo and G. Viktorin (2015). "Lineage-associated tracts defining the anatomy of the Drosophila first instar larval brain." Dev Biol **406**(1): 14-39.

Hayashi, S., K. Ito, Y. Sado, M. Taniguchi, A. Akimoto, H. Takeuchi, T. Aigaki, F. Matsuzaki, H. Nakagoshi, T. Tanimura, R. Ueda, T. Uemura, M. Yoshihara and S. Goto (2002). "GETDB, a database compiling expression patterns and molecular locations of a collection of Gal4 enhancer traps." Genesis **34**(1-2): 58-61.

Heckscher, E. S., S. R. Lockery and C. Q. Doe (2012). "Characterization of Drosophila Larval Crawling at the Level of Organism, Segment, and Somatic Body Wall Musculature." The Journal of neuroscience : the official journal of the Society for Neuroscience **32**(36): 12460-12471.

Heckscher, E. S., S. R. Lockery and C. Q. Doe (2012). "Characterization of Drosophila larval crawling at the level of organism, segment, and somatic body wall musculature." J Neurosci **32**(36): 12460-12471.

Hernandez-Nunez, L., J. Belina, M. Klein, G. Si, L. Claus, J. R. Carlson and A. D. T. Samuel (2015). "Reverse-correlation analysis of navigation dynamics inDrosophilalarva using optogenetics." eLife **4**.

Hong, S.-T., S. Bang, S. Hyun, J. Kang, K. Jeong, D. Paik, J. Chung and J. Kim (2008). "cAMP signalling in mushroom bodies modulates temperature preference behaviour in Drosophila." Nature **454**(7205): 771-775.

Hsu, C. T. and V. Bhandawat (2016). "Organization of descending neurons in Drosophila melanogaster." Scientific Reports **6**: 20259.

Hückesfeld, S., A. Schoofs, P. Schlegel, A. Miroschnikow and M. J. Pankratz (2015). "Localization of Motor Neurons and Central Pattern Generators for Motor Patterns Underlying Feeding Behavior in <italic>Drosophila</italic> Larvae." PLoS ONE **10**(8): e0135011.

Hughes, C. L. and J. B. Thomas (2007). "A sensory feedback circuit coordinates muscle activity in Drosophila." Molecular and Cellular Neuroscience **35**(2): 383-396.

Hwang, R. Y., L. Zhong, Y. Xu, T. Johnson, F. Zhang, K. Deisseroth and W. D. Tracey (2007). "Nociceptive neurons protect Drosophila larvae from parasitoid wasps." Curr Biol **17**(24): 2105-2116.

Inada, K., H. Kohsaka, E. Takasu, T. Matsunaga and A. Nose (2011). "Optical dissection of neural circuits responsible for Drosophila larval locomotion with halorhodopsin." PLoS One **6**(12): e29019.

Inagaki, H. K., Y. Jung, E. D. Hoopfer, A. M. Wong, N. Mishra, J. Y. Lin, R. Y. Tsien and D. J. Anderson (2014). "Optogenetic control of

Drosophila using a red-shifted channelrhodopsin reveals experience-dependent influences on courtship." Nat Methods **11**(3): 325-332.

Ito, M., N. Masuda, K. Shinomiya, K. Endo and K. Ito (2013). "Systematic Analysis of Neural Projections Reveals Clonal Composition of the Drosophila Brain." Current Biology **23**(8): 644-655.

Jefferis, G. S., E. C. Marin, R. F. Stocker and L. Luo (2001). "Target neuron prespecification in the olfactory map of Drosophila." Nature **414**(6860): 204-208.

Jefferis, G. S., C. J. Potter, A. M. Chan, E. C. Marin, T. Rohlfing, C. R. Maurer, Jr. and L. Luo (2007). "Comprehensive maps of Drosophila higher olfactory centers: spatially segregated fruit and pheromone representation." Cell **128**(6): 1187-1203.

Jenett, A., G. M. Rubin, T. T. Ngo, D. Shepherd, C. Murphy, H. Dionne, B. D. Pfeiffer, A. Cavallaro, D. Hall, J. Jeter, N. Iyer, D. Fetter, J. H. Hausenfluck, H. Peng, E. T. Trautman, R. R. Svirskas, E. W. Myers, Z. R. Iwinski, Y. Aso, G. M. DePasquale, A. Enos, P. Hulamm, S. C. Lam, H. H. Li, T. R. Laverty, F. Long, L. Qu, S. D. Murphy, K. Rokicki, T. Safford, K. Shaw, J. H. Simpson, A. Sowell, S. Tae, Y. Yu and C. T. Zugates (2012). "A GAL4-driver line resource for Drosophila neurobiology." Cell Rep **2**(4): 991-1001.

Kane, E. A., M. Gershow, B. Afonso, I. Larderet, M. Klein, A. R. Carter, B. L. de Bivort, S. G. Sprecher and A. D. Samuel (2013). "Sensorimotor structure of Drosophila larva phototaxis." Proc Natl Acad Sci U S A **110**(40): E3868-3877.

Kanzaki, R., A. Ikeda and T. Shibuya (1994). "Morphological and physiological properties of pheromone-triggered flipflopping descending interneurons of the male silkworm moth, Bombyx mori." Journal of Comparative Physiology A **175**(1): 1-14.

Katz, P. S. (2016). "Evolution of central pattern generators and rhythmic behaviours." Philos Trans R Soc Lond B Biol Sci **371**(1685): 20150057.

Katz, P. S. and R. M. Harris-Warrick (1999). "The evolution of neuronal circuits underlying species-specific behavior." Current Opinion in Neurobiology **9**(5): 628-633.

Kay, L. M. and M. Stopfer (2006). "Information processing in the olfactory systems of insects and vertebrates." Semin Cell Dev Biol **17**(4): 433-442.

Keene, A. C. and S. Waddell (2007). "Drosophila olfactory memory: single genes to complex neural circuits." Nature Reviews Neuroscience **8**(5): 341-354.

Kido, A. and K. Ito (2002). "Mushroom bodies are not required for courtship behavior by normal and sexually mosaic Drosophila." J Neurobiol **52**(4): 302-311.

Kim, A. J., A. A. Lazar and Y. B. Slutskiy (2015). "Projection neurons in Drosophila antennal lobes signal the acceleration of odor concentrations." eLife **4**: e06651.

Kitamoto, T. (2002). "Conditional disruption of synaptic transmission induces male-male courtship behavior in Drosophila." Proc Natl Acad Sci U S A **99**(20): 13232-13237.

Klapoetke, N. C., Y. Murata, S. S. Kim, S. R. Pulver, A. Birdsey-Benson, Y. K. Cho, T. K. Morimoto, A. S. Chuong, E. J. Carpenter, Z. Tian, J. Wang, Y. Xie, Z. Yan, Y. Zhang, B. Y. Chow, B. Surek, M. Melkonian, V. Jayaraman, M. Constantine-Paton, G. K. Wong and E. S. Boyden (2014). "Independent optical excitation of distinct neural populations." Nat Methods **11**(3): 338-346.

Klein, M., B. Afonso, A. J. Vonner, L. Hernandez-Nunez, M. Berck, C. J. Tabone, E. A. Kane, V. A. Pieribone, M. N. Nitabach, A. Cardona, M. Zlatic, S. G. Sprecher, M. Gershow, P. A. Garrity and A. D. Samuel (2015). "Sensory determinants of behavioral dynamics in Drosophila thermotaxis." Proc Natl Acad Sci U S A **112**(2): E220-229.

Koch, C., & Laurent, G. (1999). "Complexity and the nervous system." Science,**284**(5411), 96-98.

Kohsaka, H., S. Okusawa, Y. Itakura, A. Fushiki and A. Nose (2012). "Development of larval motor circuits in Drosophila." Dev Growth Differ **54**(3): 408-419.

Kohsaka, H., E. Takasu, T. Morimoto and A. Nose (2014). "A group of segmental premotor interneurons regulates the speed of axial locomotion in Drosophila larvae." Curr Biol **24**(22): 2632-2642.

Krashes, M. J., S. DasGupta, A. Vreede, B. White, J. D. Armstrong and S. Waddell (2009). "A neural circuit mechanism integrating motivational state with memory expression in Drosophila." Cell **139**(2): 416-427.

Kreher, S. A., J. Y. Kwon and J. R. Carlson (2005). "The Molecular Basis of Odor Coding in the Drosophila Larva." Neuron **46**(3): 445-456.

Kreher, S. A., D. Mathew, J. Kim and J. R. Carlson (2008). "Translation of sensory input into behavioral output via an olfactory system." Neuron **59**(1): 110-124.

Kreher, S. A., D. Mathew, J. Kim and J. R. Carlson (2008). "Translation of Sensory Input into Behavioral Output via an Olfactory System." Neuron **59**(1): 110-124.

Kunz, T., K. F. Kraft, G. M. Technau and R. Urbach (2012). "Origin of Drosophila mushroom body neuroblasts and generation of divergent embryonic lineages." Development **139**(14): 2510-2522.

Kupfermann, I. and K. R. Weiss (1978). "The command neuron concept." Behavioral and Brain Sciences **1**(01): 3-10.

Kwon, J. Y., A. Dahanukar, L. A. Weiss and J. R. Carlson (2011). "Molecular and cellular organization of the taste system in the Drosophila larva." J Neurosci **31**(43): 15300-15309.

Lahiri, S., K. Shen, M. Klein, A. Tang, E. Kane, M. Gershow, P. Garrity and A. D. Samuel (2011). "Two alternating motor programs drive navigation in Drosophila larva." PLoS One **6**(8): e23180.

Landgraf, M., V. Jeffrey, M. Fujioka, J. B. Jaynes and M. Bate (2003). "Embryonic origins of a motor system: motor dendrites form a myotopic map in Drosophila." PLoS Biol **1**(2): E41.

Larsson, M. C., A. I. Domingos, W. D. Jones, M. E. Chiappe, H. Amrein and L. B. Vosshall (2004). "Or83b encodes a broadly expressed odorant receptor essential for Drosophila olfaction." Neuron **43**(5): 703-714.

Lemon, W. C., S. R. Pulver, B. Hockendorf, K. McDole, K. Branson, J. Freeman and P. J. Keller (2015). "Whole-central nervous system functional imaging in larval Drosophila." Nat Commun **6**: 7924.

Lewis, L. P., K. P. Siju, Y. Aso, A. B. Friedrich, A. J. Bulteel, G. M. Rubin and I. C. Grunwald Kadow (2015). "A Higher Brain Circuit for Immediate Integration of Conflicting Sensory Information in Drosophila." Curr Biol **25**(17): 2203-2214.

Li, H. H., J. R. Kroll, S. M. Lennox, O. Ogundeyi, J. Jeter, G. Depasquale and J. W. Truman (2014). "A GAL4 driver resource for developmental and behavioral studies on the larval CNS of Drosophila." Cell Rep **8**(3): 897-908.

Libersat, F. and R. Gal (2013). "What can parasitoid wasps teach us about decision-making in insects?" J Exp Biol **216**(Pt 1): 47-55.

Lin, S., D. Owald, V. Chandra, C. Talbot, W. Huetteroth and S. Waddell (2014). "Neural correlates of water reward in thirsty Drosophila." Nature neuroscience **17**(11): 1536-1542.

Louis, M., T. Huber, R. Benton, T. P. Sakmar and L. B. Vosshall (2008). "Bilateral olfactory sensory input enhances chemotaxis behavior." Nat Neurosci **11**(2): 187-199.

Luan, H., N. C. Peabody, C. R. Vinson and B. H. White (2006). "Refined spatial manipulation of neuronal function by combinatorial restriction of transgene expression." Neuron **52**(3): 425-436.

Luo, L., E. M. Callaway and K. Svoboda (2008). "Genetic dissection of neural circuits." Neuron **57**(5): 634-660.

Luo, L., M. Gershow, M. Rosenzweig, K. Kang, C. Fang-Yen, P. A. Garrity and A. D. Samuel (2010). "Navigational decision making in Drosophila thermotaxis." J Neurosci **30**(12): 4261-4272.

Luo, L., Q. Wen, J. Ren, M. Hendricks, M. Gershow, Y. Qin, J. Greenwood, E. R. Soucy, M. Klein, H. K. Smith-Parker, A. C. Calvo, D. A. Colon-Ramos, A. D. Samuel and Y. Zhang (2014). "Dynamic encoding of perception, memory, and movement in a C. elegans chemotaxis circuit." Neuron **82**(5): 1115-1128.

Marder, E. and R. L. Calabrese (1996). "Principles of rhythmic motor pattern generation." Physiol Rev **76**(3): 687-717.

Marella, S., K. Mann and K. Scott (2012). "Dopaminergic modulation of sucrose acceptance behavior in Drosophila." Neuron **73**(5): 941-950.

Marin, E. C., G. S. Jefferis, T. Komiyama, H. Zhu and L. Luo (2002). "Representation of the glomerular olfactory map in the Drosophila brain." Cell **109**(2): 243-255.

Marin, E. C., R. J. Watts, N. K. Tanaka, K. Ito and L. Luo (2005). "Developmentally programmed remodeling of the Drosophila olfactory circuit." Development **132**(4): 725-737.

Masuda-Nakagawa, L. M., T. Awasaki, K. Ito and C. J. O'Kane (2010). "Targeting expression to projection neurons that innervate specific mushroom body calyx and antennal lobe glomeruli in larval Drosophila." Gene Expression Patterns **10**(7-8): 328-337.

Masuda-Nakagawa, L. M., N. Gendre, C. J. O'Kane and R. F. Stocker (2009). "Localized olfactory representation in mushroom bodies of Drosophila larvae." Proc Natl Acad Sci U S A **106**(25): 10314-10319.

Masuda-Nakagawa, L. M., N. Gendre, C. J. O'Kane and R. F. Stocker (2009). "Localized olfactory representation in mushroom bodies of Drosophila larvae." Proceedings of the National Academy of Sciences **106**(25): 10314-10319.

Masuda-Nakagawa, L. M., N. K. Tanaka and C. J. O'Kane (2005). "Stereotypic and random patterns of connectivity in the larval mushroom body calyx of Drosophila." Proceedings of the National Academy of Sciences **102**(52): 19027-19032.

Mathew, D., C. Martelli, E. Kelley-Swift, C. Brusalis, M. Gershow, A. D. T. Samuel, T. Emonet and J. R. Carlson (2013). "Functional diversity

among sensory receptors in aDrosophilaolfactory circuit." Proceedings of the National Academy of Sciences **110**(23): E2134-E2143.

Matsunaga, T., A. Fushiki, A. Nose and H. Kohsaka (2013). "Optogenetic perturbation of neural activity with laser illumination in semi-intact drosophila larvae in motion." J Vis Exp(77): e50513.

McGuire, S. E., Z. Mao and R. L. Davis (2004). "Spatiotemporal gene expression targeting with the TARGET and gene-switch systems in Drosophila." Sci STKE **2004**(220): pl6.

Namiki, S., & Kanzaki, R. (2016)."Comparative neuroanatomy of the lateral accessory lobe in the insect brain." Frontiers in Physiology, 7, 244.

Nern, A., B. D. Pfeiffer and G. M. Rubin (2015). "Optimized tools for multicolor stochastic labeling reveal diverse stereotyped cell arrangements in the fly visual system." Proc Natl Acad Sci U S A **112**(22): E2967-2976.

Oh, S. W., J. A. Harris, L. Ng, B. Winslow, N. Cain, S. Mihalas, Q. Wang, C. Lau, L. Kuan, A. M. Henry, M. T. Mortrud, B. Ouellette, T. N. Nguyen, S. A. Sorensen, C. R. Slaughterbeck, W. Wakeman, Y. Li, D. Feng, A. Ho, E. Nicholas, K. E. Hirokawa, P. Bohn, K. M. Joines, H. Peng, M. J. Hawrylycz, J. W. Phillips, J. G. Hohmann, P. Wohnoutka, C. R. Gerfen, C. Koch, A. Bernard, C. Dang, A. R. Jones and H. Zeng (2014). "A mesoscale connectome of the mouse brain." Nature **508**(7495): 207-214.

Ohyama, T., C. M. Schneider-Mizell, R. D. Fetter, J. V. Aleman, R. Franconville, M. Rivera-Alba, B. D. Mensh, K. M. Branson, J. H. Simpson, J. W. Truman, A. Cardona and M. Zlatic (2015). "A multilevel multimodal circuit enhances action selection in Drosophila." Nature **520**(7549): 633-639.

Olsen, S. R., V. Bhandawat and R. I. Wilson (2010). "Divisive normalization in olfactory population codes." Neuron **66**(2): 287-299.

Olsen, S. R. and R. I. Wilson (2008). "Cracking neural circuits in a tiny brain: new approaches for understanding the neural circuitry of Drosophila." Trends Neurosci **31**(10): 512-520.

Olsen, S. R. and R. I. Wilson (2008). "Lateral presynaptic inhibition mediates gain control in an olfactory circuit." Nature **452**(7190): 956-960.

Owald, D., J. Felsenberg, C. B. Talbot, G. Das, E. Perisse, W. Huetteroth and S. Waddell (2015). "Activity of defined mushroom body output neurons underlies learned olfactory behavior in Drosophila." Neuron **86**(2): 417-427.

Owald, D., S. Lin and S. Waddell (2015). "Light, heat, action: neural control of fruit fly behaviour." Philos Trans R Soc Lond B Biol Sci **370**(1677): 20140211.

Pauls, D., M. Selcho, N. Gendre, R. F. Stocker and A. S. Thum (2010). "Drosophila larvae establish appetitive olfactory memories via mushroom body neurons of embryonic origin." J Neurosci **30**(32): 10655-10666.

Pfeiffer, B. D., A. Jenett, A. S. Hammonds, T. T. Ngo, S. Misra, C. Murphy, A. Scully, J. W. Carlson, K. H. Wan, T. R. Laverty, C. Mungall, R. Svirskas, J. T. Kadonaga, C. Q. Doe, M. B. Eisen, S. E. Celniker and G. M. Rubin (2008). "Tools for neuroanatomy and neurogenetics in Drosophila." Proc Natl Acad Sci U S A **105**(28): 9715-9720.

Pfeiffer, B. D., T. T. Ngo, K. L. Hibbard, C. Murphy, A. Jenett, J. W. Truman and G. M. Rubin (2010). "Refinement of tools for targeted gene expression in Drosophila." Genetics **186**(2): 735-755.

Pfeiffer, B. D., J. W. Truman and G. M. Rubin (2012). "Using translational enhancers to increase transgene expression in Drosophila." Proc Natl Acad Sci U S A **109**(17): 6626-6631.

Pulver, S. R., T. G. Bayley, A. L. Taylor, J. Berni, M. Bate and B. Hedwig (2015). "Imaging fictive locomotor patterns in larval Drosophila." J Neurophysiol **114**(5): 2564-2577.

Pulver, S. R., S. L. Pashkovski, N. J. Hornstein, P. A. Garrity and L. C. Griffith (2009). "Temporal dynamics of neuronal activation by Channelrhodopsin-2 and TRPA1 determine behavioral output in Drosophila larvae." J Neurophysiol **101**(6): 3075-3088.

Python, F. and R. F. Stocker (2002). "Adult-like complexity of the larval antennal lobe of D. melanogaster despite markedly low numbers of odorant receptor neurons." J Comp Neurol **445**(4): 374-387.

Ramaekers, A., E. Magnenat, E. C. Marin, N. Gendre, G. S. X. E. Jefferis, L. Luo and R. F. Stocker (2005). "Glomerular Maps without Cellular Redundancy at Successive Levels of the Drosophila Larval Olfactory Circuit." Current Biology **15**(11): 982-992.

Rohwedder, A., N. L. Wenz, B. Stehle, A. Huser, N. Yamagata, M. Zlatic, J. W. Truman, H. Tanimoto, T. Saumweber, B. Gerber and A. S. Thum (2016). "Four Individually Identified Paired Dopamine Neurons Signal Reward in Larval Drosophila." Curr Biol **26**(5): 661-669.

Rosenzweig, M., K. Kang and P. A. Garrity (2008). "Distinct TRP channels are required for warm and cool avoidance in Drosophila melanogaster." Proc Natl Acad Sci U S A **105**(38): 14668-14673.

Roth, G. (2015). "Convergent evolution of complex brains and high intelligence." Philos Trans R Soc Lond B Biol Sci **370**(1684).

Schleyer, M., S. F. Reid, E. Pamir, T. Saumweber, E. Paisios, A. Davies, B. Gerber and M. Louis (2015). "The impact of odor-reward memory on chemotaxis in larval Drosophila." Learn Mem **22**(5): 267-277.

Schneider-Mizell, C. M., S. Gerhard, M. Longair, T. Kazimiers, F. Li, M. F. Zwart, A. Champion, F. M. Midgley, R. D. Fetter, S. Saalfeld and A. Cardona (2016). "Quantitative neuroanatomy for connectomics in Drosophila." Elife **5**.

Schroll, C., T. Riemensperger, D. Bucher, J. Ehmer, T. Voller, K. Erbguth, B. Gerber, T. Hendel, G. Nagel, E. Buchner and A. Fiala (2006). "Light-induced activation of distinct modulatory neurons triggers appetitive or aversive learning in Drosophila larvae." Curr Biol **16**(17): 1741-1747.

Schulze, A., A. Gomez-Marin, V. G. Rajendran, G. Lott, M. Musy, P. Ahammad, A. Deogade, J. Sharpe, J. Riedl, D. Jarriault, E. T. Trautman, C. Werner, M. Venkadesan, S. Druckmann, V. Jayaraman and M. Louis (2015). "Dynamical feature extraction at the sensory periphery guides chemotaxis." eLife **4**.

Shoval, O. and U. Alon (2010). "SnapShot: network motifs." Cell **143**(2): 326-e321.

Simpson, J. H. (2009). "Mapping and manipulating neural circuits in the fly brain." Adv Genet **65**: 79-143.

Sitaraman, D., Y. Aso, G. M. Rubin and M. N. Nitabach (2015). "Control of Sleep by Dopaminergic Inputs to the Drosophila Mushroom Body." Frontiers in Neural Circuits **9**: 73.

Slater, G., P. Levy, K. L. Chan and C. Larsen (2015). "A central neural pathway controlling odor tracking in Drosophila." J Neurosci **35**(5): 1831-1848.

Sprecher, S. G., A. Cardona and V. Hartenstein (2011). "The Drosophila larval visual system: high-resolution analysis of a simple visual neuropil." Dev Biol **358**(1): 33-43.

Staudacher, E. M. (2001). "Sensory responses of descending brain neurons in the walking cricket, Gryllus bimaculatus." Journal of comparative physiology A **187**(1): 1-17.

Strutz, A., J. Soelter, A. Baschwitz, A. Farhan, V. Grabe, J. Rybak, M. Knaden, M. Schmuker, B. S. Hansson and S. Sachse (2014). "Decoding odor quality and intensity in the Drosophila brain." Elife **3**: e04147.

Sweeney, S. T., K. Broadie, J. Keane, H. Niemann and C. J. O'Kane (1995). "Targeted expression of tetanus toxin light chain in Drosophila specifically eliminates synaptic transmission and causes behavioral defects." Neuron **14**(2): 341-351.

Swierczek, N. A., A. C. Giles, C. H. Rankin and R. A. Kerr (2011). "High-throughput behavioral analysis in C. elegans." Nat Meth **8**(7): 592-598.

Szigeti, B., A. Deogade and B. Webb (2015). "Searching for motifs in the behaviour of larval Drosophila melanogaster and Caenorhabditis elegans reveals continuity between behavioural states." J R Soc Interface **12**(113): 20150899.

Taborsky, M. and M. Hauber (2014). "Tribute to Tinbergen: The Four Problems of Biology. A Critical Appraisal." Ethology **120**(3): 224-227.

Tanaka, N. K., T. Awasaki, T. Shimada and K. Ito (2004). "Integration of chemosensory pathways in the Drosophila second-order olfactory centers." Curr Biol **14**(6): 449-457.

Tastekin, I., J. Riedl, V. Schilling-Kurz, A. Gomez-Marin, J. W. Truman and M. Louis (2015). "Role of the subesophageal zone in sensorimotor control of orientation in Drosophila larva." Curr Biol **25**(11): 1448-1460.

Thum, A. S., S. Knapek, J. Rister, E. Dierichs-Schmitt, M. Heisenberg and H. Tanimoto (2006). "Differential potencies of effector genes in adult Drosophila." J Comp Neurol **498**(2): 194-203.

Thum, A. S., B. Leisibach, N. Gendre, M. Selcho and R. F. Stocker (2011). "Diversity, variability, and suboesophageal connectivity of antennal lobe neurons in D. melanogaster larvae." J Comp Neurol **519**(17): 3415-3432.

Tinbergen, N. (1963). "On aims and methods of ethology." Zeitschrift für Tierpsychologie **20**(4): 410-433.

Träger, U. and U. Homberg (2011). "Polarization-Sensitive Descending Neurons in the Locust: Connecting the Brain to Thoracic Ganglia." The Journal of Neuroscience **31**(6): 2238-2247.

van Breugel, F., & Dickinson, M. H. (2014). "Plume-tracking behavior of flying Drosophila emerges from a set of distinct sensory-motor reflexes." Current Biology, **24**(3), 274-286.

Van Essen, D. C., S. M. Smith, D. M. Barch, T. E. J. Behrens, E. Yacoub and K. Ugurbil (2013). "The WU-Minn Human Connectome Project: An overview." NeuroImage **80**: 62-79.

Varshney, L. R., Chen, B. L., Paniagua, E., Hall, D. H., & Chklovskii, D. B. (2011). "Structural properties of the Caenorhabditis elegans neuronal network." PLoS Comput Biol, 7(2), e1001066.

Venken, K. J., J. H. Simpson and H. J. Bellen (2011). "Genetic manipulation of genes and cells in the nervous system of the fruit fly." Neuron **72**(2): 202-230.

Vogelstein, J. T., Y. Park, T. Ohyama, R. A. Kerr, J. W. Truman, C. E. Priebe and M. Zlatic (2014). "Discovery of brainwide neural-behavioral maps via multiscale unsupervised structure learning." Science **344**(6182): 386-392.

Vogt, K., C. Schnaitmann, K. V. Dylla, S. Knapek, Y. Aso, G. M. Rubin and H. Tanimoto (2014). "Shared mushroom body circuits underlie visual and olfactory memories in Drosophila." Elife **3**: e02395.

von Philipsborn, A. C., T. Liu, J. Y. Yu, C. Masser, S. S. Bidaye and B. J. Dickson (2011). "Neuronal control of Drosophila courtship song." Neuron **69**(3): 509-522.

Vosshall, L. B. and R. F. Stocker (2007). "Molecular architecture of smell and taste in Drosophila." Annu Rev Neurosci **30**: 505-533.

Wang, Y., Y. Pu and P. Shen (2013). "Neuropeptide-gated perception of appetitive olfactory inputs in Drosophila larvae." Cell Rep **3**(3): 820-830.

White, J. G., Southgate, E., Thomson, J. N., & Brenner, S. (1986). "The structure of the nervous system of the nematode Caenorhabditis elegans." Philos Trans R Soc Lond B Biol Sci, **314**(1165), 1-340.

Wiersma, C. A. G., & Ikeda, K. (1964). "Interneurons commanding swimmeret movements in the crayfish, Procambarus clarki (Girard)."Comparative Biochemistry and Physiology, **12**(4), 509-525.

Wilson, R. I. (2013). "Early Olfactory Processing inDrosophila: Mechanisms and Principles." Annual Review of Neuroscience **36**(1): 217-241.

Wilson, R. I., G. C. Turner and G. Laurent (2004). "Transformation of olfactory representations in the Drosophila antennal lobe." Science **303**(5656): 366-370.

Wong, A. M., J. W. Wang and R. Axel (2002). "Spatial representation of the glomerular map in the Drosophila protocerebrum." Cell **109**(2): 229-241.

Yoshikawa, S., H. Long and J. B. Thomas (2016). "A subset of interneurons required for Drosophila larval locomotion." Mol Cell Neurosci **70**: 22-29.

Younossi-Hartenstein, A., P. M. Salvaterra and V. Hartenstein (2003). "Early development of the Drosophila brain: IV. Larval neuropile compartments defined by glial septa." J Comp Neurol **455**(4): 435-450.

Zhang, W., W. Ge and Z. Wang (2007). "A toolbox for light control of Drosophila behaviors through Channelrhodopsin 2-mediated photoactivation of targeted neurons." Eur J Neurosci **26**(9): 2405-2416.

Zhang, W., Z. Yan, L. Y. Jan and Y. N. Jan (2013). "Sound response mediated by the TRP channels NOMPC, NANCHUNG, and INACTIVE in chordotonal organs of Drosophila larvae." Proc Natl Acad Sci U S A **110**(33): 13612-13617.

Zimmermann, G., L. P. Wang, A. G. Vaughan, D. S. Manoli, F. Zhang, K. Deisseroth, B. S. Baker and M. P. Scott (2009). "Manipulation of an innate escape response in Drosophila: photoexcitation of acj6 neurons induces the escape response." PLoS One **4**(4): e5100.

Zlatic, M., F. Li, M. Strigini, W. Grueber and M. Bate (2009). "Positional Cues in the <italic>Drosophila</italic> Nerve Cord: Semaphorins Pattern the Dorso-Ventral Axis." PLoS Biol **7**(6): e1000135.

Zwart, M. F., S. R. Pulver, J. W. Truman, A. Fushiki, R. D. Fetter, A. Cardona and M. Landgraf (2016). "Selective Inhibition Mediates the Sequential Recruitment of Motor Pools." Neuron **91**(3): 615-628.